ORIGINAL

VanNess Feldman
ATTORNEYS AT LAW

A PROFESSIONAL CORPORATION
1050 Thomas Jefferson Street N.W.
Washington, D.C. 20007-3877
(202) 298-1800 Telephone
(202) 338-2416 Facsimile

Seattle, Washington
(206) 623-9372

John H. Burnes, Jr.
(202) 298-1865

PUBLIC

Volume 2; Part 3 of 3

January 26, 2004

The Honorable Magalie R. Salas
Secretary
Federal Energy Regulatory Commission
888 First Street N.E.
Washington, D.C. 20426

Re: Sound Energy Solutions, Application for Authority To Site, Construct, And Operate LNG Import Terminal Facilities, Docket No. CP04 58 -000

Dear Ms. Salas:

Enclosed for filing pursuant to Section 3 of the Natural Gas Act and Part 153 of the Commission's Regulations thereunder, is an "Application for Authority to Site, Construct, and Operate LNG Import Terminal Facilities" ("Application") by Sound Energy Solutions ("SES").

SES respectfully requests that the Commission issue a final order granting SES all necessary authorizations by October 20, 2004.

The Application consists of the following 10 volumes and additional material:

- Transmittal letter, Application, Form of Notice, and Exhibits A, B, and C required by Section 153.8(a)(1), (2) and (3) of the Commission's regulations, 18 C.F.R. § 153.8(a)(1), (2) and (3). **(PUBLIC)**;

- Volume I (Environmental Report – Resource Report Numbers 1, 2, 3, 4, and 5 and Appendices) **(PUBLIC)**;

- Volume II (Environmental Report – Resource Report Number 6 and Appendices) **(PUBLIC)**;
- Volume III (Environmental Report – Resource Report Numbers 7, 8, 9, 10 and 11 and applicable Appendices for Resource Report Numbers 7, 8, 9, 10 and 11) **(PUBLIC)**;
- Volume IV (Environmental Report – Resource Report Number 9-Appendices only) **(PUBLIC)**;
- Volume V (Environmental Report – Resource Report Numbers 1, 4, 5, 6, 8, 9, 10, and 11) **(NON-INTERNET PUBLIC)**;
- Volume VI (Environmental Report – Resource Report Number 13, Appendix 13-1 Drawings) **(CRITICAL ENERGY INFRASTRUCTURE INFORMATION)**;
- Volume VII (Environmental Report – Resource Report Number 13, Appendix 13-2, Specifications and Data Sheets) **(CRITICAL ENERGY INFRASTRUCTURE INFORMATION)**;
- Volume VIII (Environmental Report – Resource Report Number 13, Appendix 13-3.1, Manufacturer Data) **(CRITICAL ENERGY INFRASTRUCTURE INFORMATION)**;
- Volume IX (Environmental Report – Resource Report Number 13, Appendix 13.3-2, Manufacturer Data) **(CRITICAL ENERGY INFRASTRUCTURE INFORMATION)**;
- Volume X (Environmental Report – Resource Report Number 13, Appendices 13.4.1, and 13.4.2 Dispersion, Release, and Threat Analyses) **(CRITICAL ENERGY INFRASTRUCTURE INFORMATION)**;
- Envelope (Environmental Report Resource Report Number 4, Cultural Resource Figures) **(PRIVILEGED AND CONFIDENTIAL)**

Pursuant to Rule 388.112 of the Commission's Rules of Practice and Procedure, 18 C.F.R. § 388.112, SES submits an original and seven (7) copies of the Transmittal letter and the body of the Application, including Exhibits A, B, and C; and Volumes Nos. I. II, III, and IV, each of which has been marked **PUBLIC**. SES is also submitting an original and seven (7) copies of Volume No. V which is marked **NON-INTERNET PUBLIC**. Volume Nos. VI, VII, VIII, IX, and X contain information which is sensitive, protected critical energy infrastructure information ("CEII") as defined in 18 C.F.R. § 388.113(c). Accordingly, SES is filing an original and two (2) copies of Volume Nos.

VI, VII, VIII, IX, and X, each of which is marked in bold print **CONTAINS CRITICAL ENERGY INFRASTRUCTURE INFORMATION – DO NOT RELEASE.** Finally, SES is submitting a separate envelope which contains location, character, and ownership information about cultural resources. The envelope is marked in bold print, **"CONTAINS PRIVILEGED AND CONFIDENTIAL INFORMATION – DO NOT RELEASE".**

SES is also submitting one Compact Disc containing Volumes I-V, labeled "FERC Application, Resource Reports 1 through 12"; Two Separate Compact Discs are provided containing the body of the Application and a Form of Notice suitable for the Federal Register, and are labeled "FERC Application" and "Form of Notice", respectively. All Compact Discs are formatted in MS Word.

In accordance with Rule 2011(c)(5) of the Commission's Rules of Practice and Procedure, 18 C.F.R. § 385.2011(c)(5), the undersigned states that the paper copies of this filing contain the same information as the electronic medium, and that, to the best of his information, knowledge, and belief, the contents as stated in the paper copies and the electronic medium are true.

Respectfully submitted,

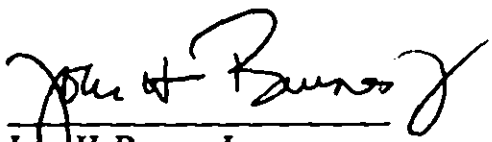

John H. Burnes, Jr.
Attorney for
Sound Energy Solutions

cc: Michael Boyle – 1 copy of Volumes I-X, Application, and Cultural Resources
Confidential Material
3 copies of Volumes VI-X

4.0 REGIONAL SEISMICITY

4.1 SOURCES OF DATA

Regional seismicity data were compiled from the following sources: (1) National Oceanic and Atmospheric Administration (NOAA) of Boulder, Colorado, and (2) National Earthquake Information Center (NEIC) of the U.S. Geological Survey (USGS). The NEIC incorporates data from several sources, including the California Geological Survey (CGS), which was formerly the California Division of Mines and Geology (CDMG). A master seismicity catalog was created from these information sources and used in the development of earthquake recurrence rates for the PSHA. This catalog contains the locations and magnitudes of all recorded earthquakes of magnitude, M≥3, in the region containing the relevant seismic sources, which are within the boundaries, 33° – 35°N and 116° – 120°W.

4.2 SPATIAL DISTRIBUTION OF SEISMICITY

The LNG terminal site is located in a region of high seismic activity. The epicenters of significant regional earthquakes from the Southern California Earthquake Center (SCEC) website (www.scecdc.scec.org/clickmap.html) are plotted in Figure 4–1, which also shows the locations of active faults (in light blue). The seismicity in this figure is concentrated to the northwest, north and southeast of the LNG site, and these earthquakes are primarily associated with the mapped fault zones. The larger historical earthquakes in the immediate vicinity of the LNG terminal (i.e., within about 20 km of the site) include the: (1) 1993 Long Beach earthquake, a moment magnitude M_w 6.4 event generated by the Newport-Inglewood fault, and (2) two local magnitude M_L 4.8 earthquakes in October and November of 1941 in the Carson-Long Beach-Wilmington area within the Newport-Inglewood fault zone. Although the epicenter of the 1933 event was approximately 30 km southeast of the site, the fault rupture proceeded to the northwest along the Newport-Inglewood fault into Long Beach. The closest distance of the rupture to the site was about 7 km.

4.3 SIGNIFICANT HISTORICAL EARTHQUAKES

The regional earthquakes of magnitude, M≥~6, in southern California and northern Baja are shown in Figure 4–2. The large events ($M_w \geq 6.5$) within 100 km of the site are listed in Table 4-1.

Table 4-1. Earthquakes of Magnitude $M_w \geq 6.5$ Within 100 km of Site

Date (MO-DY-YR)	Earthquake	Causative Fault	M_w	Epicentral Distance (km)
12-8-1812	Wrightwood	San Andreas?	7.5 est.	81?
1-9-1857	Fort Tejon	San Andreas	7.9 est.	81 (1)
2-9-1971	San Fernando	San Fernando	6.6	77
1-17-1994	Northridge	Northridge blind thrust	6.7	60
(1) Closest distance from fault rupture to site; epicentral distance was approximately 300 km northwest of site.				

The exact location of the 1812 event is unknown. Evidence from sediments along the San Andreas fault and tree-rings of pines growing near this fault, suggest the Mojave segment of the San Andreas fault system is the causative fault, possibly generating as much as 170 km (106 miles) of surface rupture (Jacoby et al., 1988; Sieh et al., 1988).

4.4 HISTORICAL SITE GROUND MOTION

The largest ground motion at the site generated by the events shown in Figure 4-2 is estimated to have been produced by the 1933 Long Beach earthquake. Peak ground accelerations (PGA) of 0.20 g (NS component) and 0.29 g (vertical component) were recorded at the nearby Long Beach Public Utilities Building during this event. At the nearby Fire Station 111 site on Terminal Island, PGA values of 0.20 g (330°- horizontal component) and 0.05 g (vertical component) were recorded during the 1994 Northridge earthquake.

Besides those from the 1933 Long Beach and 1994 Northridge events, no PGA value greater than 0.1 g has been recorded in the immediate site vicinity since the first strong motions were recorded there (Long Beach Public Utilities Building) in 1933. For example, PGA values less than 0.1 g were recorded at (1) the nearby Southern California Edison site on Terminal Island during the 1971 San Fernando earthquake, (2) the Fire Station 111 site during the 1987 Whittier Narrows earthquake (M_w 6.0), and (3) the Long Beach Public Utilities Building during the November 1941 Wilmington earthquake (M_L 4.8).

Site ground motions from pre-1933 earthquakes judged to produce the largest PGA at the site were estimated using the attenuation equations of Abrahamson and Silva (1997). These events were the aforementioned 1812 and 1857 earthquakes. If the 1812 event occurred on the San Andreas fault as the evidence suggests, then both the 1812 and 1857 events occurred approximately 81 km (closest approach of the fault rupture) from the site. Because the 1857 M_w 7.9 event had a larger magnitude, the PGA from this event would also be larger. The Abrahamson and Silva (1997) equations for soil sites predict a median PGA of 0.09 g and an 84th percentile PGA of 0.14 g from the 1857 event. The PGA values for the 1812 event are somewhat smaller (0.07 g – median and 0.11 g – 84th percentile).

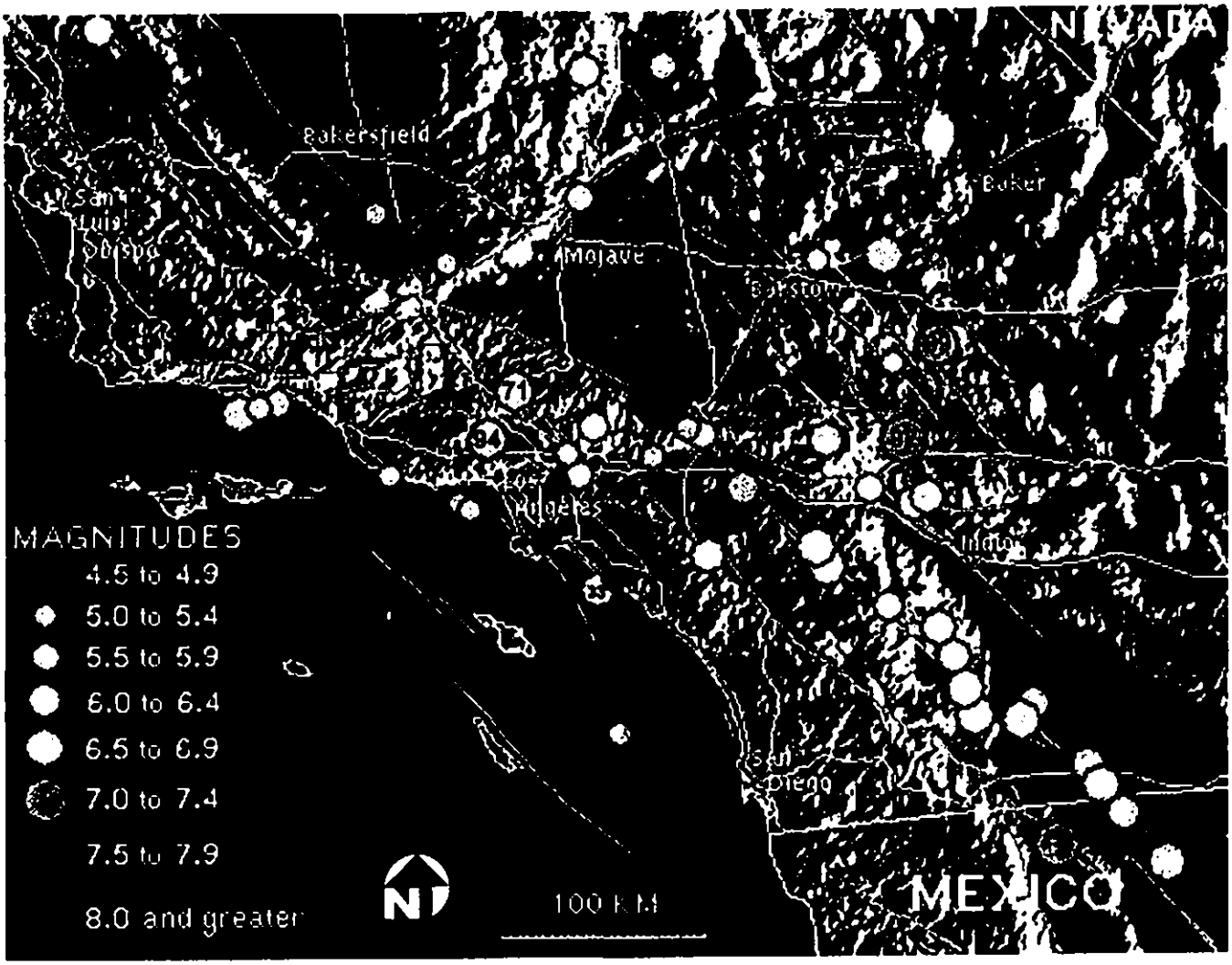

Source: http://www.scedc.scec.org/clickmap.html

This web site was developed by the Southern California Earthquake Center. By clicking on a color circle (an epicenter of a particular earthquake), pertinent information on the event will be displayed. In the figure above, two-digit numbers have been inserted into circles to reference the more significant or more recent larger magnitude earthquakes. These events are listed below (from west to east). Magnitudes are listed in Figure 4-2.

27 = 1927 Lompoc

57 = 1857 Fort Tejon

52 = 1952 Kern County

94 = 1994 Northridge

71 = 1971 San Fernando

33 = 1933 Long Beach

12 = 1812 Wrightwood

92 = 1992 Landers

99 = 1999 Hector Mine

Figure 4-1

Job No. 33756066

Significant Seismicity of Site Region of M ≥ 4.5 (1800 - 2003)

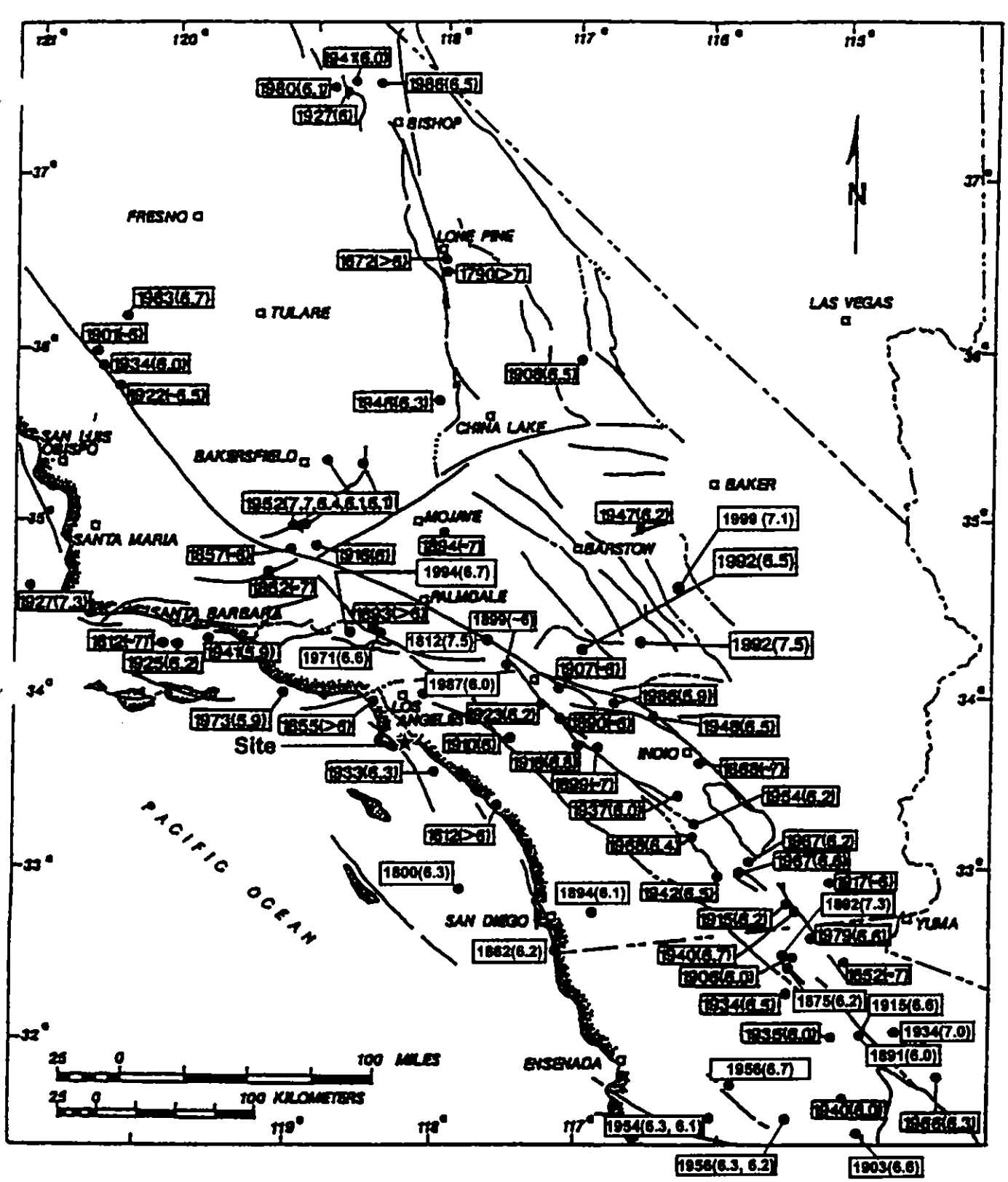

Updated from Slosson and Gray (1984), Doser (1994), and Toppozada et al. (2000)

Figure 4-2

Large Earthquakes in Southern California and Northern Baja California of M ≥ 6.0

Job No. 33756066

5.0 SEISMIC SOURCES

Southern California is a tectonically active region comprised of many potential seismic sources. The level of information for these sources varies in amount and reliability, and for many sources is incomplete for the purposes of hazard characterization. For this reason, a number of techniques must be used to model the sources for the computation of seismic hazard at the POLB LNG site. This study has relied on existing available information to develop the input parameters (i.e., maximum earthquake magnitude, slip-rate, and recurrence interval) for the probabilistic seismic hazard analysis (PSHA). Data have been drawn from a number of different sources to characterize the major seismic sources in the region. Where sufficient data were not available to model a fault for the hazard assessment, tectonic provinces were defined and treated as areal source zones.

Faults that were treated as individual seismic sources in our seismic hazard model are listed in Table 5-1; the location of these faults is shown on Figure 5-1. Three of the relevant parameters for the PSHA (fault type, M_{max}, and distance to the site) are also listed in Table 5-1. The maximum magnitude (M_{max}) estimated for each source was based on the empirical relationships for fault rupture length versus magnitude (Wells and Coppersmith, 1994), fault rupture length and slip rate versus magnitude (Anderson et al., 1996), and fault rupture area versus magnitude for Southern California faults (Dolan et al., 1995). Fault rupture lengths for each fault are typically based on the total fault length for faults of less than 100-km total length, and the longest segment or multi-segment rupture of a fault inferred to likely rupture in a single earthquake for faults greater than 100-km length. The depths and dip of the fault planes used with the rupture length to calculate the rupture area for a fault are based on published data on the depth of seismicity for the fault and site region, interpreted results of geophysical surveys, and balanced geologic cross-sections.

Table 5-1. Summary of Fault Parameters

Fault Name	Abbreviation	Type	M_{max} (M_w)	Distance (km)
THUMS-Huntington Beach	THUMS - HB	R-RL	7.0	2.2
Palos Verdes – PV & San Pedro Shelf Segments	PVF	RL-R	7.0-7.4	4
Newport-Inglewood - Onshore	NIF	RL	7.0-7.2	7
Palos Verdes-Santa Monica Bay	PVF-SMB	RL	6.6	18
Puente Hills Thrust—Santa Fe Springs & Coyote Hills segments	PHT-SFS CH	R	7.1	17
Puente Hills Thrust—Los Angeles segment	PHT-LA	R	6.9	24
Elysian Park Thrust	EPT	R	6.6	29
Whittier-Elsinore-Whittier segment	WEWhittier	RL	6.9	31
Newport-Inglewood - Offshore	NIOF	RL	7.0	35
Santa Monica	SantaMon	LL-RO	7.0	38
Hollywood	Hollywd	LL-RO	6.6	39
Raymond	Raymond	LL-RO	6.5	40
Malibu Coast	Malibu CT	LL-RO	6.7	42
Verdugo	Verdugo	R	6.7	42
Sierra Madre	SierraMa	R	7.4	48
Northridge	Northrdg	R	6.9	56
San Fernando	SanFern	R	6.7	57
Cucamonga	Cucamong	R	7.0	58
Whittier-Elsinore-Glen Ivy segment	WEGlenIvy	RL	6.9	61
Santa Susana	SantaSus	R	6.8	65
Whittier-Elsinore-Temecula segment	WETemecula	RL	7.0	75
San Andreas-Mojave segment	SAMojave	RL	7.5	81
San Jacinto-San Bernardino segment	SJSanBer	RL	6.75	84
San Andreas-San Bernardino segment	SASanBer	RL	7.25	87
San Jacinto-San Jacinto segment	SJ SanJac	RL	7.0	90
San Jacinto-Anza segment	SJAnza	RL	7.4	119
San Andreas-Coachella Valley segment	SACoache	RL	7.5	160
San Andreas-Carrizo segment	SACarriz	RL	7.75	170

Notes: LL-RO = Left lateral reverse oblique; R = Reverse; RL = Right-lateral; M_w = Moment Magnitude; Distance = closest distance from fault to site

The potential seismic sources included in the PSHA source model are described in the following sub-sections. Only those sources potentially having a significant contribution to the ground-motion hazard at the site are described. The sources are consistent with those of the California Geological Survey (formally California Division of Mines and Geology) and U.S. Geological Survey in their joint PSHA for California (CDMG/USGS 1996) except as follows:

- The Compton Thrust (Shaw and Suppe, 1996), a northwest-southeast trending blind thrust fault interpreted to underlie the central Los Angeles basin, was not included as a seismic source. Subsequent studies by Karl Mueller and Tom Rockwell have determined that latest Pleistocene (15,000 to 20,000 years old) and Holocene deposits

that overlie the subsurface trace of this fault and its associated folding are not deformed (SCEC, 2001; T.K. Rockwell, personal communication).

- The THUMS-Huntington Beach fault is included as a potential seismic source based on correlation of recent (Edwards et al., 2001, 2002, 2003; D. Ponti, personal communication, 2003) subsurface borehole and high-resolution seismic reflection data. The data indicate uplift on the Wilmington anticline has apparently deformed latest Pleistocene and possibly early Holocene strata. This uplift is inferred to be a result of reverse displacement on the blind THUMS-HB fault.

- The Puente Hills Thrust fault is included as a seismic source based on several published studies since 1996.

In general, the M_{max} values selected for the PSHA are similar to those used by CDMG/USGS (1996). Best estimate values for M_{max} are used except for the two faults located close to the site: the Palos Verdes and Newport-Inglewood faults. Because these faults contribute the greatest amount to the seismic hazard at the site and there is uncertainty associated with some of the fault parameters (e.g. slip rate, rupture length and type, etc.), a logic tree was developed for each of these faults to account for the uncertainty in M_{max} as well as the recurrence rate. The range of M_{max} presented for these two faults in Table 5-1 reflects the range of values used in the logic trees. A simpler logic tree was also developed for the recurrence of M_{max} on the THUMS-HB fault. The more detailed logic trees for the Palos Verdes and Newport-Inglewood faults and discussion of the methodology used to develop recurrence rates for them are presented in Section 6.0.

5.1 PALOS VERDES

The Palos Verdes fault is a northwest-trending right-lateral strike-slip fault zone, with a minor component of oblique slip near the Palos Verdes Peninsula. The fault extends south from northern Santa Monica Bay offshore (west) of the Los Angeles Basin, across the northeastern base of the Palos Verdes Hills of the onshore Palos Verdes Peninsula, and across the San Pedro Shelf (Darrow and Fischer, 1983; Fischer et al, 1987, 1992; Fisher et al, 2003) to Lasuen Knoll.

At Lasuen Knoll, the fault bifurcates around the knoll, which is considered a major structural segment boundary (Fisher et al., 2003). The fault continues south and possibly connects with the offshore Coronado Bank fault within the Continental Borderlands Province.

Deformation along the Palos Verdes fault has resulted in uplift of the peninsula and preservation of a series of marine terraces. Correlation of these terraces with global eustatic sea-level fluctuations provides an estimate of the late Pleistocene uplift rate of the peninsula, and thus this portion of the fault zone. Although there remains some disagreement as to the ages of all the terraces, most studies yield late Pleistocene uplift rates of approximately 0.3 to 0.4 mm/yr (Ponti et al., 1991; Muhs et al., 1992; Ward and Valensise, 1994). McNeilan et al. (1996) indicate a similar Holocene vertical slip rate of 0.35 mm/yr based on an offset paleochannel in the Los Angeles harbor.

The amount of horizontal slip versus vertical slip has been addressed by several previous studies. Darrow and Fischer (1983) suggested that the sense of slip is partitioned roughly equally between the horizontal and vertical components. Ward and Valensise (1994) conclude that on the Palos Verdes Peninsula, the fault is dominated by horizontal slip (10:1) with an oblique slip rate of 3 –3.7 mm/yr. Stephenson et al. (1995) and McNeilan et al. (1996) also indicate the fault is predominately strike-slip with a strike-slip rate of 2.5-3.8 mm/yr and 2.7 to 3.0 mm/yr, respectively, with horizontal to vertical ratios of between 7:1 and 8:1. The resultant vertical slip rate is estimated to be 0.35 mm/yr, which is consistent with the uplift rates determined from the marine terrace record. A horizontal slip-rate of approximately 3 mm/yr is assigned to the Palos Verdes fault for this study.

Recent structural modeling of faults in the LA Basin area suggest that the Palos Verdes fault is a blind thrust fault with essentially no strike-slip motion (Davis et al., 1989; Davis and Namson, 1998; Shaw and Suppe, 1996). These models, however, predict higher uplift rates than are resolvable from the height and age of the marine terraces on the Palos Verdes Peninsula and are inconsistent with the near surface (uppermost 2 km) morphology of the offshore fault south of the site (Fisher et al., 2003), and late Pleistocene-Holocene, right-lateral horizontal slip (Stephenson et al., 1995; McNeilan et al., 1996). The late Pleistocene-Holocene vertical slip is interpreted as a result of a restraining and releasing bends on the fault. Shaw (1999) suggests

that 8 to 12 km deep earthquake hypocenters with thrust focal mechanisms located offshore to the west of the surface trace of the Palos Verdes fault may be associated with the southwest dipping fault at depth that becomes steeply dipping near surface. Thus, it is possible that strain partitioning may cause both reverse and strike-slip movement on the Palos Verdes fault.

The estimated maximum earthquake magnitude for the Palos Verdes fault is based on analysis of segmentation models along the fault zone. Fisher et al. (2003) used high-resolution seismic-reflection data with other geophysical and geologic data to characterize the offshore fault between the Palos Verdes Peninsula and Lasuen Knoll. The data indicate that the fault dip direction and sense of vertical slip vary with varying bends in the strike of the fault, but that the fault is a relatively continuous structure to the bifurcation near Lasuen Knoll where relatively recent movement is observed. Furthermore, in Santa Monica Bay north of the Palos Verdes Peninsula and the transverse Redondo Canyon fault, the Palos Verdes fault does not exhibit evidence of significant recent movement (Clarke et al., 1987). For the source model, it is assumed that Lasuen Knoll is a major structural boundary and the fault south of the knoll ruptures independently of the fault to the north.

The total fault length from northern Santa Monica Bay to Lasuen Knoll is approximately 96 km. Rupture of the total length (M_W 7.2-7.4) is included in the logic tree, but the most likely fault rupture scenario is interpreted to include two rupture segments: (1) the 28-km Santa Monica Bay and (2) the 68-km combined onshore and San Pedro Shelf segments. The Santa Monica Bay segment extends from the Redondo Canyon fault on the south to the southern margin of the Transverse Ranges. Rupture of the Santa Monica Bay segment would be expected to produce an earthquake of M_W 6.6. Rupture of the 68 km segment that includes the onshore portion of the fault combined with the offshore extension across the San Pedro shelf to Lasuen Knoll has an estimated M_{max} of M_W 7.0-7.2. Slip rates ranging from 2.5 to 3.8 mm/yr, with a preferred rate of 3.0 mm/yr, were selected for the PSHA.

5.2 THUMS-HUNTINGTON BEACH FAULT

The THUMS-Huntington Beach (THUMS-HB) fault is a northwest-southeast trending fault that extends for approximately 38 km from its intersection with the Palos Verdes fault to the

southeast, where it apparently connects with the Newport-Inglewood fault offshore Newport Beach (Wright, 1991; Williams, 2003). Late Quaternary displacement on the fault has been interpreted as primarily reverse, which has caused renewed growth of the Wilmington anticline (Edwards et al., 2001, 2002, 2003; Williams, 2003). There are varying interpretations on the origin, style, and subsurface geometry of the fault as discussed below.

There is a difference of opinion as to the geometry and style of faulting on the THUMS-HB fault. The fault was originally revealed by a seismic survey in 1969 (Truex and Hunter, 1973). The buried fault has been interpreted as both a high angle down-to-the-north normal fault and an oblique right-lateral normal fault (Truex, 1974; Clarke et al. 1987; Wright, 1991). Davis and Namson (1992) interpret the THUMS-HB fault to be a high-angle (80°), reverse fault in the upper plate of a 45° NE-dipping blind thrust (Torrance-Wilmington) fault (see Figure 3-4). The inferred depth to the buried fault-tip ranges from less than 1 km (Wright, 1991) to approximately 2.4 km (Davis and Namson, 1992). The inferred depth to the buried Torrance-Wilmington fault-tip is approximately 4.2 km (Davis and Namson, 1992).

More recent 3D seismic survey data suggest that the THUMS-HB fault is a northeast dipping, blind thrust fault (Williams, 2003) with the shallowest depth to the tipline of the fault is believed to be approximately 1.4 km (4,500 feet) (John Shaw, personal communication, 2003). The dip of the fault approximately 38 degrees to the NE (Williams, 2003), but the fault may be locally steeper at shallower depths.

The fault surface is well defined where Catalina Schist Basement rocks are thrust over Tertiary strata. Syntectonic Pliocene-age Repetto Formation strata clearly demonstrate fold growth of the Wilmington Anticline and thus fault movement occurred in the Pliocene. These strata are overlain by a prominent unconformity that was previously interpreted as representing cessation of fold growth and fault movement. The more recent subsurface mapping by Davis and Namson (1998) and Williams (2003) indicate that the unconformity and overlying early Pleistocene strata are folded during a second period of late Pleistocene reactivation of the THUMS-HB fault. The results of USGS age dating of these strata in boreholes in the southern Los Angeles basin suggested the second phase of fault movement was initiated approximately 400,000 to

600,000 ybp (Dan Ponti, pers. communication) and has continued into the early Holocene (Edwards et al., 2001, 2002, 2003).

The ongoing USGS study (subsurface drilling, stratigraphic analysis and age dating, and high-resolution geophysical surveys) of Late Quaternary strata in the southern Los Angeles Basin indicate these strata have been tilted by about 6 degrees on the north flank of the Wilmington Anticline (Edwards et al., 2001, 2002, 2003). Dipping pre-Holocene, pre-Gaspur aquifer strata have been dated at approximately 90,000 years to 115,00 ybp at depths ranging from about 26 m below ground surface (bgs) to about 30 m bgs. Shallow, flatlying Holocene (Gaspur) sediments have been dated at about 1,400 ybp (7.4 m depth) to 2,400 ybp (12 m depth). The USGS interprets the currently available data as evidence that the THUMS-HB fault has likely experienced one significant earthquake and associated Wilmington anticline uplift event in the early Holocene (approximately 7,500 to 11,000 ybp), but has not experienced a significant earthquake event in at least the past 2,400 years (D. Ponti, personal communication, 2003).

The USGS (J. Tinsley, personal communication, 2003) also reports that detailed 1:24,000 topographic maps from the 1920s show that that the Wilmington anticline had clear but low approximately 10-20 feet of topographic relief, with antecedent drainage cutting the flanks of the structure. Urbanization of the southern LA basin has subsequently obscured much of the low relief of the Wilmington anticline. However, there is still a linear depression north of the Wilmington anticline with small drainages on the north flank that flow north, away from the Long Beach Harbor area, rather than to the south. Thus, geomorphic expression of the Wilmington anticline appears to be supporting evidence of Holocene uplift.

Based on the currently available data, the THUMS-HB fault is interpreted to be a Miocene normal fault that has been reactivated as a right-lateral oblique reverse fault that accommodates compression between the Newport-Inglewood and Palos Verdes faults. The fault may also transfer lateral motion from the Newport-Inglewood fault to the Palos Verdes fault. The relative components of vertical (reverse) versus lateral (strike-slip) motion are unconstrained by the currently available data, but reverse movement is inferred to be the dominant component. The fault has been active in the late Pleistocene and probably the early Holocene; thus it is considered to be a potential seismic source.

Shaw (personal communication, 2003) believes an appropriate recurrence interval for the THUMS-HB fault is on the order of several 1,000s of years, comparable to other blind reverse structures in the Los Angeles basin such as the Puente Hills and Sierra Madre faults. Shaw also suggests that larger but less frequent events are also possible. This speculation is compatible with the USGS data, which suggest that the fault was active in the late Pleistocene and into the early Holocene, but has been dormant for at least the past several thousand years. For the purposes of this seismic hazard assessment, average recurrence intervals of 5,000 years $\pm$ 2,500 years were used for the logic tree of the THUMS-HB fault. The weights assigned to these intervals were 0.25 (2,500 years), 0.5 (5,000 years), and 0.25 (7,500 years). Based on the fault length and rupture area versus magnitude relationships, an M_{max} of M_w 7.0 is used for this fault.

Based on the depth to the fault tip and 38° fault dip reported by Williams (2003) and the plan view location of Wright (1991) shown on Figure 3-6, the closest distance of the THUMS-HB fault to the site is estimated to be 2.2 km (Figure 5-2).

5.3 NEWPORT-INGLEWOOD

The Newport-Inglewood fault zone, comprises a closely spaced system of northwest-trending, active, strike-slip and/or oblique-slip faults. The northern, onshore portion of the Newport-Inglewood fault zone extends through the Los Angeles Basin from the Santa Monica Mountains to Newport Beach, where it trends offshore (Figure 3-1). This onshore segment is characteristically a series of aligned, low-relief hills and mesas and en echelon buried faults which are a result of compressional folding and uplift along the fault zone. The Newport-Inglewood fault zone is terminated on the north by the southern frontal fault system of the Santa Monica Mountains in the Transverse Ranges province.

Offshore, the surface trace of the fault zone is primarily along the margin of the mainland shelf, generally around the 100-m depth. Southward, the fault zone extends onshore again at Rose Canyon in the San Diego area, and trends southerly into the Descanso fault zone offshore northern Baja California, Mexico. The southern extent of this zone of deformation is poorly defined, but appears to merge with the northwest trending, active Agua Blanca fault in Baja California.

Historical earthquakes have been most abundant on the southern, onshore portion of the fault zone. Most of these events were aftershocks of the 1933 M_w 6.4 Long Beach earthquake, the largest historical earthquake on the fault zone. Farther south, late Quaternary uplift of the San Joaquin Hills may be due to the Newport-Inglewood zone or an associated blind thrust fault. The most recent uplift event occurred since 1635 A.D. (Grant et al., 1999, 2002). Subsurface investigation of the fault south of the 1933 rupture detected evidence for three to five surface rupture events in the past 11,700 years (Grant et al., 1997). Grant and Rockwell (2002) consider the Newport-Inglewood fault zone to be the northern portion of a 300+ km long series of onshore and offshore, kinematically linked, active faults that extend from northern Baja California to southern California. Paleoseismic and historical seismicity data suggest a series of contemporaneous or sequential M 6.5-7 earthquakes have occurred on the zone since approximately 1650 A.D. Currently, there is no evidence that the northernmost onshore segment (north of the 1933 earthquake rupture) has ruptured during this time period.

The onshore portion of the fault is the closest segment to the POLB site. Based on the combined length of the two onshore segments of the zone and the tectonic relationships, an M_{max} of 7.0-7.2 is estimated for the onshore Newport-Inglewood fault zone. An M_{max} of 7.0 is estimated for the offshore Newport-Inglewood fault zone. The slip rate of the Newport-Inglewood zone cannot be precisely estimated from available surface data because of the many uncertainties regarding interpreted offsets and ages of geomorphic features. Calculated slip rates vary by an order of magnitude from 0.1 mm/yr to about 1.5 mm/yr (Peterson and Wesnousky, 1994; WGCEP, 1995; SCEC, 2001). Slip rates ranging from 0.5 to 1.5 mm/yr, with a preferred rate of 1.0 mm/yr are included in the logic tree.

5.4 PUENTE HILLS THRUST

The Puente Hills Thrust (PHT) is a north-dipping thrust fault that extends for approximately 40 km along the northern margin of the Los Angeles Basin from beneath Los Angeles to northern Orange County. Based on the most recent interpretations of Shaw and Shearer (1999), Pratt et al. (2002), and Shaw et al.(2002), the PHT consists of three distinct segments: (1) Los Angeles, (2) Santa Fe Springs, and (3) Coyote Hills. The PHT structurally overlies the lower Elysian Park Thrust (EPT) and underlies the upper EPT (Davis et al., 1989; Davis and Namson,

1998; Shaw and Suppe, 1996; Shaw et al., 2002). The Santa Fe Springs segment was the probable source of the 1987 M_W 6.0 Whittier Narrows earthquake (Shaw and Shearer, 1999).

High-resolution seismic profiles and subsurface exploration across the Santa Fe Springs and Coyote Hills segments indicate that shallow, late Quaternary deposits are folded above the PHT in the area of topographic escarpments (Pratt et al., 2002; Shaw et al., 2002; Dolan et al., 2003). Preferred rates of Late Quaternary slip rates for the three segments are 0.62 mm/yr (Santa Fe Springs), 0.85 mm/yr (Los Angeles), and 1.28 mm/yr (Coyote Hills) (Dolan et al., 2001; Shaw et al., 2002). The minimum and maximum slip rates are 0.44 mm/yr and 1.70 mm/yr, respectively. There have been four surface deformation events on the Santa Fe Springs segment in the last 11,000 ybp (Dolan et al., 2003). The displacement per event and recurrence rate suggests large magnitude earthquakes that probably involved more than one segment (Dolan, personal communication, 2002; Shaw et al., 2002).

Based on the segment geometry and different slip rates, the PHT was modeled as two sources, the Los Angeles segment and the combined Santa Fe Springs and Coyote Hills segments. The M_{max} used for both sources (M_w 6.9 and 7.1, respectively) is estimated based on the rupture areas indicated by Dolan et al. (2001, 2003) and Shaw et al. (2002), and the magnitude/rupture area relationships of Wells and Coppersmith (1994) and Dolan et al. (1995). These magnitudes are consistent with the estimates presented by Shaw et al. (2002). Dolan et al. (2003) indicate conservative estimates of magnitude for the earthquakes that caused the paleoseismic ruptures are M_w 7.2 to 7.5 based on average displacement–magnitude relationships. It is our opinion that these magnitudes are overly conservative values. The M_{max} recurrence intervals of 2,500 years and 5,000 years, respectively, used in the PSHA model are based on the paleoseismic data for the Santa Fe Springs segment (Dolan et al., 2003) and the slip rate for the Los Angeles segment.

5.5 ELYSIAN PARK THRUST

The Elysian Park Thrust (EPT) underlies a northwest trending anticlinorium that deforms Miocene through recent strata (Davis et al, 1989; Davis and Namson, 1998; Shaw and Suppe, 1996). A series of south vergent parasitic folds and flexures are interpreted to result from contractional deformation above the north-dipping blind thrust fault (Oskin and Sieh, 1998). The

Elysian Park anticlinorium is interpreted to be a southward migrating fault-propagation fold linked to the EPT. The subsurface geometry of the Elysian Park anticlinorium was initially modeled as being underlain by two subparallel thrust faults by Davis et al., (1989) and the southwestern margin of the trend is interpreted by Shaw and Suppe (1996) to contain at least two distinct zones of faults and folds. The anticlinorium is expressed as the uplifted Elysian and Repetto Hills and is bounded by the Hollywood and Alhambra Wash faults (Davis et al, 1989; Bullard and Lettis, 1993; Oskin et al., 2000).

Initial analysis of instrumentally recorded seismicity indicated that the EPT was the likely source of the 1987 Whittier Narrows earthquake (Hauksson and Jones, 1989). However, more recent analysis (Shaw and Shearer, 1999) indicates the east-west trending Puente Hills Thrust fault, which structurally underlies the upper EPT, was the probable source of this earthquake. Active seismicity in the vicinity of the EPT and clear evidence of Quaternary deformation indicates that the EPT may be the source of future moderate magnitude earthquakes.

Prior interpretations also considered the EPT as both a single segment and multiple segments. Based on the current data, it is our opinion that the single segment model is the most probable. In addition, the CDMG/USGS (1996) treat the Elysian Park trend as a single segment in development of the recent seismic hazard model for the State of California.

Based on the available data, the EPT is modeled as the uppermost thrust and a single segment for this seismic hazard assessment. A length of 20 km and a rupture area of 255 km is assigned to the EPT assuming a 30° dip sub-parallel to the underlying Puente Hills Thrust. The source geometry is modified from CDMG/USGS (1996) and Shaw and Suppe (1996) to reflect the interpretations of Shaw and Shearer (1999), Oskin et al. (2000), and Shaw et al. (2002). The northern termination of the EPT is defined in this report as the subsurface intersection with the Raymond-Hollywood fault. We interpret this system of east-west trending faults to form a logical termination point for the northwest trending EPT. Based on the magnitude to area/length relationships of Wells and Coppersmith (1994) and Dolan et al. (1995), an M_{max} of M_w 6.6 is used for the EPT.

The fault slip rate for the Elysian Park Thrust has been assessed through use of both balanced cross-section techniques (Davis et al., 1989; Shaw and Suppe, 1996) and quantitative morphometric techniques (Bullard and Lettis, 1993; Oskin et al. 2000). The slip rates reported through the balanced cross-section techniques range from 1.3 to 4.6 mm/yr. The slip rates obtained through quantitative morphometric techniques range from 0.3 to 1.1 mm/yr. The slip rates predicted from the balanced cross-section method are considered to over-estimate the late Pleistocene-Holocene slip rate on the fault. This assessment is based on several factors: (1) Slip rates above 1 mm/yr would be expected to produce significant geomorphic expression of the EPT, which is much less pronounced than reverse-slip faults in southern California with slip-rates of greater than 1 mm/yr, such as the Sierra Madre or Cucamonga; (2) The balanced cross-section estimates base slip rates on the length of kink bands in Plio-Pleistocene strata, which have uncertainties in the age and amount of deformation. In addition, Plio-Pleistocene deposits are much older than the period of concern for seismic hazard assessments in southern California and slip rates may have changed considerably over the past 4 million years; (3) Balanced cross-sections assume that no material moves into, or out of, the plane of the section; therefore, this assumption may not be valid, if there is considerable oblique slip along on the EPT; and, (4) Balanced cross-sections are non-unique solutions with considerable variability in the predicted geometry and fault slip rates.

Quantitative morphometric techniques are considered to provide estimates of deformation rates that are more realistic over the period of concern for seismic hazard assessment. The results of Bullard and Lettis (1993) and Oskin et al. (2000) provide estimates of late Quaternary contraction rates that are based on verifiable geomorphic data. The results provided by these studies are also more consistent with the qualitative comparison of the Elysian Park trend to other reverse, or reverse oblique-slip faults. The earthquake recurrence interval for the M_{max} is estimated between 530 and 1,730 years based on the rupture area, range of potential fault dips (30°–60°), and range of morphometrically derived slip rate values. Based on the preferred dip of 30°, the estimated slip rate is 0.35 to 1.3 mm/yr. Using the preferred 30° dip and 1.0 mm/yr dip rate, a recurrence interval of 1,200 years was estimated for the Elysian Park thrust. This value was used in the PSHA.

5.6 TRANSVERSE RANGES SOUTHERN BOUNDARY FAULT SYSTEM: RAYMOND-HOLLYWOOD-SANTA MONICA FAULTS

The southern boundary of the Transverse Ranges province is bounded by a system of east-trending reverse, oblique slip, and left-lateral strike slip faults that extend for more than 200 km. This system accommodates the westward translation of the Transverse Ranges block, relative to the Los Angeles basin, along the Raymond (Jones et al., 1990), Hollywood (Dolan et al, 1997), Santa Monica (Dolan and Sieh, 1992), Anacapa-Dume (Ellsworth 1990), Malibu Coast (Treiman, 1994), Santa Cruz Island (Pinter and Sorlien, 1991), and Santa Rosa Island (Colson et al., 1995) faults. Paleomagnetic studies of upper Pliocene strata (1 to 3 Ma) indicate that parts of the Transverse Ranges have undergone more than 20 degrees of clockwise rotation (Liddicoat, 1992). This observation suggests that the left lateral deformation along the southern boundary system is accompanied by active clockwise rotation of the Transverse Ranges. The major faults of the boundary system are described below.

5.6.1 Santa Monica Fault

The Santa Monica fault extends approximately 35-40 km from Beverly Hills on the east to offshore of Pt. Dume on the west (Dolan et al., 1997, 2000b; Pratt et al., 1998; Tsutsumi et al., 2001; Catchings et al., 2002). The fault is interpreted as a left-lateral reverse oblique structure. Left-lateral slip along the Hollywood fault steps southward along the West Beverly Hills lineament to the Santa Monica fault (Dolan et al., 2000b). Although now extensively developed, geomorphic features indicative of Holocene activity are reported from historical photographs and topographic maps of the area. Features observed include well-defined linear scarps and ridges, closed depressions, sag ponds, and springs (Real, 1987; Dolan et al., 2000b). A well-defined groundwater barrier exists along the fault zone (Hill et al., 1979). Uplift of late Pleistocene deposits indicate a reverse slip rate of 0.5 to 0.6 mm/yr (Dolan and Pratt, 1997; McGill, 1989; Dolan et al., 2000b). There are limited data on the strike-slip rate on the fault, but Treiman (1994) estimated it to be < 0.5 mm/yr.

Paleoseismic studies indicate two surface rupturing events in the last 10,000 to 17,000 ybp, with the most recent between 1,000 to 3,000 ybp (Dolan et al., 2000b). Based on the paleoseismic evidence, the fault is considered active. Using the empirical relationship of Wells and

Coppersmith (1994) and a fault length of 40 km, we estimate a maximum earthquake magnitude of M_w 7.0 for the Santa Monica fault. A slip rate of 1 mm/yr is assigned to the Santa Monica fault in CDMG/USGS (1996) based on general geomorphic criteria, and comparison with other structures of the Transverse Ranges Southern Boundary zone. This value is slightly higher than the dip-slip rate of 0.5-0.6 mm/yr reported by Dolan and Pratt (1997) and Dolan et al. (2000b) and yields recurrence rates considerably shorter than the paleoseismic data indicate. Dolan et al (2000b) consider it to be unlikely that evidence for large magnitude earthquakes on the Santa Monica fault would not have been preserved at their study location; therefore, the paleoseismic-based recurrence rate of 7,500 years is used for the M_{max} in this study.

5.6.2 Malibu Coast Fault

The Malibu Coast fault is an east-west trending, north-dipping reverse fault that is exposed on land along the southern margin of the Santa Monica Mountains between Malibu Point and Pt. Dume (Dibblee and Ehrenspeck, 1990, 1992, 1993, 1994; Treiman, 1994), and extends offshore to the east and southwest. The fault is inferred to extend for at least 55 km from its intersection with the Santa Monica fault, near the coastline at Pacific Palisades, to 15 km southwest of Port Hueneme. At its offshore western margin, slip on the Malibu Coast fault appears to transfer to the Santa Cruz Island fault via an 8 km wide left step (Sorlien, 1994). The fault exhibits evidence for left-lateral and reverse slip, and the most recent displacement occurred during the Holocene (Rzonca et al., 1991; Treiman, 1994; California Division of Mines and Geology, 1995a,b). The estimated strike-slip rate is <<0.5 mm/yr (Treiman, 1994). For this study, an M_{max} of M_w 6.7 and an associated average recurrence interval of 2,900 years are used (CDMG/USGS, 1996).

5.6.3 Hollywood Fault

The Hollywood fault extends east-northeast along the southern edge of the Santa Monica Mountains. The Hollywood fault is a steeply north-dipping fault that juxtaposes Cretaceous quartz diorite and Miocene volcanic and sedimentary rocks of the Santa Monica Mountains against Quaternary and Tertiary sedimentary rocks to the south (Tsutsumi et al., 2001). The fault is marked by a narrow, steeply southward sloping gravity gradient (Dolan et al., 1997; Chapman and Chase, 1979). The fault has had at least one surface fault rupturing event since early

Holocene time, and has an estimated vertical slip rate of 0.75 mm/yr (Dolan et al., 1997, 2000a; Lindvall et al., 2001; Quinn et al., 2001). Previous studies of the Hollywood fault suggest that the left-lateral rate along the fault is greater than 0.25 mm/yr and may be closer to 1 mm/yr (Dolan et al. 1997; S. Lindvall, personal communication, 1998). Based on a length of 17 km, the Hollywood fault is estimated to be capable of producing an M_{max} of M_w 6.6. A recurrence consistent with CDMG/USGS (1996) was used for M_{max}.

5.6.4 Raymond Fault

The Raymond fault splays from the Sierra Madre fault in Monrovia and extends westward approximately 21 km to its western termination south of the Hollywood fault (Dibblee, 1989). However, there is no consensus on the location and continuity of the fault in the Repetto Hills (Lamar, 1970; Hill et al., 1979; Weber et al., 1980; Dibblee, 1989). The Raymond fault exhibits reverse and left-lateral displacement of Holocene deposits and its geomorphic expression is consistent with the left-lateral focal mechanisms and aftershock patterns from the 1988 M_L 4.9 Pasadena Earthquake.

The fault shows well-defined evidence of repeated fault movements in late Quaternary time (Crook et al., 1987; Weaver and Dolan, 2000, 2001; Dolan et al, in review). The estimated slip rate ranges from 1.5 mm/yr to a maximum of 4 mm/yr (Weaver and Dolan, 2000; Marin et al., 2000, Dolan et al., in review). Based on alluvial fan stratigraphy five to eight surface rupturing earthquakes are estimated to have occurred between approximately 40,000 to 2,000 ybp. A recurrence interval of approximately 3,000 years was inferred by (Crook et al., 1987) and the maximum recurrence interval is 5,700 to 10,000 years (SCEC, 2001; Weaver and Dolan, 2000). The paleoseismic recurrence intervals are considerably longer than expected based on the slip rate. Based on a fault length of 21 km, the Raymond fault is estimated to be capable of producing an M_{max} of M_w 6.5.

5.7 TRANSVERSE RANGES

The Transverse Ranges province comprises a series of closely-spaced, east-west trending mountain ranges which transect the predominantly north-northwest trend of the California geologic structure and physiography. The Channel Islands are the exposed tops of mountains that are offshore

extensions of the Santa Monica Mountains. The major mountain ranges are the Santa Ynez, Santa Susana, Topatopa, and Santa Monica mountains. A major portion of the province consists of the Santa Barbara Channel which is a major geologic downwarp between the mountain ranges that form the northern and southern portions of the province. The downwarp extends onshore as the Ventura Trough and narrows easterly into the Santa Clara River Valley, which extends nearly to the San Andreas fault zone.

The mountain ranges in the Transverse Ranges province consist largely of folded and faulted sedimentary strata with most major structures aligned east-west. The east-west trending physiography and geologic structure in this province is a result of north-south to north-northeast crustal compression. Most of the faults are reverse or thrust faults with the north side upthrown. The reverse faults commonly have left-lateral components of displacement.

Numerous faults in this province have had late-Quaternary movement, and late-Quaternary uplift rates in the Ventura region are among the highest in the world. Some of the major Quaternary faults are the Big Pine, Santa Ynez, Arroyo Parida, Oakridge, Santa Cruz Island, Malibu Coast, Sierra Madre, Cucamonga, and Santa Susana faults (Figure 3-1). This tectonic regime is probably related to geometrical constrictions of the plate motion along the plate boundary. This is supported by the presence of the San Gabriel fault in this province. The San Gabriel fault is thought by many geoscientists to be an ancestral trace of the plate boundary.

The Transverse Ranges province is characterized by a high level of historical seismicity. The earthquake epicenters are most dense in a belt trending westerly from the San Gabriel and Santa Susana faults, near San Fernando, through the Ventura and Santa Barbara regions. This belt generally coincides with the area of most-abundant late-Quaternary faulting, but few events have been correlated directly to specific faults because the faults dip both northerly and southerly in the subsurface. Earthquake focal-mechanism solutions indicate a dominant north-northeasterly to south-southwesterly compressional tectonic regime.

The Transverse Ranges province has experienced several moderate-magnitude events in recent decades, notably the 1971 San Fernando (M_w 6.6), 1973 Pt. Mugu (M_L 5.9), 1979 Malibu (M_L 5.0), 1987 Whittier (M_w 6.0), 1994 Northridge (M_w 6.7), and several events in the Santa Barbara

Channel. Based on focal-mechanism determinations, all of these events had a reverse sense of displacement. The only event with a documented surface displacement was the San Fernando earthquake, but many of the other earthquakes occurred offshore and it is not certain that they did not rupture the seafloor surface.

The largest historical event in the province is believed to have been the December 21, 1812, earthquake, which is thought to have occurred in the Santa Barbara Channel region. The 1812 event had a maximum Modified Mercalli Intensity of X and an estimated magnitude of about 7.1 (Ellsworth, 1990). Based on these seismic data and on the presence of numerous long faults, the M_{max} within the province is estimated to be a M_w 7.25 event.

Recent investigations of specific faults within the Transverse Ranges have led to important revisions to the perceived hazard within the province. The major faults in the province that were included in the PSHA are described below.

5.7.1 Sierra Madre Fault

The Sierra Madre fault is a Holocene active reverse fault that extends approximately 57 km along the south flank of the San Gabriel Mountains. The fault dips to the north and has a down-dip seismogenic width of 18 km. There are two distinct segments of this fault: (1) The west segment is bounded by the San Fernando earthquake fault rupture and the intersection with the Raymond fault; and (2) The east segment is between the Raymond and Cucamonga faults. Crook et al.(1987) concluded that there is a lack of demonstrable evidence for Holocene activity along the fault. However, recent paleoseismic investigations of the western segment of the fault show that it has ruptured in large magnitude earthquakes of M_w 7.2 to 7.6 at least twice in the past 15,000 years (Rubin et al., 1998). The east segment last ruptured prior to 8,000 ybp, but exhibits 14m of reverse slip between 8,000 years and 24,000 ybp (Tucker and Dolan, 2001).

The slip rate on the Sierra Madre fault is based on the paleoseismic displacements. Rubin et al. (1998) report 10.5m slip in two events in the last 18,000 years, or a minimum fault slip rate of 0.6 mm/yr. The eastern segment also has a long term rate of 0.6 mm/yr (Tucker and Dolan, 2001). Using the Wells and Coppersmith empirical relationship between rupture area and moment magnitude yields an M_{max} magnitude of M_w 7.0, consistent with the M_{max} assigned to

the Sierra Madre by the CDMG/USGS (1996). However, the more recent paleoseismic results of Rubin et al. (1998) and Tucker and Dolan (2001) support the occurrence of less frequent, larger magnitude events on the Sierra Madre. Therefore, an M_{max} of M_w 7.4 with a recurrence interval of 6,600 years is assigned to the Sierra Madre fault for this study.

5.7.2 San Fernando

The San Fernando fault is a steeply north-dipping reverse fault, and is the western-most segment of the Sierra Madre fault zone. The San Fernando fault ruptured causing the M_w 6.6 San Fernando earthquake in 1971. This segment is the most active of the Sierra Madre fault zone based on the available geological information (Crook et al., 1987) and was also the likely source of the 1991 M_L 5.8 Sierra Madre earthquake.

The zone of surface rupture along the San Fernando fault in 1971 was about 15 km long, extending from the western side of San Fernando to Big Tujunga Canyon. Displacements of up to 2.1 meters were observed along the fault zone and showed a predominantly left-oblique sense of deformation. The zone of surface faulting coincided with a groundwater barrier in Quaternary alluvium formed by pre-1971 faulting. The two previous events before the 1971 earthquake occurred in the past 3,500 to 4,000 ybp (Fumal et al., 1995; Bonilla, 1973). Lindvall et al. (1995) indicate a minimum slip-rate of 1 mm/yr and possibly up to 2 mm/yr. A M_{max} of M_w 6.7 is assigned to the San Fernando fault based on rupture area, and historical precedence.

5.7.3 Northridge Blind Thrust

The Northridge blind thrust is located near the northern edge of the San Fernando Valley. The fault dips 35 degrees to the south and has a length of approximately 31 km. Unlike other blind thrusts in the Los Angeles basin the Northridge blind thrust is not obviously associated with surface geological structures (Hudnut et al., 1996).

The Northridge blind thrust produced the January 17, 1994 Northridge earthquake of M_w 6.7. The mainshock hypocenter was located at a depth of 19 km in the lower crust. Aftershock distributions define a fault plane that extends from a depth of 7 to 10 km near the upper termination of the rupture to a depth of 23 km. The west side of the aftershock zone is characterized by a north-northeast striking and steeply dipping planar cluster of aftershocks with

mostly thrust-type focal mechanism solutions. This cluster coincides with the Gillibrand lateral ramp described by Yeats (1987) along the Santa Susana fault. The eastern edge of the rupture area is also characterized by thrust faulting focal mechanism solutions (Hauksson et al., 1995).

Both the 1971 San Fernando and 1994 Northridge earthquakes accommodated contractional deformation of the Transverse Ranges. The San Fernando earthquake ruptured a north-dipping thrust fault from a depth of approximately 10 to 12 km to the ground surface. The Northridge earthquake ruptured a south-dipping thrust fault from a depth of 19 km to approximately 7 km, where it partially abutted the rupture surface of the San Fernando fault at a depth of ~3 to 5 km (Hauksson et al., 1995). However, the relationship of the Northridge fault to other structures of the Transverse Ranges remains ambiguous. Based on the inferred area of the Northridge thrust fault, an M_{max} of M_w 6.9 was assigned. Davis and Namson (1994) and Huftile and Yeats (1996) interpret the Quaternary slip rate to be 1.7 mm/yr.

5.7.4 Santa Susana

The Santa Susana fault extends along the southern edge of the Santa Susana Mountains, approximately 27 km from its intersection with the Oak Ridge fault on the west to the San Fernando segment of the Sierra Madre fault on the east. The Santa Susana fault is a north dipping structure that dips gently near the surface and steepens with depth (Yeats, 1987). The fault separates two different stratigraphic sequences. The Santa Susana Mountains on the north side of the fault comprise a folded and uplifted sequence of middle Miocene to Pliocene age sediments. The sequence on the south side of the fault consists of discontinuous late Cretaceous and Tertiary age sediments that are offset by both north-dipping and south-dipping thrust faults. The faulted sequence on the south side of the fault is unconformably overlain by Pleistocene age Saugus formation. The Saugus formation and Quaternary age alluvial fan deposits are overthrust by the Santa Susana fault (Yeats, 1987).

Displacement varies along strike of the Santa Susana fault. No displacement is measured at the west-end of the fault near the Oak Ridge oil field, while more than 4 km of displacement is measured near the Aliso Canyon oil field. Several significant changes in fault strike may form segmentation points along the fault. At Gillibrand Canyon and at the west edge of Sylmar Basin the fault steps left, steepens in dip, and forms a lateral ramp. Aftershocks occurred along the

left-step near Sylmar following the 1971 San Fernando earthquake. Structural relations along the fault, and older faults within the system (i.e., Frew fault) suggest that fault slip rates have accelerated from ~5 to 8 mm/yr between 975,000 to 500,000 ybp to around 10 to 14 mm/yr since 500,000 ybp (Huftile and Yeats, 1995). No slip-rate, or recurrence data from paleoseismic investigations of the Santa Susana fault are available (Lung and Weick, 1987). CDMG/USGS (1996) have adopted a fault slip rate of 5 mm/yr for the Santa Susana fault.

Based on empirical relationships among fault length/fault area and magnitude (Wells and Coppersmith, 1994; Dolan et al. 1995) the Santa Susana fault is estimated to be capable of generating an M_{max} of M_w 6.8.

5.7.5 Cucamonga

The Cucamonga fault is the eastern-most segment of the Transverse Ranges frontal fault zone. The structure extends approximately 28 km along the southern flank of the San Gabriel Mountains, initiating near the San Jacinto fault and continuing westward to the eastern end of the Sierra Madre fault. Morton and Matti (1987) found the height and age distribution of fault scarps along the Cucamonga fault to be consistent with an average repeat time for 2-meter displacements every 684 years. The slip-rate for the fault is estimated, based on cumulative offset of alluvial fans, between 4.5 and 5.5 mm/yr during the last 13,000 years.

The fault length of 28 km results in an estimated magnitude of M_w 6.7. This is consistent with the estimated magnitude for paleoearthquakes by Dolan et al. (1996). However, the empirical estimate of displacement for a M_w 6.7 event is less than the >2m paleoseismic displacements reported by Morton and Matti (1987). To account for the observed >2m displacements along the Cucamonga fault, we assign an M_{max} of M_w 7.0.

5.8 VERDUGO-EAGLE ROCK FAULT

The Verdugo-Eagle Rock fault is a northwest trending reverse fault that extends for approximately 29 km along the base of the Verdugo Mountains, Pacoima Hills, and San Rafael Hills (Weber et al., 1980; Davis et al., 1989; Ziony and Jones, 1989; Tsutsumi and Yeats, 1999). The fault is situated between the San Fernando fault on the north and Raymond fault on the south

and may structurally link with these two faults. The fault is delineated by 2-3 m, southwest-facing scarps in Holocene age alluvial deposits, subsurface faults in alluvial deposits exposed in gravel pits, and apparent gravity and groundwater anomalies (Weber et al., 1980). Historical seismicity is not known to be associated with the fault, there is no paleoseismic data, and the late Quaternary slip rate is not well constrained. Based on the fault length, an M_{max} of M_w 6.7 is estimated. An M_{max} recurrence interval consistent with the CDMG/USGS (1996) model was used in the PSHA.

5.9 WHITTIER-ELSINORE FAULT

The Elsinore fault is one of the major tectonic elements of the San Andreas Fault System in southern California. The fault extends approximately 280 km from the Los Angeles Basin to northern Baja California. The fault zone comprises six major segments including from north to south: the Whittier, Glen Ivy, Temecula, Julian, Coyote Mountain, and Laguna Salada segments. These fault segments vary from 37 to 67 km in length (CDMG/USGS, 1996) and are capable of earthquake magnitudes up to M_w 7.1.

The geological and seismological characteristics of the fault zone change at approximately 33.5°N latitude. North of this point on the fault zone, the Elsinore consists of relatively simple fault strands that occupy the narrow Elsinore Trough (Hull and Nicholson, 1992). South of 33.5°N the zone comprises a number of fault traces parallel to and east of the main fault trace. The distribution of earthquakes similarly occupies a narrow zone to the north and a wider zone to the southeast (Magistrale and Rockwell, 1996).

Paleoseismic investigations along the Elsinore fault demonstrate repeated Holocene surface rupturing events. Four to five prehistorical surface-rupture events have been documented along the Glen Ivy segment of the fault, with a recurrence interval for large magnitude earthquakes of approximately 250 years. This segment has a best estimate Holocene slip rate of 5 mm/yr (Rockwell et al., 1986, 1990; Bergmann and Rockwell, 1993; WGCEP, 1995).

The Whittier segment of the Elsinore fault is the closest segment to the site. This segment extends approximately 45 km to its junction with the Chino fault and Glen Ivy segment of the

Elsinore fault. Holocene age right-lateral displacement along the fault zone has been identified through exploratory trenching and is supported by right-lateral deflections of stream channels across strands of the fault (Leighton and Associates, Inc., 1987). The Whittier fault has a Holocene slip-rate of 1.7 to 2.5 mm/yr (Rockwell et al, 1988, 1992; Gath et al., 1992, 1994).

Although the Whittier-Elsinore fault is interpreted to have a relatively high slip rate, the rate of historical earthquakes along the fault is low. The 1910 M6.0 event near Lake Elsinore is the largest earthquake reported for the northern portion of the zone. Although the historical record does not provide any examples of larger magnitude earthquakes on the Whittier-Elsinore fault zone, the paleoseismic data, segment lengths, and slip rate suggest that large frequent events are possible. The M_{max} for each segment, taken from the WGCEP (1995) study, was used in the PSHA.

5.10 SAN ANDREAS

The San Andreas fault forms a relatively linear narrow zone extending from Cape Mendocino in northern California to the Salton Sea in southern California, a distance of about 1,100 km. Based on varying slip rates, earthquake recurrence intervals, and maximum earthquakes, the system can be divided into several segments. The WGCEP (1995) subdivided the southern half of the San Andreas fault into seven segments. For the site, the four southernmost segments (Carrizo, Mojave, San Bernardino Mountains, and Coachella Valley) are the closest to the site, and are considered in the analysis.

Seismic activity is low along the southern San Andreas fault. Since 1932, when earthquakes began to be systematically recorded in southern California, only a few small-magnitude events have been recorded near this fault. Two moderate events, the 1986 Palm Springs (M_L 5.9) and the 1948 Desert Hot Springs (M_L 6.5) earthquakes, were probably associated with the Banning fault (Nicholson, 1987), a splay of the San Andreas fault near the north end of the Coachella Valley segment. The latest known great earthquake on the southern San Andreas fault system was the 1857 event, which ruptured the Carrizo and Mojave segments from just north of the Carrizo Plain to Cajon Pass near San Bernardino, a distance of about 300 km. The magnitude of this event is believed to have been about M_W 7.8-7.9. This is the largest earthquake known to have occurred in

southern California. The epicenter of this event is believed to have been at the northern portion of the surface rupture, about 150 to 250 km from the Los Angeles area.

Since the WGCEP studies (USGS, 1988; WGCEP, 1995), considerably more information has become available on slip rates, recurrence intervals and maximum earthquakes for the southern San Andreas fault (Grant and Lettis, 2002). The pertinent available data for each of the recognized segments on the fault in southern California are briefly summarized below.

The recurrence intervals between ground-rupture events on the Mojave segment range from 74 years to about 282 years, with an average of about 135 years (Biasi et al., 2002, in press). Sieh et al. (1989) suggest these events and their associated earthquakes occur in clusters. Recurrence intervals within clusters are less than 100 years, but between clusters they are about 200 to 300 years. Several of the rupture events, including the 1857 Ft. Tejon earthquake, ruptured both the San Bernardino and Mojave segments. Paleoseismic studies at Wrightwood near the northwestern end of the San Bernardino Mountain segment show 14 surface-faulting events have occurred since 534 A.D. (Weldon et al., 2002). The recurrence intervals range from 62 to 192 years, which correspond to an average recurrence interval of about 105 years (Biasi et al., 2002, in press). At Pitman Canyon on the southern portion of the San Bernardino segment, the average recurrence interval is approximately 150 years (Sietz et al., 1997). Fumal et al. (2002) identified five paleoseismic events in the last 1200 years on the Mission Creek strand. Geologic data on the Coachella Valley segment indicate three large earthquakes between the years 1000 A.D. and 1700 A.D., with the most recent event in 1690 A.D. (Sieh and Williams, 1990). The average recurrence interval for these events is about 220 years.

Geologic data indicate that slip during prehistoric earthquakes along the Carrizo segment has been as much as 12 m per event. Coseismic slip on the Mojave segment ranges from about 20 cm to 4.5 m per event. The geologic data also indicate that the slip rate is about 30 to 35 mm/yr on the Carrizo and Mojave segments and about 20 to 25 mm/yr on the San Bernardino Mountain and Coachella Valley segments. Individual segments are capable of generating maximum earthquakes of about M_w 7.25 to 7.75, depending on the segment length (Table 5-1).

5.11 SAN JACINTO

The San Jacinto fault zone consists of several northwest-striking, strike-slip faults that extend from the San Gabriel Mountains on the northwest (Figure 5-1) to the Imperial fault on the southeast. The WGCEP (USGS, 1988) and CDMG/USGS (1996) subdivided the zone into five segments based on varying fault-slip rates and historic earthquakes. For the site, the three northernmost segments (San Bernardino Valley, San Jacinto Valley, and Anza) are closest to the site and therefore are considered in the analysis.

During historical times, the San Jacinto fault system has produced more earthquakes than any other fault system in Southern California. Since 1890, as many as 11 earthquakes in the magnitude 6 to 7 range have occurred (Figure 4-2). The largest earthquake appears to have been the 1918 event (M_w 6.8) on the San Jacinto Valley segment. The maximum earthquake capable of occurring on this fault zone is estimated to be a M_w 7.5 event if more than one segment ruptures. Individual segments are capable of generating smaller maximum earthquakes of about M_w 6.75 up to 7.4, depending on the segment length (Table 5-1). The best estimate slip rate for these segments is 12 mm/yr.

5.12 PENINSULAR RANGES PROVINCE

The Peninsular Ranges Province is a northwest trending mountain belt that includes the Santa Ana, Laguna, Jacumba, and Sierra Juarez mountains. Except for a relatively narrow strip of Cenozoic and Mesozoic sedimentary rocks along the western flank of the ranges, the Peninsular Ranges is primarily a massive granitic batholith of Cretaceous age.

The province boundaries are based on the internal geological and seismological characteristics as well as the location of major active faults. The Peninsular Ranges province has only a very limited number of Quaternary faults (e.g., La Nacion fault near San Diego; Jennings, 1994) and a very low rate of seismic activity. These factors suggest the province is a relatively stable tectonic block. This province is bound by the Elsinore fault on the northeast and the Newport-Inglewood-Rose Canyon and Vallecitos-San Miguel faults on the southwest. The eastern boundary in northern Baja coincides with a north-south trending structure that also delineates a change in the regional rate of seismicity.

The M_{max} for the Peninsular Ranges province is estimated to be M_w 6.5. This is considered to be the maximum background earthquake that is likely to occur without developing recognizable geomorphic features related to repeated surface fault rupturing events. This maximum magnitude also encompasses the potential M_{max} for earthquakes on the few Quaternary faults in the region, based on empirical length-magnitude relationships of Wells and Coppersmith (1994).

5.13 CATALINA PROVINCE

The offshore area between the San Clemente and Palos Verdes fault zones, north of San Clemente Island, is included in the Catalina province. This offshore area includes several major structures including the San Pedro Basin, Avalon Knoll, Catalina Escarpment, San Clemente, and Santa Cruz-Santa Catalina Ridge fault zones. These faults generally coincide with prominent seafloor escarpments. This zone is similar to the Continental borderlands province, but is treated separately based on the more westerly strike of fault segments and a change in the level of seismic activity. This zone is interpreted as a transition zone between the offshore faults of the borderland and the faults of the Channel Islands. A number of historical small to moderate magnitude earthquakes have occurred in this region.

The major faults within the province appear to be similar in size and tectonic style to the Palos Verdes fault. They are associated with major uplift along some part of their length, and consist of complex anastamozing splays with alternating Holocene and late-Quaternary displacements (Clarke et al, 1987; Marlow et al., 2000; Legg, 2001). Based on the length of the major fault segments, this province is assigned an M_{max} of M_w 7.

LARGE-FORMAT IMAGES

One or more large-format images (over 8 ½" X 11") go here.
These images are available in FERRIS at:

For Large-Format(s):
Accession No.: 20040202-0043

Security/Availability:

- [X] PUBLIC
- [ ] NIP
- [ ] CEII
- [ ] NON-PUBLIC/PRIVILEGED

File Date: 1/26/04 Docket No.: CP04-58

Parent Accession No.: 20040202-0042

Set No.: 1 of 1

Number of page(s) in set: 2

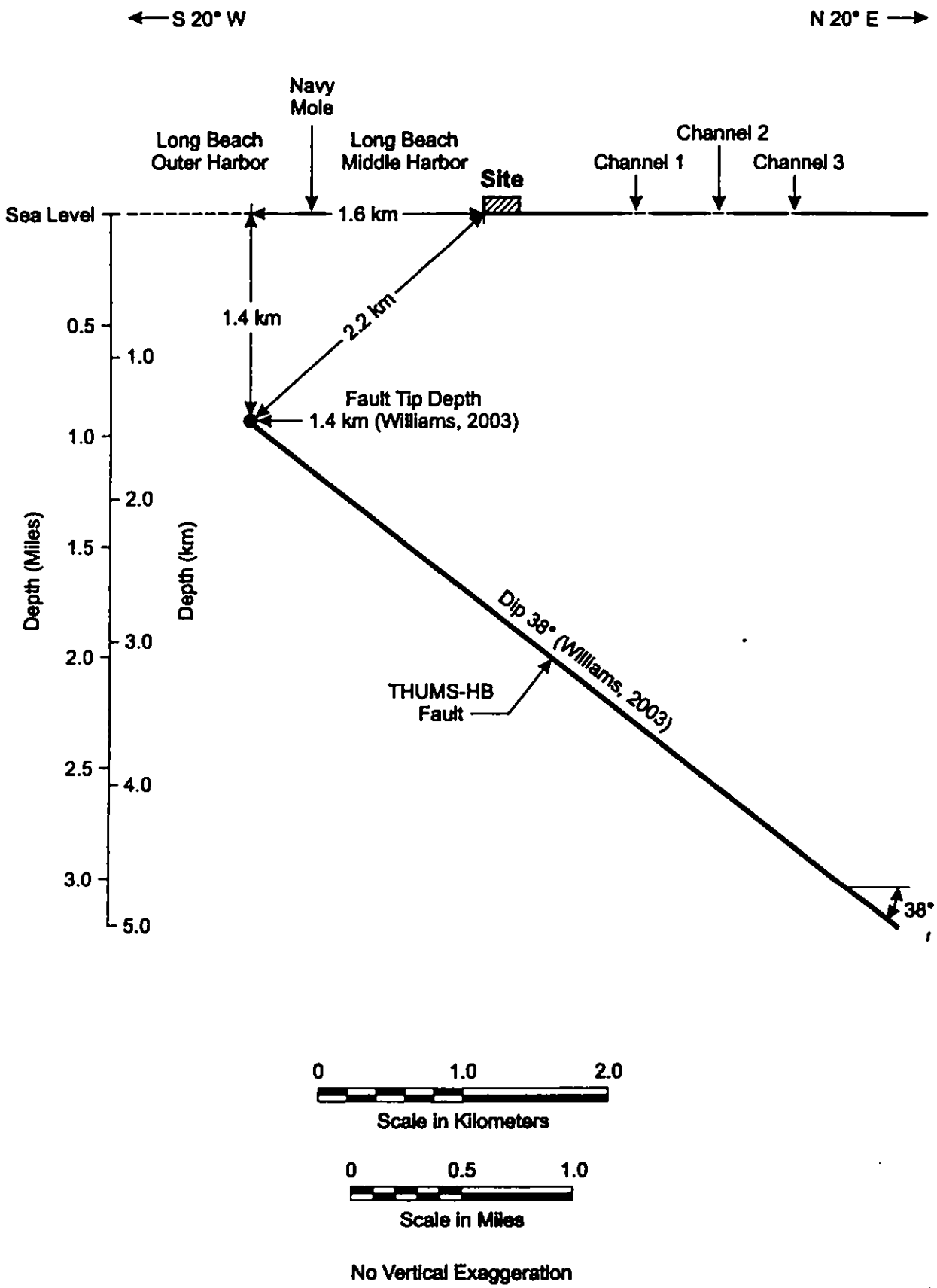

Figure 5-2

THUMS-HB Fault Cross Section

6.0 PROBABILISTIC SEISMIC HAZARD ANALYSIS

A probabilistic seismic hazard analysis (PSHA) was performed to estimate the seismic ground motions at the site. The analytical model used for the PSHA is based on models originally developed by Cornell (1968), and Kiureghian and Ang (1975). The basic assumption of these models is that the occurrence of earthquakes in space and time within a particular seismic zone is completely random (i.e., a Poisson process). This type of probabilistic model is commonly used for seismic hazard analyses of important facilities throughout the world.

Through the use of weighted alternatives cast in a logic tree format, the PSHA incorporated uncertainties associated with (1) three key seismic sources (Palos Verdes, Newport-Inglewood, and THUMS – HB faults) included in PSHA, and (2) the ground-motion attenuation.

6.1 PROBABILISTIC HAZARD MODEL

The two basic components of the probabilistic model are:

1. The seismic source models, which specify the spatial, temporal, and magnitude distribution of earthquake occurrences expected in each of the seismic sources.

2. The ground-motion attenuation models, which determine the distribution of ground motions expected at the site for an earthquake occurrence (characterized by magnitude and location, and usually by other factors) on a seismic source.

These components, which are discussed in Sections 6.2 and 6.3, comprised the inputs to the seismic hazard analysis. In this analysis, probability-of-exceedance rates were computed for a range of horizontal and vertical ground motions. These ground motions are expressed in terms of peak ground acceleration (PGA) and 5 percent-damped spectral accelerations (S_a) at 14 oscillator periods, T, of 0.04, 0.1, 0.15, 0.2, 0.3, 0.4, 0.5, 0.6, 0.8, 1.0, 1.5, 2.0, 3.0 and 4.0 seconds. From the probability-of-exceedance rates, uniform probability spectra corresponding to probabilities of exceedance of 10% in 50 years, 2% in 50 years, and 1% in 50 years, were computed, and the results are presented in Section 6.4. The spectra with these probabilities have average return periods of 475 years, 2475 years, and 4975 years, respectively. These ground-

motion return periods, adopted in the 2001 edition of the NFPA 59A standards for LNG tanks, are the basis for defining the Operating Basis Earthquake (OBE) and Safe Shutdown Earthquake (SSE) ground motions.

6.2 SEISMIC SOURCE MODELS

Based on information in Section 5.0, two types of seismic sources were defined for the PSHA: (1) seismotectonic provinces and broad fault zones modeled as areas, and (2) individual faults or fault segments modeled as points or lines. A total of ten (10) provinces, all or portions of which were less than 100 km from the LNG site, are shown in Figure 6–1. The provinces and broad fault zones are numbered 1 through 10 in this figure, while the faults or fault segments are numbered 11 through 38.

Other potential seismotectonic provinces are too far from the site to impact the ground-motion hazard.

6.2.1 Earthquake Recurrence Models for Area Sources

The earthquake recurrence rate estimated for each area source (seismotectonic province or broad fault zone—Nos. 1 through 10 in Figure 6-1) was based on the subset of seismicity within these sources. These rates were calculated with consideration given to the time periods during which the seismicity records for earthquakes above certain magnitude thresholds were considered to be complete. The completeness intervals for each source were determined by tabulating the number of earthquakes of various magnitudes in selected time intervals from 1800 AD to the present. These time periods and magnitude thresholds were selected based on discussions with Dr. T. Toppozada, seismologist with the California Geological Survey, and information in Stein and Hanks (1998). With the exception of the Newport-Inglewood fault zone, the time periods and magnitude thresholds were as follows:

Time Interval	Magnitudes
1932 – 2003	$3.0 \leq M_w \leq 5.9$
1900 – 2003	$6.0 \leq M_w \leq 6.9$
1850 – 2003	$7.0 \leq M_w$

For the Newport-Inglewood fault zone (No. 6 in Figure 6-1), the time period prior to 1940 was ignored in order to eliminate the 1933 Long Beach earthquake and its aftershocks. Inclusion of these data would have resulted in an overly conservative rate of activity inconsistent with the relatively small slip rate measured for the fault.

Annual recurrence rates were computed for the seismicity meeting the above completeness criteria. These rate data, denoted by solid diamond symbols, are plotted in Figures 6–2 through 6–10 for sources 1 through 10. The data developed in Figure 6-2 was judged to appropriately characterize the earthquake recurrence rate for both source No. 1 (ETRP – Eastern Transverse Ranges Province) and Source No. 2 (WTRP – Western Transverse Ranges Province). The Transverse Ranges Province was divided into an Eastern (ETRP) and a Western (WTRP) province to properly account for the way the faults were modeled in each province. The recurrence data in Figures 6-2 through 6-10 were used to develop recurrence equations of the form:

$$log\ (N) = a - bM_w \qquad (6\text{-}1)$$

where: N is the annual number of earthquakes of moment magnitude greater than or equal to M_w, and a and b are constants determined by least squares fit to the recurrence data. Plots of the equations are also presented in Figures 6–2 through 6–10. For the PSHA, the a-values reported in these figures (in which the recurrence rates have been normalized by 1,000 km ^{2} of area) were adjusted to account for the actual areas of the sources modeled in the PSHA code. The resulting a-values, and the b-values from Figures 6-2 through 6-10, are listed in Table 6-1.

For the PSHA, the recurrence curves were truncated at a maximum moment magnitude, M_{max}, of the largest random earthquake in the source (i.e., an event not associated with one of the twenty-eight modeled fault segments). An $M_{max} = 6.5$ was selected for source No. 1 and source Nos. 4 through 10. An $M_{max} = 7.0$ was selected for source No. 3 (Catalina) to account for the possibility of larger random earthquakes in this offshore province where less information is available on the potentially active faults. An $M_{max} = 7.25$ was selected for source No. 2 (WTRP) because individual faults capable of generating n $M_w > 6.5$ events in this province were not individually modeled, as was done for the closer ETRP, which was assigned an $M_{max} = 6.5$.

Table 6-1. Recurrence Parameters for Seismic Sources in PSHA

Seismic Source			Eqn. (6-1) Parameters			Maximum Earthquake Parameters	
Type	No.	Abbreviated Name[1]	a	b	M_{max}	Rate (#/yr)	M_{max}
Areas							
	1	ETRP	3.5070	0.8045	6.5		
	2	WTRP	3.5994	0.8045	7.25		
	3	Catalina	3.8855	1.1272	7.0		
	4	PVFZ	2.4812	0.8139	6.5		
	5	PVFZ-SMB	4.5014	1.5482	6.5		
	6	NIFZ	3.0210	0.9362	6.5		
	7	NIOFZ	1.2937	0.7414	6.5		
	8	PRP-NW	3.5863	1.1562	6.5		
	9	WhitEls zone	4.0836	1.1706	6.5		
	10	SJFZ	3.7808	0.8571	6.5		
Faults							
	11	a. PVF-M6.5-6.9(ss)	2.4099	0.8139	6.9		
		b. PVF-M6.5-6.9(rv)	1.9327	0.8139	6.9		
		c. PVF-M7.0(ss)				4.70E-04	7.0
		d. PVF-M7.2(ss)				3.79E-04	7.2
		e. PVF-M7.4(ss)				5.20E-05	7.4
		f. PVF-M7.0(rv)				1.57E-04	7.0
		g. PVF-M7.2(rv)				1.26E-04	7.2
		h. PVF-M7.4(rv)				1.73E-05	7.4
	12	PVF-SMB				3.40E-03	6.6
	13	a. NIF-M6.5-6.9(ss)	2.8961	0.9362	6.9		
		b. NIF-M6.5-6.9(rv)	2.4189	0.9362	6.9		
		c. NIF-M7.0(ss)				1.85E-04	7.0
		d. NIF-M7.2(ss)				1.00E-04	7.2
		e. NIF-M7.0(rv)				6.15E-05	7.0
		f. NIF-M7.2(rv)				3.33E-05	7.2
	14	NIOF				5.40E-04	7.0
	15	WEWhittier				1.71E-03	6.9
	16	WEGlenIvy				4.26E-03	6.9
	17	WETemecula				5.81E-03	7.0
	18	SJSanBer				1.54E-02	6.75
	19	SJSanJac				1.87E-02	7.0
	20	SJAnza				6.21E-03	7.4
	21	SACarriz				6.62E-03	7.75
	22	SAMojave				1.00E-02	7.5
	23	SASanBer				1.09E-02	7.25
	24	SACoache				8.28E-03	7.5
	25	EPT				8.33E-04	6.6
	26	SANTASUS				3.85E-03	6.8
	27	SANFERN				1.00E-03	6.7
	28	SIERRAM				1.51E-04	7.4
	29	VERDUGO				6.22E-04	6.7
	30	CUCAMONG				1.54E-03	7.0
	31	MALIBUCT				3.44E-04	6.7
	32	SANTAMON				1.33E-04	7.0
	33	HOLLYWD				1.58E-03	6.6
	34	RAYMOND				6.49E-04	6.5
	35	NORTHRDG				1.22E-03	6.9
	36	PHT-LA				2.00E-04	6.9
	37	PHT-SFS+CH				4.00E-04	7.1
	38	THBF				2.33E-04	7.0

[1] See Figure 6-1 for full names of seismic sources.

For the area sources (Nos. 1 through 10), two minimum magnitude (M_{min}) values were used in the PSHA: one for the OBE and one for the SSE. Because the 10% in 50 year and 2% in 50 year motions are used for defining the OBE design ground motion, an $M_{min} = 5.0$ was selected in the PSHA for these probabilities. On the other hand, the M_{min} value was raised to 6.0 for the PSHA runs for the SSE at the 1% in 50 year probability level. Different M_{min} values were selected because the performance criteria for the OBE and SSE are different. For the OBE the terminal shall be designed to withstand the earthquake without major damage and the complex can become operational after normal commissioning and minor repairs, if needed. For the SSE, significant damage is permitted as long as catastrophic failure, leading to a major loss of containment of LNG, does not occur. Thus, the M_{min} of 5.0 for the OBE is based on past experience, which indicates that earthquakes of smaller magnitude have little or no potential to seriously affect the continued operation of the facility, including tanks, designed to modern seismic provisions. The M_{min} of 6.0 for the SSE is also based on the same performance record, which indicates that earthquakes of smaller magnitude have little or no potential to cause catastrophic failure to structures designed to modern seismic provisions.

6.2.2 Earthquake Recurrence Models for Palos Verdes and Newport-Inglewood Faults

In the case of the Palos Verdes and Newport-Inglewood faults (source Nos. 11 and 13 in Figure 6-1), which are key faults in the PSHA because of their activity and proximity to the terminal site, logic trees were established (Figures 6–11 and 6-12) to characterize the uncertainties in the segmentation, M_{max}, rupture type and recurrence rates for these sources.

The weights assigned to the various branches of these logic trees in Figures 6-11 and 6-12 were based on judgments. The information affecting these judgments was discussed in Sections 5.1 and 5.3. In the logic tree for the Palos Verdes fault (Figure 6-11), weights of 0.25 and 0.75 were assigned to unsegmented and segmented models, respectively. The possible rupture-type scenarios proposed in the next set of branches of the tree favor a strike-slip over a reverse type of rupture, with respective weights of 0.75 and 0.25. These weights do not imply that there is a 25% likelihood that the fault is reverse and a 75% likelihood that it is strike slip. Rather, the

weights indicate that the major component of the motion is strike slip with a small reverse component. Instead of attempting to select a value for the fault-rupture parameter (F) to model this condition in the attenuation equations (Section 6.3), which are better suited to handle strike slip or reverse faults, we elected to give 0.75 (strike slip) and 0.25 (reverse) weights in the logic tree and assign F = 0 (strike slip) and F = 1 (reverse) values to the attenuation equations for these options, which are listed at the bottom of Figure 6-11.

Under the strike-slip and reverse rupture scenarios, the logic tree in Figure 6-11 includes other branches defining M_{max} - recurrence options associated with different slip rates. As stated previously, the M_{max} assigned to the Palos Verdes fault zone (source No. 4) is $M_{max} = 6.5$, which corresponds to the size of the largest random earthquake not associated with the Palos Verdes fault. The M_{max} range as shown in the logic tree for the Palos Verdes fault is $M_{max} = 7.0 - 7.4$.

To account for possible events in the magnitude range 6.5 –6.9 (which were assumed to occur on the Palos Verdes fault), the associated recurrence rates were computed from an extrapolation of the recurrence equation for the Palos Verdes fault zone, with allowance for the 0.75 (strike slip) and 0.25 reverse weighting scheme. These two strike slip and reverse sources are designated as PVF-M6.5-6.9 (ss) and PVF-M6.5-6.9 (rv) in Table 6-1.

The slip rates assigned to the Palos Verdes fault based on the information in Section 5.1 were 3.8 mm/yr, 3.0 mm/yr, and 2.5 mm/yr with weights of 0.2, 0.6, and 0.2, respectively. The rates were assumed to apply to the generation of earthquakes of M 6.5 – 6.9 and M 7.0 – 7.4. Thus, the slip rates in the logic tree (Figure 6-11) were adjusted to account for the portion of the slip rate corresponding to the M 6.5 – 6.9 events. The M 6.5 – 6.9 slip rate was computed by the moment-rate method (Anderson, 1979) and subtracted from the 3.8-, 3.0- and 2.5-mm/yr values to obtain the values listed in Figure 6-11.

The "recurrence interval" values in Figure 6-11 were computed as the inverse of the "recurrence rate" values, listed in the second to last column in this figure. Each of these rates was computed as the weighted average of rates obtained by two methods. The first or preferred method (assigned weight of 0.6) consisted of using the Southern California earthquake data in Dolan et al. (1995). In this method, regressions of the logarithm of average fault displacement (D) versus

moment magnitude (M_w) and logarithm of fault-rupture area (RA) versus M_w were performed on essentially the same data in Table 1 of Dolan et al (1995). Where ranges are listed for some values in this table, we used an average value so that for each earthquake, single values of M_w, D and RA were used in the regressions. A given rupture area, computed as the fault width (estimated to be 13 km) times the fault length (96 km or 68 km), was substituted into the M_w versus log (RA) regression equation and the resulting M_w was substituted into the log (D) versus M_w regression to obtain a value of D. The slip rate was divided by this D-value to obtain the corresponding recurrence rate.

The second method (assigned weight of 0.4) consisted of the moment-rate approach, in which the Hanks and Kanamori (1979) formula relating seismic moment (M_o) and M_w was used to compute M_o for a given M_w. The seismic moment rate of the fault ($M_o = \mu$ A s, where μ = the fault rigidity of 3.3 x10^{11} dyne/cm^2, A = rupture area, and s = slip rate) was divided by M_o to obtain the recurrence rate.

The weighted average of the two recurrence rates from both methods was computed to obtain the recurrence rate for each end branch shown in the second to last column in Figure 6-11. This rate was multiplied by the end-branch weight in the column to the right of the "End Branch #."[1] The resulting weighted rates for all end branches are listed in the last column of Figure 6-11. The sum of these weighted rates (0.00120) is shown at the bottom of this column next to "ave rate = ." This value is the average annual rate of M 7.0 – 7.4 earthquakes for the Palos Verdes fault. The reciprocal of this rate (832 years) is the corresponding average return period (ARP), which is also listed in Figure 6-11.

For the PSHA, the twenty-four (24) weighted rates in the last column of Figure 6-11 were consolidated into "Effective Recurrence Rate" values corresponding to the two distinct fault types and the three distinct M_{max} values in the logic tree. These effective rates, obtained by summing the appropriate end-branch weighted rates, are listed in bold at the bottom of Figure 6-11, and in Table 6-1 for source No. 11 (c through h).

[1] The end-branch weights represent the relative frequencies of the end branches and have a sum equal to 1.0. Each end-branch weight is obtained by multiplying the branch weights leading to the end branch. For example, the weight of 0.0225 for End Branch #1 in Figure 6-11 is the product, 0.25 x 0.75 x 0.6 x 0.2.

The logic tree for the Newport-Inglewood Fault (Figure 6-12) was similar in construction to the Palos Verdes logic tree, except that the segmented fault option was not considered because the offshore segment of the fault system was defined as a separate source. However, the methods to compute the rates listed in Figure 6-12 were identical to those used for the Palos Verdes fault. The effective rates listed at the bottom of this figure are also listed in Table 6-1 for source No. 13 (d through f).

Because distance from the site to the Santa Monica Bay segment of the Palos Verdes fault (18 km) is much greater than that (4 km) for the Palos Verdes fault, a logic tree was not considered necessary for this source (No. 12 in Figure 6-1). Instead, a single M_{max} and associated recurrence rate were estimated for this segment. The recurrence rate was computed by the moment-rate method, and the resulting value is listed in Table 6-1 for source No. 12.

The recurrence rate for the offshore segment of the Newport-Inglewood fault (source No. 14 in Figure 6-11) was computed with the same moment-rate method used for the Santa Monica Bay segment. The resulting recurrence rate is listed in Table 6-1 for source No. 14.

6.2.3 Earthquake Recurrence Models for Whittier-Elsinore, San Jacinto and San Andreas Faults

Segmentation models were adopted for the Whittier-Elsinore, San Jacinto, and San Andreas fault zones. The segments included in the PSHA for the Whittier-Elsinore fault were the Whittier, Glen Ivy and Temecula; the San Jacinto segments were the San Bernardino, San Jacinto Valley, and Anza; the San Andreas segments were Carrizo, Mojave Dessert, San Bernardino, and Coachella Valley. These segments are source Nos. 15 through 24 in Figure 6-1. The annual recurrence rates for characteristic earthquakes on the various fault segments comprising the Whittier-Elsinore, San Jacinto, and San Andreas faults were estimated from the 30-year mean probabilities (p30) of these characteristic earthquakes reported in Table 2 of WGCEP (1995). The rates were computed under the assumption that the temporal occurrence of the characteristic events was Poissonian. Thus, each rate, v, was computed from $v = - \ln (1 - p30) / 30$.

The characteristic magnitudes for the various segments of the Whittier Elsinore, San Jacinto, and San Andreas faults were based on WGCEP (1995).

6.2.4 Earthquake Recurrence Models for Thrust and Reverse Faults

The characteristic earthquake magnitudes and associated annual recurrence rates were taken from Appendix A of CDMG/USGS (1996) for the following thrust and reverse faults (Figure 6-1) within the Eastern Transverse Ranges.

No.	Fault Name
27	San Fernando
29	Verdugo
30	Cucamonga
31	Malibu Coast
34	Raymond
35	Northridge

The recurrence rate and M_{max} for the Elysian Park Thrust (source No. 25), Puente Hills Thrust (source Nos. 36 and 37) and THUMS-HB fault (source No. 38) are presented in Sections 5.5, 5.4, and 5.2, respectively.

The recurrence rate and characteristic magnitude for the Santa Susana fault (source No. 26) given in CDMG/USGS (1996) were modified to account for our estimated fault length of 32 km. The magnitude estimated from Wells and Coppersmith (1994) was M_w=6.8 and the associated annual recurrence rate computed from the moment method (with w=16 km and s=5 mm/yr) was 0.0038.

Recent studies by Rubin et al. (1998) suggest the Sierra Madre fault (source No. 28) has generated large fault displacements during relatively infrequent large characteristic earthquakes. Based on these studies, an M_{max} of 7.4 and a 6,600-year recurrence interval were assigned to this fault.

The annual recurrence rate for the Hollywood fault (source No. 33) was also taken from Appendix A of CDMG/USGS (1996), but the M_{max} was elevated from 6.4 to 6.6 based on Dolan et al. (1997).

The recurrence rates and M_{max} values for the above seismic sources are given in Table 6-1.

6.3 ATTENUATION EQUATIONS

In the PSHA, the Abrahamson and Silva (1997), Dames and Moore (1995), and Campbell and Bozorgnia (2003) attenuation equations were incorporated into the computational model. These equations were judged to be equally applicable to the site. Therefore, equal weights were assigned to each model in the PSHA. The analysis was carried out under the assumption that the soils underneath the LNG tanks will have to be improved to mitigate the liquefaction potential in the upper 70 ft approximately. This recommendation is based on the available geotechnical data for the site (URS, 2003a). Regardless of the improvement method (e.g. stone columns, deep soil mixing, etc), the Soil Profile Type of the improved site in our judgment will be S_D per Table 16-J of the 1997 Uniform Building Code (UBC). The local geology parameters in the attenuation equations were selected to represent this stiff soil subsurface condition at the LNG tank locations.

The attenuation equations are briefly described in the following subsections. These three equations were selected because (1) they include sets for horizontal and vertical components, (2) the oscillator period band covered by the equations extends to 4 or 5 sec to account for the possibility that the LNG tanks will be base isolated, and (3) they were derived from strong motion accelerogram data recorded primarily in California, including data from the 1994 Northridge earthquake.

The values selected for the various fault and geologic parameters in these equations are given in Table 6-2.

Table 6-2. Attenuation Equation Parameters

Seismic Source		Abrahamson & Silva (1997)			Dames & Moore (1995)			Campbell & Bozorgnia (2003)					
No.	Name	*S*	*F*	*HW*	*S*	*F*	*D*	S_{VFS}	S_{SR}	S_{FR}	F_{RV}	F_{TH}	δ(°)
1	ETRP	1	1	0	1	1	2.1	0	0	0	1	0	80
2	WTRP	1	1	0	1	1	2.1	0	0	0	1	0	80
3	Catalina	1	0	0	1	0	2.1	0	0	0	0	0	90
4	PVFZ	1	0	0	1	0	2.1	0	0	0	0	0	90
5	PVFZ-SMB	1	0	0	1	0	2.1	0	0	0	0	0	90
6	NIFZ	1	0	0	1	0	2.1	0	0	0	0	0	90
7	NIOFZ	1	0	0	1	0	2.1	0	0	0	0	0	90
8	PRP-NW	1	0	0	1	0	2.1	0	0	0	0	0	90
9	WhitEls zone	1	0	0	1	0	2.1	0	0	0	0	0	90
10	SJFZ	1	0	0	1	0	2.1	0	0	0	0	0	90
11	a. PVF-M6.5-6.9(ss)	1	0	0	1	0	2.1	0	0	0	0	0	90
	b. PVF-M6.5-6.9(rv)	1	1	0	1	1	2.1	0	0	0	1	0	80
	c. PVF-M7.0(ss)	1	0	0	1	0	2.1	0	0	0	0	0	90
	d. PVF-M7.2(ss)	1	0	0	1	0	2.1	0	0	0	0	0	90
	e. PVF-M7.4(ss)	1	0	0	1	0	2.1	0	0	0	0	0	90
	f. PVF-M7.0(rv)	1	1	0	1	1	2.1	0	0	0	1	0	80
	g. PVF-M7.2(rv)	1	1	0	1	1	2.1	0	0	0	1	0	80
	h. PVF-M7.4(rv)	1	1	0	1	1	2.1	0	0	0	1	0	80
12	PVF-SMB	1	0	0	1	0	2.1	0	0	0	0	0	90
13	a. NIF-M6.5-6.9(ss)	1	0	0	1	0	2.1	0	0	0	0	0	90
	b. NIF-M6.5-6.9(rv)	1	1	0	1	1	2.1	0	0	0	1	0	80
	c. NIF-M7.0(ss)	1	0	0	1	0	2.1	0	0	0	0	0	90
	d. NIF-M7.2(ss)	1	0	0	1	0	2.1	0	0	0	0	0	90
	e. NIF-M7.0(rv)	1	1	0	1	1	2.1	0	0	0	1	0	80
	f. NIF-M7.2(rv)	1	1	0	1	1	2.1	0	0	0	1	0	80
14	NIOF	1	0	0	1	0	2.1	0	0	0	0	0	90
15	WEWhittier	1	0	0	1	0	2.1	0	0	0	0	0	90
16	WEGlenIvy	1	0	0	1	0	2.1	0	0	0	0	0	90
17	WETemecula	1	0	0	1	0	2.1	0	0	0	0	0	90
18	SJSanBer	1	0	0	1	0	2.1	0	0	0	0	0	90
19	SJSanJac	1	0	0	1	0	2.1	0	0	0	0	0	90
20	SJAnza	1	0	0	1	0	2.1	0	0	0	0	0	90
21	SACarriz	1	0	0	1	0	2.1	0	0	0	0	0	90
22	SAMojave	1	0	0	1	0	2.1	0	0	0	0	0	90
23	SASanBer	1	0	0	1	0	2.1	0	0	0	0	0	90
24	SACoache	1	0	0	1	0	2.1	0	0	0	0	0	90
25	EPT	1	1	0	1	1	2.1	0	0	0	0	1	40
26	SANTASUS	1	1	0	1	1	2.1	0	0	0	1	0	80
27	SANFERN	1	1	0	1	1	2.1	0	0	0	1	0	50
28	SIERRAM	1	1	0	1	1	2.1	0	0	0	1	0	80
29	VERDUGO	1	1	0	1	1	2.1	0	0	0	1	0	80
30	CUCAMONG	1	1	0	1	1	2.1	0	0	0	1	0	80
31	MALIBUCT	1	1	0	1	1	2.1	0	0	0	1	0	80
32	SANTAMON	1	1	0	1	1	2.1	0	0	0	1	0	80
33	HOLLYWD	1	1	0	1	1	2.1	0	0	0	1	0	80
34	RAYMOND	1	1	0	1	1	2.1	0	0	0	1	0	80
35	NORTHRDG	1	1	0	1	1	2.1	0	0	0	0	1	40
36	PHT-LA	1	1	0	1	1	2.1	0	0	0	0	1	40
37	PHT-SFS+CH	1	1	0	1	1	2.1	0	0	0	0	1	40
38	THBF	1	1	1	1	1	2.1	0	0	0	0	1	40

6.3.1 Abrahamson and Silva (1997)

The basic form of the attenuation equations derived by Abrahamson and Silva is

$$ln\,Y = f_1(M,r) + Ff_3(M) + HWf_4(M,r) + Sf_5(\overline{pga}_{rock}) \qquad (6\text{-}2)$$

where:
- Y = 5% damped spectral acceleration in g
- M = moment magnitude
- r = closest distance from site to fault rupture in km
- F = fault type (1 for reverse, 0.5 for reverse/oblique, and 0 otherwise)
- HW = dummy variable for hanging wall sites (1 for sites over wall, and 0 otherwise)
- S = dummy variable for site class (0 for rock or shallow soil, 1 for deep soil)
- $\overline{pga}_{rock}$ = expected value of peak ground acceleration on rock
- f_i = functions given in Abrahamson and Silva

The deep soil site designation (s = 1) in their equations represents a site geology that is appropriate for this application based on the available geotechnical data and proposed soil improvement for the site.

6.3.2 Dames & Moore (1995)

The Dames & Moore (1995) equations were derived from regression analyses of PGA and response spectra data for horizontal and vertical components of ground-motion records from stiff alluvial sites during California earthquakes occurring in the time period 1933 – 1994. The equations are of the form:

$$ln\,Y = p_1 + p_2M + p_3\,ln\,(R + p_4\exp\{p_5M\}) + p_6S + p_7F + p_8D \qquad (6\text{-}3)$$

where:
- Y = ground-motion parameter – either peak ground acceleration (PGA), or 5% damped pseudo-spectral velocity (PSV); units of PGA are g; units of PSV are cm/sec
- M = moment magnitude, M_w
- R = closest distance from site to fault rupture surface in km
- S = site classification code: S=0 for site class B, S=1 for site class C
- F = fault-type code: F=0 for strike-slip, F=1 for reverse
- D = depth to basement rock in km
- p_i = regression coefficients

Site class B refers to soft rock or stiff soil sites, whereas site class C refers to medium-stiff soil sites. Class B sites have an average shear-wave velocity, V_s, in the upper 30 m of 366 to 762 m/sec; class C sites range between 183 and 366 m/sec.

Values of the regression coefficients were taken from Equations Set (8) of Appendix B of the Dames & Moore (1995) report.

The soil parameter, S = 1, was selected based on the aforementioned geotechnical information and proposed soil improvement for the site.

The depth under the site to basement rock, D = 2.1 km, was taken from the Yerkes et al. (1965) map of basement-rock depth contours for the Los Angeles basin.

6.3.3 Campbell and Bozorgnia (2003)

The form of the Campbell and Bozorgnia equations for horizontal and vertical components is

$$ln(Y) = c_1 + f_1(M) + c_4\, ln\sqrt{f_2(M,R,S)} + f_3(F) + f_4(S) + f_5(HW,F,M,R) \quad (6\text{–}4a)$$

$$f_1(M) = c_2 M + c_3(8.5 - M)^2 \quad (6\text{–}4b)$$

$$f_2(M,R,S) = R^2 + \left[c_5 + c_6\left(S_{VS} + S_{SR}\right) + c_7 S_{FR}\right]^2 \cdot \left(\exp\left[c_8 M + c_9(8.5 - M)\right]^2\right)^2 \quad (6\text{–}4c)$$

$$f_3(F) = c_{10} F_{RV} + c_{11} F_{TH} \quad (6\text{–}4d)$$

$$f_4(S) = c_{12} S_{VFS} + c_{13} S_{SR} + c_{14} S_{FR} \quad (6\text{–}4e)$$

$$f_5(HW,F,M,R) = HW \cdot f_3(F) f_{HW}(M) f_{HW}(R) \quad (6\text{–}4f)$$

where:

Y	=	5% damped pseudo absolute spectral acceleration for horizontal or vertical components in g
M	=	moment magnitude
R	=	closest distance in km from site to seismogenic portion of the rupture
S_{VFS}	=	index site geologic variable (1 for very firm soil, 0 otherwise)
S_{SR}	=	index site geologic variable (1 for soft rock, 0 otherwise)
S_{HR}	=	index site geologic variable (1 for hard rock, 0 otherwise) ($S_{VFS} = S_{SR} = S_{HR} = 0$ signifies firm soil)
F_{RV}	=	index fault-type variable (1 for reverse, 0 otherwise)
F_{TH}	=	index fault-type variable (1 for thrust faulting, 0 otherwise) ($F_{TH} = F_{RV} = 0$ for strike-slip and normal faulting)
HW	=	0, for $r_{jb} \geq 5.0$ km and $\delta > 70°$ $(S_{VFS} + S_{SR} + S_{HR})(5 - r_{jb})$, for $r_{jb} < 5.0$ km and $\delta \leq 70°$

$f_{HW(M)}$ = 0, for $M < 5.5$
M-5.5, for $5.5 \le M \le 6.5$
1, for $M > 6.5$

$f_{HW(R)}$ = c_{15}(R/8), for R < 8.0 km
c_{15}, for R ≥ 8.0 km

f_i = functions given in Campbell and Bozorgnia (2003)

c_i = coefficients from regression analysis

The zero (0) values selected for S_{VFS}, S_{SR}, S_{HR} represent a firm soil site geology that is appropriate for this application.

6.3.4 Probabilistic Distribution of Ground Motions Predicted by Attenuation Equations

A lognormal probabilistic distribution is associated with the ground-motion variable (Y) in each attenuation equation, and the standard deviations of this distribution are given in Abrahamson and Silva (1997), Dames & Moore (1995), and Campbell and Bozorgnia (2003). Campbell and Bozorgnia offer two formulas for the standard deviation: one in terms of the median PGA value predicted by their equations, and the other in terms of magnitude. For this application, the latter was chosen.

The standard deviations in all three attenuation equations were reduced by 10% to account for the fact that these deviations include both earthquake-to-earthquake variability and site-to-site variability, whereas the PSHA is performed for a single site of specified local geology. Thus, in our judgment, the site-to-site component of the total variability in these equations should be removed when the soil profile type is defined and no unusual conditions are present within the profile, which is the case for the present study.[2] The 10% reduction is considered a lower limit of the actual value based on Joyner and Boore (1992) and prior unpublished URS calculations.

In the PSHA, the lognormal distribution was truncated at the three standard-deviation level, an assumption that is commonly employed to eliminate unrealistic extreme values of ground

[2] The shear-wave velocities measured at the site and at nearby locations within the port complex, gradually increase with depth. This velocity gradient in the upper 80 ft of loose soil would be less with the stone columns. Thus, regardless of the point within the stiff soil profile where the free-field motion is defined (either at the ground surface in the case of stone columns, or at 80-ft depth if some columns are not used), no sharp discontinuities in shear-wave velocities were measured below this depth. Therefore, no large motion amplification is expected within this soil profile.

motion. The resulting probability density functions were adjusted such that the areas under the curves were unity.

6.4 PSHA RESULTS

The PSHA was run with the URS code, GMPROB. The fault-rupture option within this code was exercised for all area and line source in Figure 6-1 in order to account for the effect of the finite rupture lengths of earthquakes of various magnitudes. The parameters for the reverse-slip or strike-slip fault regressions of Wells and Coppersmith (1994) were selected for the estimation of fault-rupture length within the code. To account for the effect of fault-rupture length for the reverse or thrust faults (source Nos. 25 through 38 in Figure 6-1), point sources were defined for these faults, and each one was placed at a location marking the closest distance of the fault to the site. For the THUMS-HB fault, this point was 2.2 km from the site (Figure 5-2).

The area sources with an M_{max} value of 6.5 (i.e., source Nos. 1, 4 through 10 in Table 6-1) were placed at 5 km depth. This depth was judged to be an appropriate value for the PSHA and was selected based on the expected depth range for earthquakes of these moderate magnitudes and their estimated rupture areas. The other two area sources (Nos. 2 and 3 in Table 6-1) were placed at the ground surface because of the larger rupture areas associated with the larger magnitude events (up to 7.25 and 7.0) included for these areas.

The PSHA was first run for horizontal components using the three attenuation equations listed in Section 6-3. The PSHA was repeated using the corresponding vertical-component equations.

The results of the PSHA for horizontal components are provided in Table 6–3, which lists (1) the 5% damped response spectral accelerations that correspond to the three probability levels of interest for the OBE and SSE per the 2001 NFPA 59A standard, and (2) the scaled spectral accelerations equal to 2/3 of the 2% in 50 year values, which are used in the determination of the OBE. The value at oscillator period, T=0.0 sec, is the PGA. The spectra corresponding to the three probability levels are termed uniform hazard spectra (UHS) because all ordinates of a given spectrum have the same probability of being exceeded in a future time period, which in this

study is 50 years. The three UHS are plotted in Figure 6–13, along with the spectrum equal to 2/3 of the 2% in 50 year spectrum.

Table 6-3. Uniform Hazard Response Spectra, PSA (g) from PSHA. Horizontal Component.

Period	10% in 50 yr	2/3 x 2% in 50 yr	2% in 50 yr	1% in 50 yr
T (sec)	*PSA* (g)	*PSA* (g)	*PSA* (g)	*PSA* (g)
0.00	0.441	0.497	0.745	0.876
0.04	0.401	0.469	0.704	0.825
0.10	0.799	0.847	1.270	1.427
0.15	0.969	1.043	1.565	1.796
0.20	1.024	1.137	1.706	1.999
0.30	1.015	1.188	1.781	2.129
0.40	0.900	1.115	1.672	2.033
0.50	0.832	1.080	1.620	1.987
0.60	0.759	1.022	1.533	1.894
0.80	0.630	0.875	1.313	1.637
1.00	0.509	0.721	1.082	1.382
1.50	0.368	0.520	0.781	1.000
2.00	0.285	0.382	0.572	0.729
3.00	0.177	0.223	0.335	0.424
4.00	0.121	0.149	0.223	0.279

The results of the PSHA for the vertical component that were obtained following the procedure described above, are provided in Table 6-4 and plotted in Figure 6-14.

Table 6-4. Uniform Hazard Response Spectra, PSA (g) from PSHA. Vertical Component.

Period	10% in 50 yr	2/3 x 2% in 50 yr	2% in 50 yr	1% in 50 yr
T (sec)	*PSA* (g)	*PSA* (g)	*PSA* (g)	*PSA* (g)
0.00	0.417	0.526	0.789	0.955
0.04	0.496	0.743	1.115	1.413
0.10	1.028	1.289	1.933	2.336
0.15	0.846	1.052	1.578	1.908
0.20	0.665	0.829	1.243	1.506
0.30	0.451	0.560	0.840	1.021
0.40	0.350	0.436	0.654	0.802
0.50	0.291	0.373	0.560	0.688
0.60	0.251	0.324	0.486	0.600
0.80	0.201	0.260	0.390	0.484
1.00	0.177	0.228	0.343	0.424
1.50	0.131	0.170	0.255	0.318
2.00	0.101	0.128	0.193	0.241
3.00	0.080	0.092	0.138	0.167
4.00	0.064	0.076	0.114	0.138

The output files of the GMPROB PSHA runs provided the contributions to the ground motion hazard by earthquake source. This deaggregation information was used to prepare Table 6-5, which lists the percentage contributions to the 10% in 50-year hazard for response spectral ordinates at oscillator periods, T = 0.0 (corresponds to PGA), 0.4 and 2.0 sec.

Not surprisingly, because of their proximity to the site and relatively high recurrence rates, the Palos Verdes fault zone (No. 4 in Table 6-5) and the Palos Verdes fault (Nos. 11a through 11h) together had the major contribution to the hazard; generally, the Newport-Inglewood fault zone (No. 6) and Newport-Inglewood fault (Nos. 13a through 13f) were collectively the second largest contributors.

6.4.1 Comparison with USGS Results

The results of the PSHA horizontal runs were compared to ground-motion estimates based on (1) bedrock motions computed by the USGS for the site, and (2) adjustments to these motions to account for the S_D soil classification for the site in its improved condition. The USGS has computed bedrock ground motions for the U.S. as part of the National Seismic Hazard Mapping Program (NSHMP) (Frankel et al., 2000; Frankel and Leyendecker, 2001). The USGS values computed in 1996 were used as the basis to establish design response spectra in building codes, such as the International Building Code and the ASCE 7-02 Standard. In 2002, the USGS completed a revision to their 1996 values, and posted them on their web site, http://geohazards.cr.usgs.gov/eq/. Table 6-6 and Figure 6-15 show a comparison of the 10% in 50-year horizontal component response spectra developed in this study and those based on the USGS 1996 and 2002 bedrock values. The values under the USGS columns in this table were obtained as follows. The USGS bedrock values are applicable to sites with $\overline{V}_s = 760$ m/sec (i.e., the boundary between S_B and S_C soil-profile types as defined in Table 16-J of the 1997 Uniform Building Code). These values were multiplied by scale factors, computed from the site-amplification factors, F_a and F_v, in Tables 4.1.2.4a and 4.1.2.4b of the 2000 NEHRP seismic provisions (FEMA, 2001).

Table 6-5. Source Contribution to Seismic Hazard at Site for Ground Motions with a 10% Probability of Exceedance in 50 yrs.

No.	Source Name	Horizontal 10% in 50 yr			Vertical 10% in 50 yr		
		PGA	T = 0.4s	T = 2.0s	PGA	T = 0.4s	T = 2.0s
		% Contribution			% Contribution		
1	Eastern Transverse Ranges Province	0.06	0.34	0.06	0.00	0.68	0.05
2	Western Transverse Ranges Province	0.00	0.00	0.05	0.00	0.03	0.02
3	Channel Islands & Catalina Province	0.03	0.06	0.08	0.04	0.11	0.08
4	Palos Verdes fault zone	17.71	12.88	3.83	17.11	12.67	3.82
5	Palos Verdes fault zone - Santa Monica Bay	0.00	0.00	0.00	0.00	0.00	0.00
6	Newport-Inglewood fault zone	8.38	6.33	1.90	7.74	6.48	1.76
7	Newport-Inglewood Offshore fault zone	0.00	0.00	0.00	0.00	0.00	0.00
8	Peninsular Ranges seismotectonic province NW	0.01	0.02	0.01	0.01	0.04	0.01
9	Whittier-Elsinore Fault Zone	0.00	0.00	0.00	0.00	0.00	0.00
10	San Jacinto Fault Zone	0.00	0.00	0.00	0.00	0.00	0.00
11a	Palos Verdes Fault Magnitude Range 6.5-6.9 Strike-Slip	7.24	7.76	7.41	9.42	8.83	8.83
11b	Palos Verdes Fault Magnitude Range 6.5-6.9 Reverse	3.74	3.64	2.01	3.57	3.68	2.65
11c	Palos Verdes fault Magnitude 7.0 Strike-Slip	11.46	12.27	14.51	12.37	11.24	13.74
11d	Palos Verdes fault Magnitude 7.2 Strike-Slip	10.21	10.95	13.86	11.13	10.15	12.99
11e	Palos Verdes fault Magnitude 7.4 Strike-Slip	1.50	1.61	2.12	1.65	1.51	1.98
11f	Palos Verdes fault Magnitude 7.0 Reverse	5.03	4.92	3.70	4.22	4.17	3.83
11g	Palos Verdes fault Magnitude 7.2 Reverse	4.77	4.64	4.09	4.21	4.05	4.09
11h	Palos Verdes fault Magnitude 7.4 Reverse	0.68	0.66	0.63	0.61	0.59	0.62
12	Palos Verdes fault - Santa Monica Bay	1.17	2.86	2.75	1.80	4.62	2.87
13a	Newport-Inglewood fault Magnitude Range 6.5-6.9 Strike-Slip	4.60	5.04	4.30	5.06	4.77	4.25
13b	Newport-Inglewood fault Magnitude Range 6.5-6.9 Reverse	2.83	2.71	1.23	2.14	2.18	1.37
13c	Newport-Inglewood fault Magnitude 7.0 Strike-Slip	3.13	3.58	4.20	3.55	3.37	3.97
13d	Newport-Inglewood fault Magnitude 7.2 Strike-Slip	1.95	2.25	2.96	2.23	2.13	2.73
13e	Newport-Inglewood fault Magnitude 7.0 Reverse	1.80	1.78	1.22	1.47	1.48	1.27
13f	Newport-Inglewood fault Magnitude 7.2 Reverse	1.06	1.06	0.86	0.90	0.90	0.86
14	Newport-Inglewood Offshore fault	0.00	0.08	0.36	0.01	0.25	0.43
15	Whittier-Elsinore fault--Whittier segment	0.02	0.39	1.08	0.11	1.02	1.23
16	Whittier-Elsinore fault--Glen Ivy segment	0.00	0.00	0.41	0.00	0.04	0.22
17	Whittier-Elsinore fault--Temecula segment	0.00	0.00	0.18	0.00	0.00	0.00
18	San Jacinto fault--San Bernardino segment	0.00	0.00	0.00	0.00	0.00	0.00
19	San Jacinto fault--San Jacinto Valley segment	0.00	0.00	0.17	0.00	0.00	0.00
20	San Jacinto fault--Anza segment	0.00	0.00	0.50	0.00	0.00	0.23
21	San Andreas fault--Carrizo segment	0.00	0.00	5.34	0.00	0.00	4.73
22	San Andreas fault--Mojave segment	0.00	0.00	7.73	0.00	0.14	7.66
23	San Andreas fault--San Bernardino segment	0.00	0.00	1.16	0.00	0.00	0.68
24	San Andreas fault--Coachella Valley segment	0.00	0.00	0.74	0.00	0.00	0.39
25	Elysian Park Thrust	0.00	0.02	0.02	0.09	0.92	0.24
26	Santa Suzanna fault	0.00	0.00	0.02	0.00	0.03	0.00
27	San Fernando fault	0.00	0.00	0.01	0.00	0.02	0.00
28	Sierra Madre fault	0.02	0.13	0.16	0.01	0.18	0.26
29	Verdugo fault	0.00	0.06	0.05	0.00	0.17	0.05
30	Cucamonga fault	0.00	0.00	0.09	0.00	0.12	0.06
31	Malibu Coast fault	0.00	0.03	0.02	0.00	0.08	0.02
32	Santa Monica fault	0.00	0.13	0.08	0.01	0.13	0.08
33	Hollywood fault	0.00	0.00	0.00	0.00	0.03	0.00
34	Raymond fault	0.00	0.03	0.02	0.00	0.09	0.02
35	Northridge fault	0.00	0.01	0.05	0.00	0.10	0.03
36	Puente Hills Thrust--Los Angeles-La cienega segment	0.28	0.60	0.19	0.23	0.82	0.43
37	Puente Hills Thrust--Puente Hills-Santa Fe Springs segment	2.99	4.12	1.99	2.26	4.34	3.33
38	Thums-HB Fault	9.32	9.04	7.81	8.04	7.84	8.12

Table 6-6. Comparison of 10% in 50-year Response Spectra, PSA (g). Horizontal Component.

Period	This Study	USGS (1996)	USGS (2002)
T (sec)	*PSA* (g)	*PSA* (g)	*PSA* (g)
0.0	0.441	0.562	0.477
0.1	0.799	0.978	NA
0.2	1.024	1.182	1.100
0.3	1.015	1.098	NA
0.5	0.832	0.929	NA
1.0	0.509	0.552	0.501
2.0	0.285	0.253	NA

NA = Not Available (as of this study)

The scale factors were computed as:

$(F_a)_D / \frac{1}{2}[(F_a)_B + (F_a)_C]$ for short periods, T=0 – 0.3 sec, and

$(F_v)_D / \frac{1}{2}[(F_v)_B + (F_v)_C]$ for long periods, T≥1.0 sec,

where: the numerator is the appropriate F_a or F_v value for site class S_D (equivalent to site Class D designation in the F_a and F_v tables), and the denominator is the average of the F values for site classes S_C and S_B (i.e. the value for the boundary between these classes).

At T = 0.5 sec, the scale factor was computed as the average of the short and long period scale factors. Multiplying these scale factors by the USGS bedrock values yields spectral accelerations that are generally comparable to our PSHA values, as shown in Table 6-6. The scaled 1996 USGS results are about 10 to 20% higher than our results at T < 2 sec, and about 10% lower than ours at T= 2.0 sec. The scaled 2002 USGS results are slightly higher than ours (by less than 10%) at T = 0 and 0.2 sec and virtually identical to ours at T = 1.0 sec.

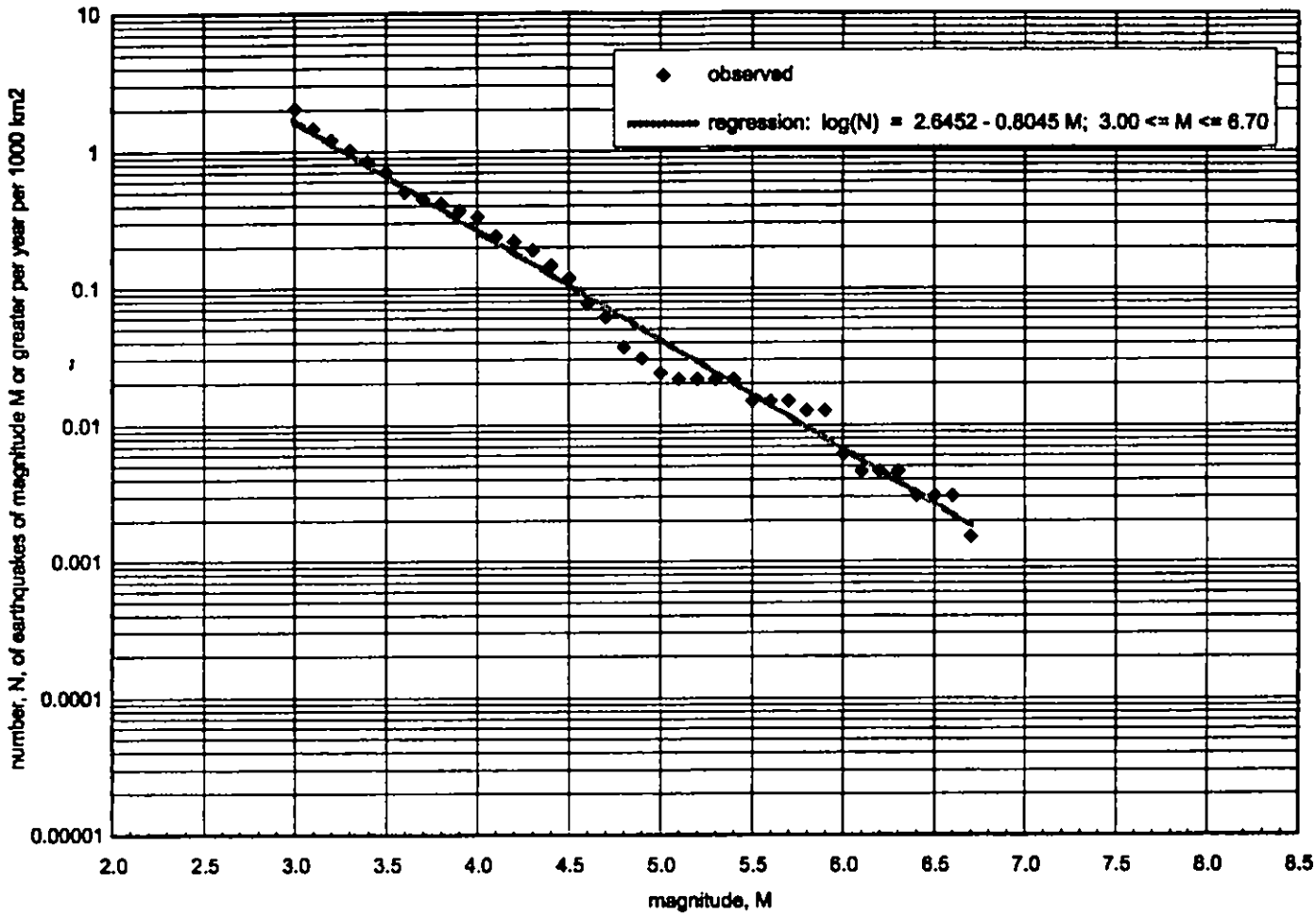

Figure 6-2
Recurrence Curve, Transverse Ranges Province (ETRP and WTRP)

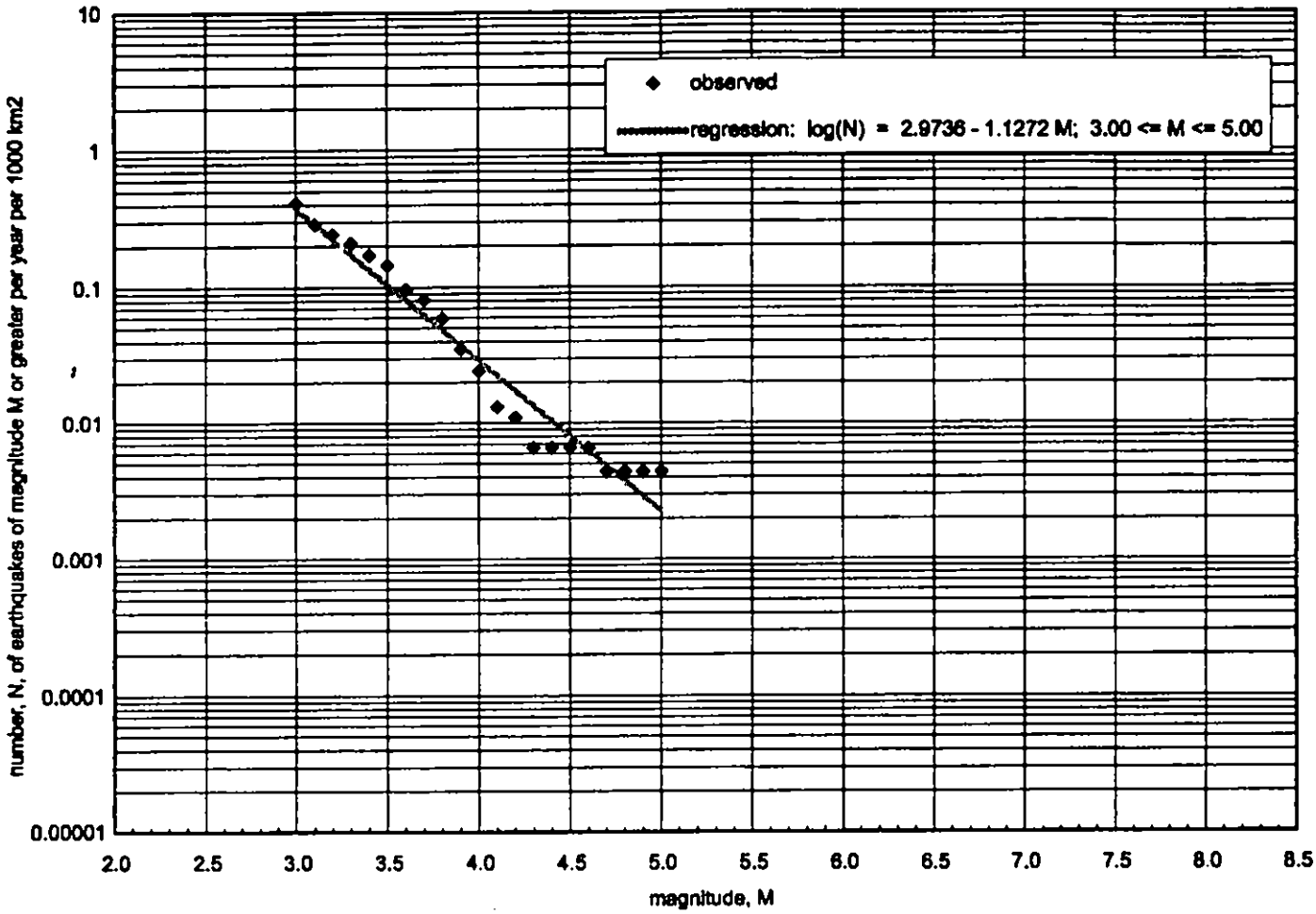

Figure 6-3

Recurrence Curve, Channel Islands-Catalina Province (Catalina)

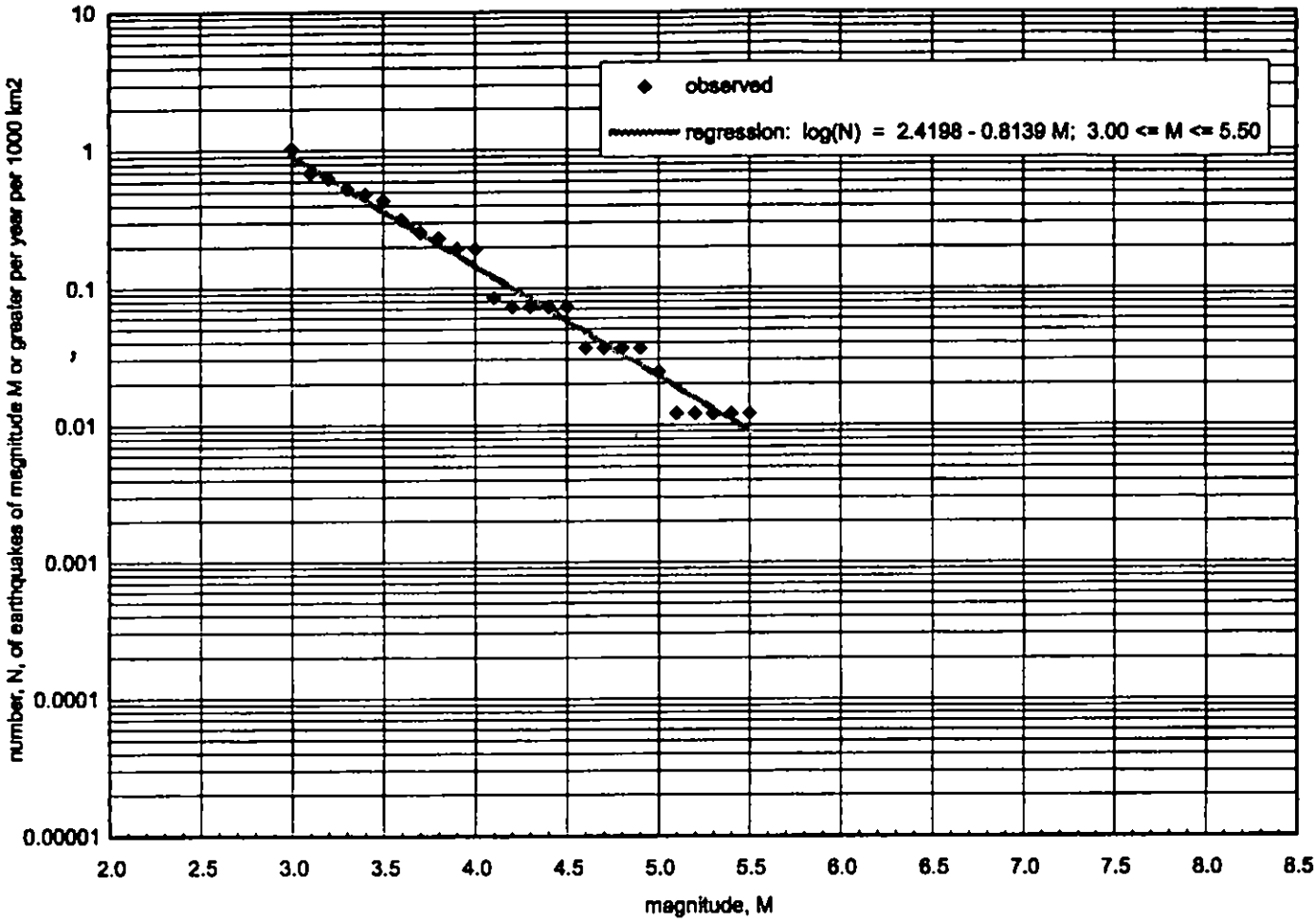

Figure 6-4
Recurrence Curve,
Palos Verdes Fault Zone (PVFZ)

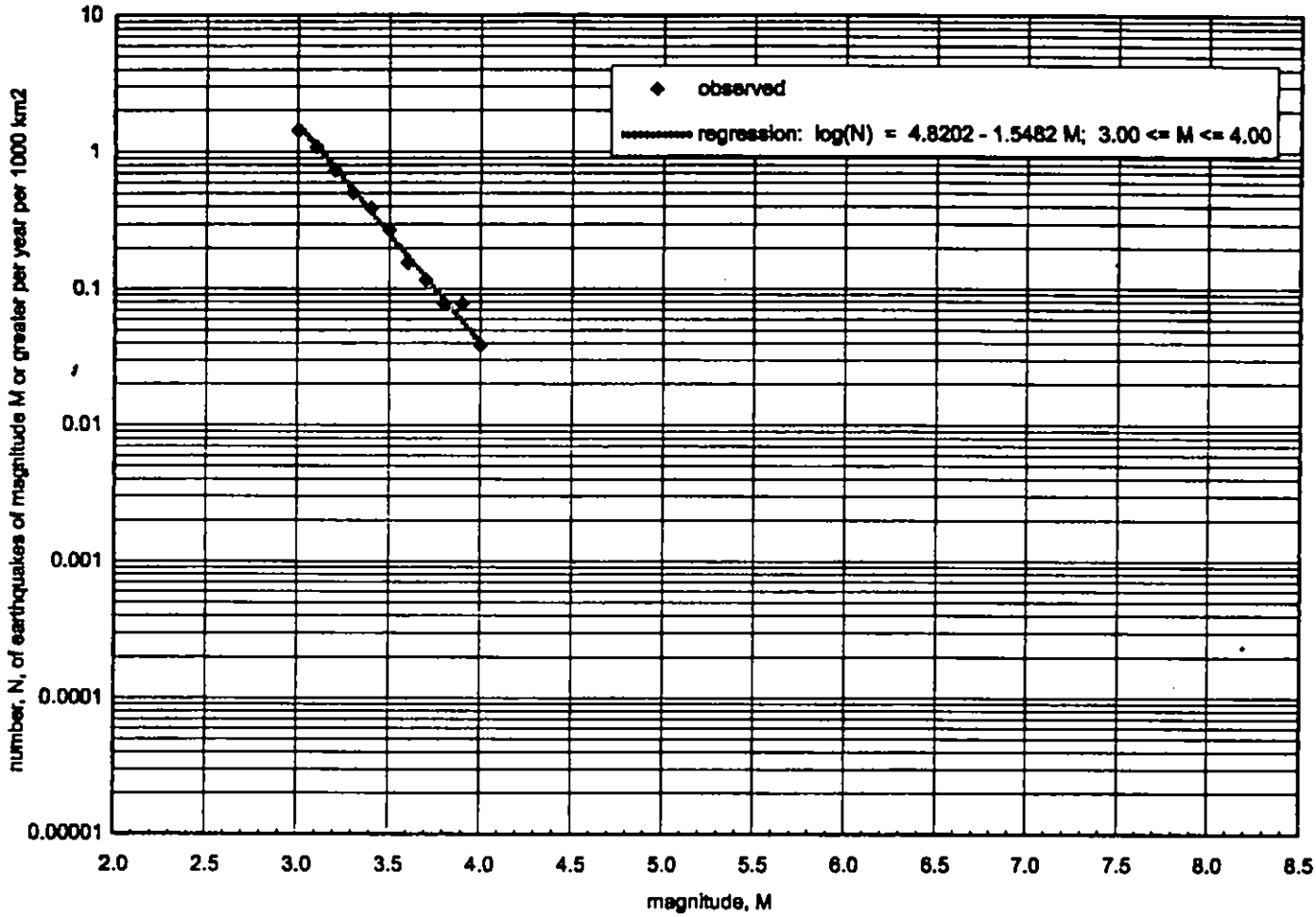

Figure 6-5

Recurrence Curve,
Palos Verdes Fault Zone-Santa Monica Bay Seismic Province
(PVFZ-SMB)

Job No. 33756066

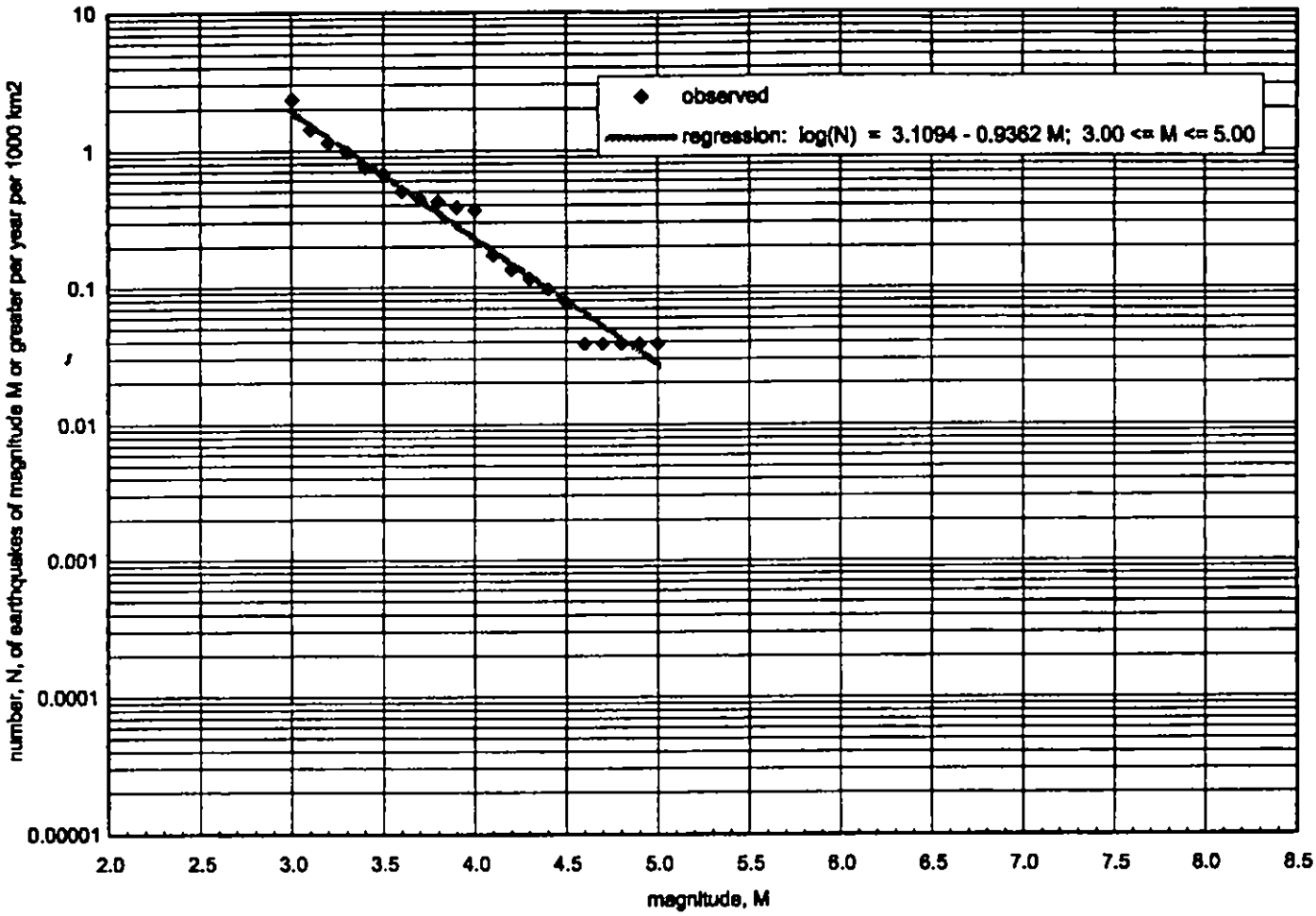

Figure 6-6
Recurrence Curve,
Newport-Inglewood Fault Zone (NIFZ)

Job No. 33756066

URS

Port of Long Beach LNG Terminal
Seismic Hazard Analysis

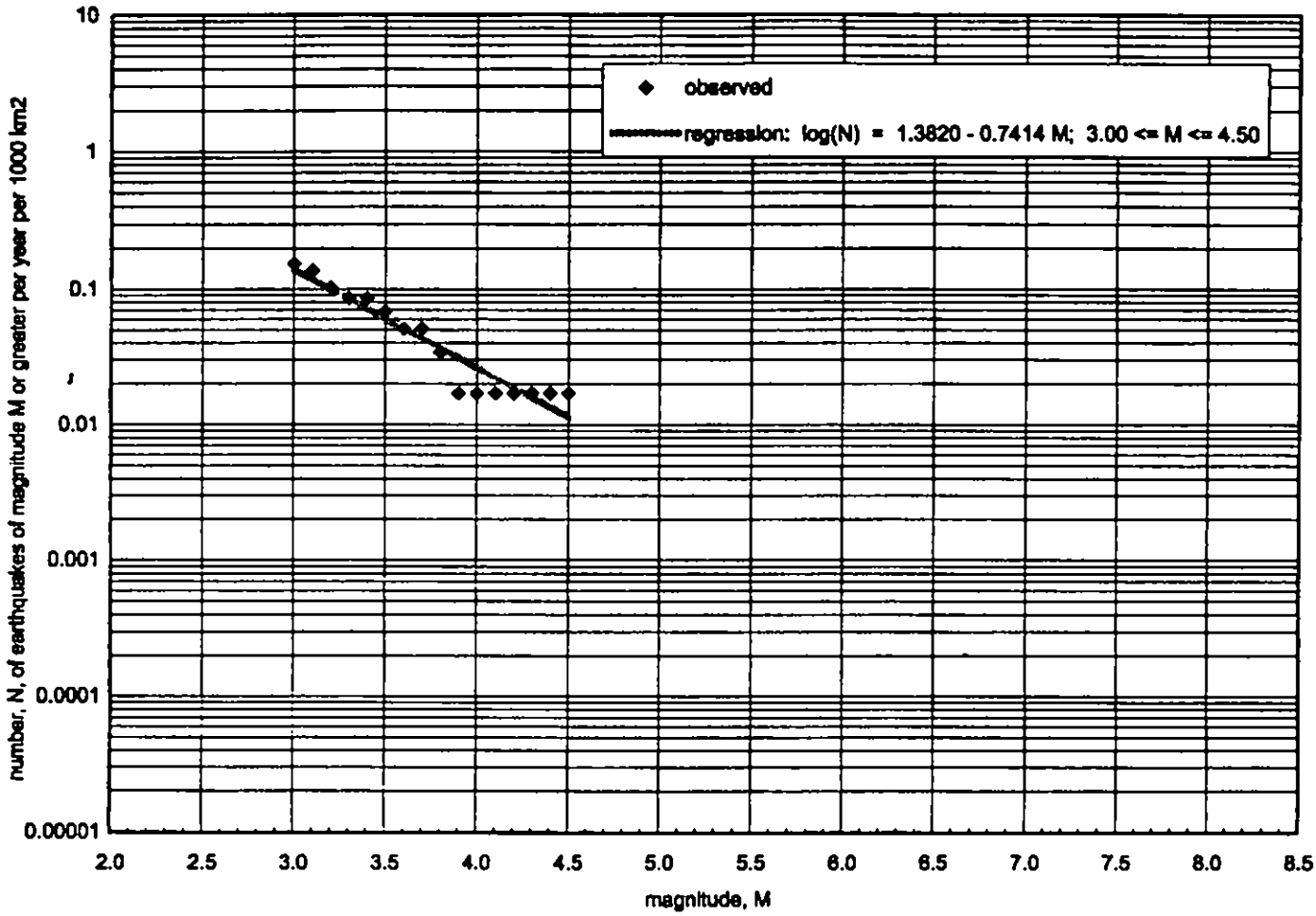

Figure 6-7

Recurrence Curve,
Newport-Inglewood Offshore Fault Zone (NIOFZ)

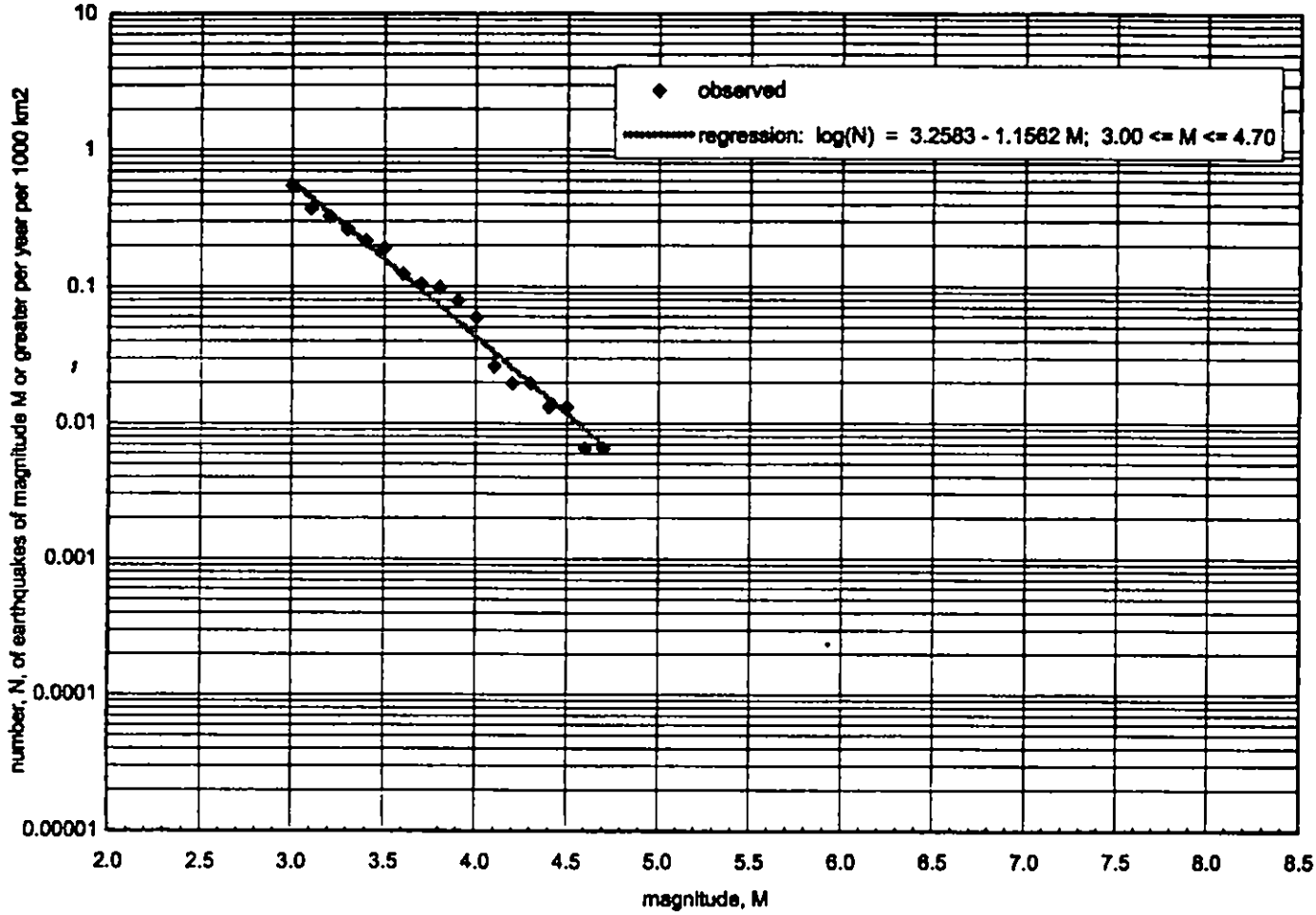

Figure 6-8

Recurrence Curve, Peninsular Ranges Seismic Province NW (PRP-NW)

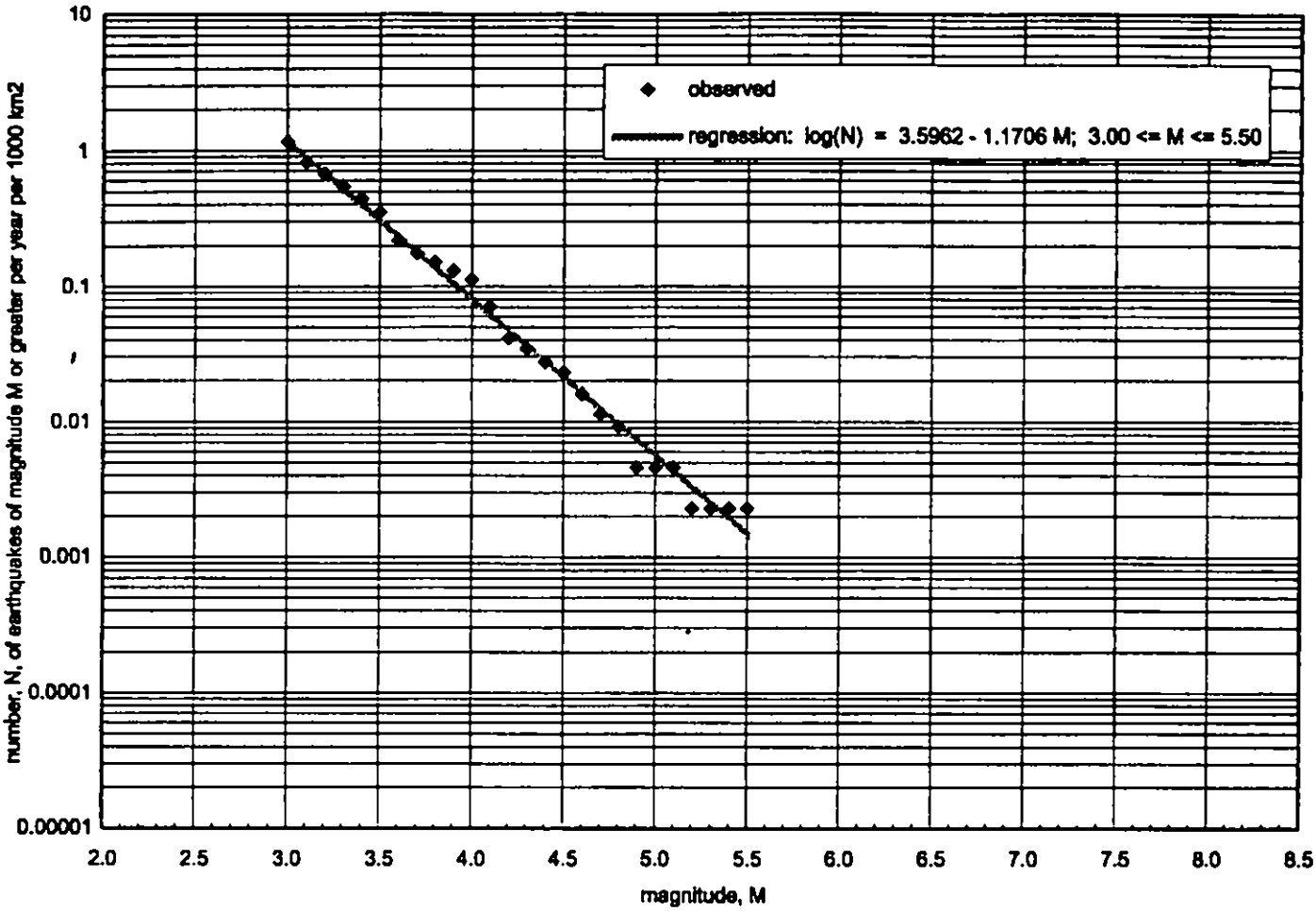

Figure 6-9
Recurrence Curve,
Whittier--Elsinore Fault Zone (WhitEls zone)

Job No. 33756066

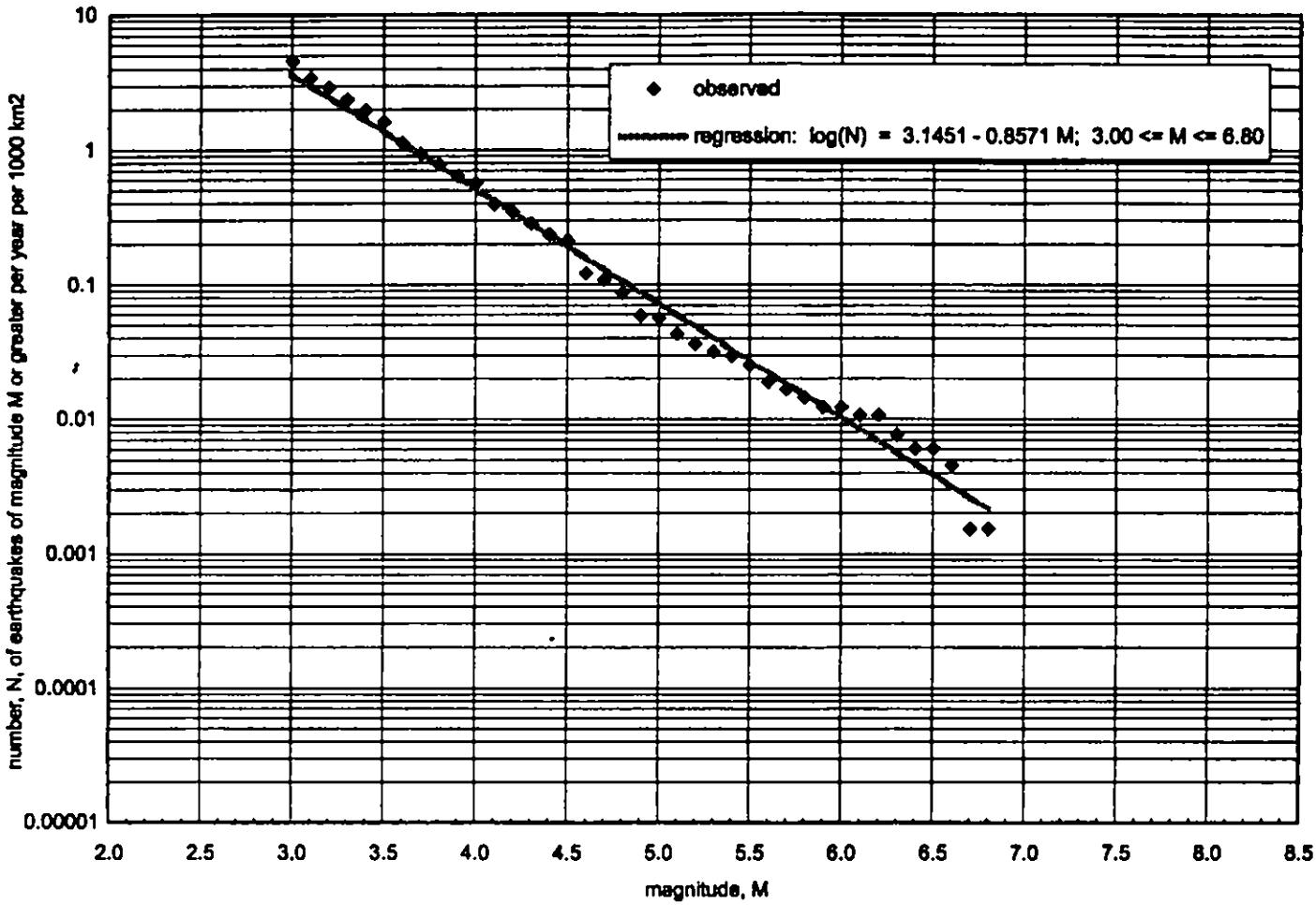

Figure 6-10
Recurrence Curve,
San Jacinto Fault Zone (SJFZ)

33756066_10.cdr

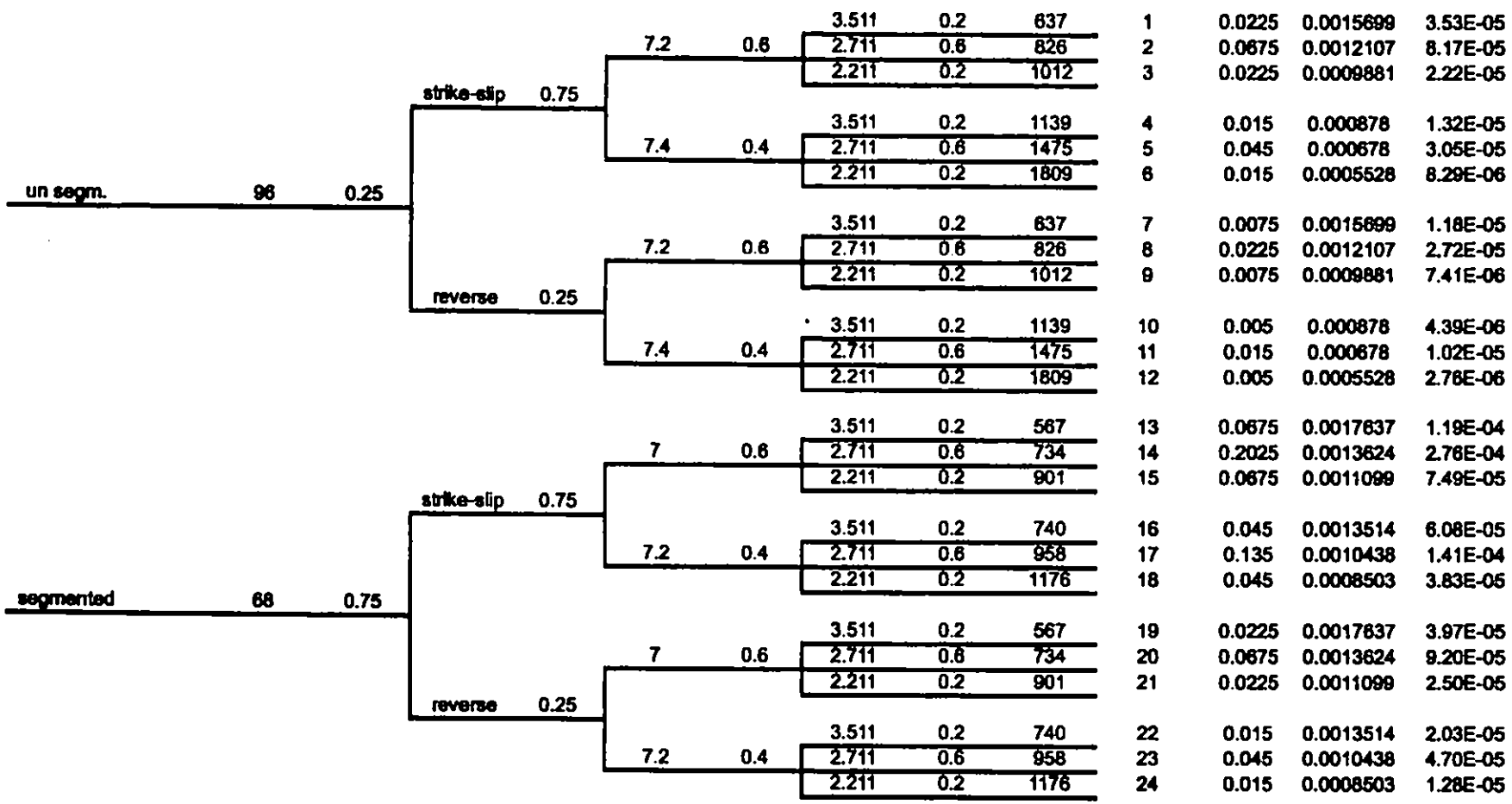

Effective Recurrence Rate		Effect. Rate 1/yr
A. (strike slip, M7.0)	End Branches (13+14+15)	4.70E-04
B. (strike slip, M7.2)	End branches (1+2+3+16+17+18)	3.79E-04
C. (strike slip, M7.4)	End Branches (4+5+6)	5.20E-05
D. (reverse, M7.0)	End Branches (19+20+21)	1.57E-04
E. (reverse, M7.2)	End Branches (7+8+9+22+23+24)	1.26E-04
F. (reverse, M7.4)	End Branches (10+11+12)	1.73E-05

Job No. 33756066

Figure 6-11
Logic Tree
Palos Verdes Fault
(Slip Rate Adjusted for M 6.5-6.9 Increment)

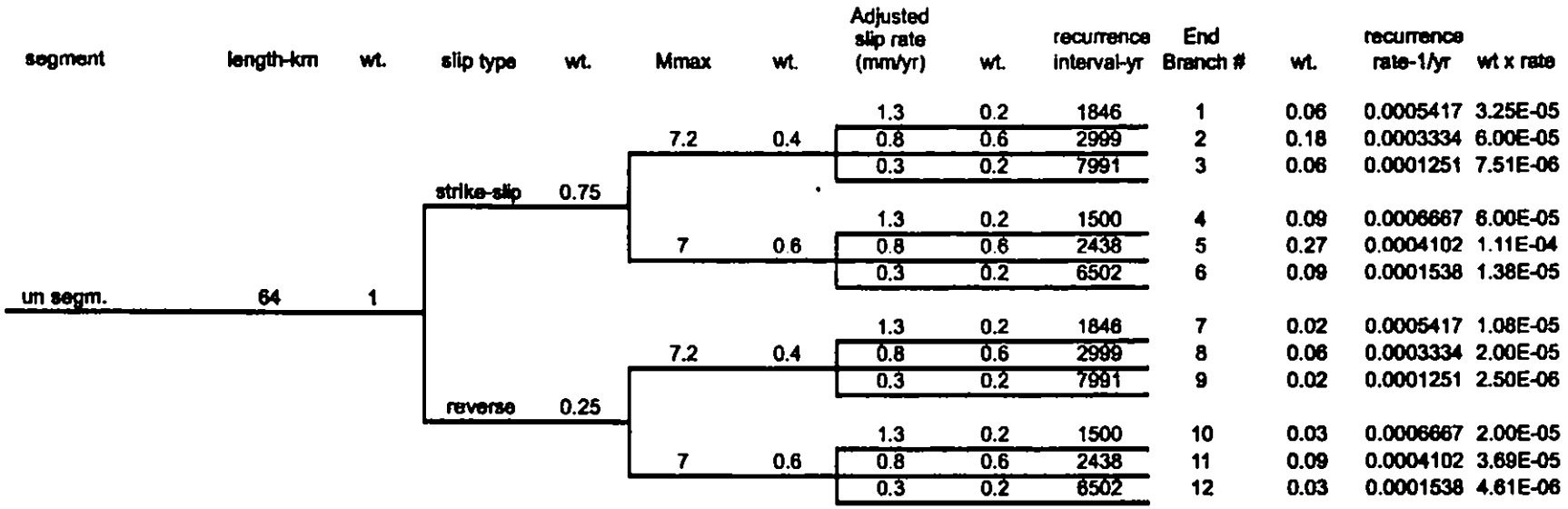

Effective Recurrence Rate		Effect. Rate 1/yr
A. (strike slip, M7.0)	End Branches (4+5+6)	1.85E-04
B. (strike slip, M7.2)	End Branches (1+2+3)	1.00E-04
C. (reverse, M7.0)	End Branches (10+11+12)	6.15E-05
D. (reverse, M7.2)	End Branches (7+8+9)	3.33E-05

Figure 6-12

Logic Tree
Newport-Inglewood Fault (NIF) - Onshore
(Slip Rate Adjusted for M 6.5-6.9 Increment)

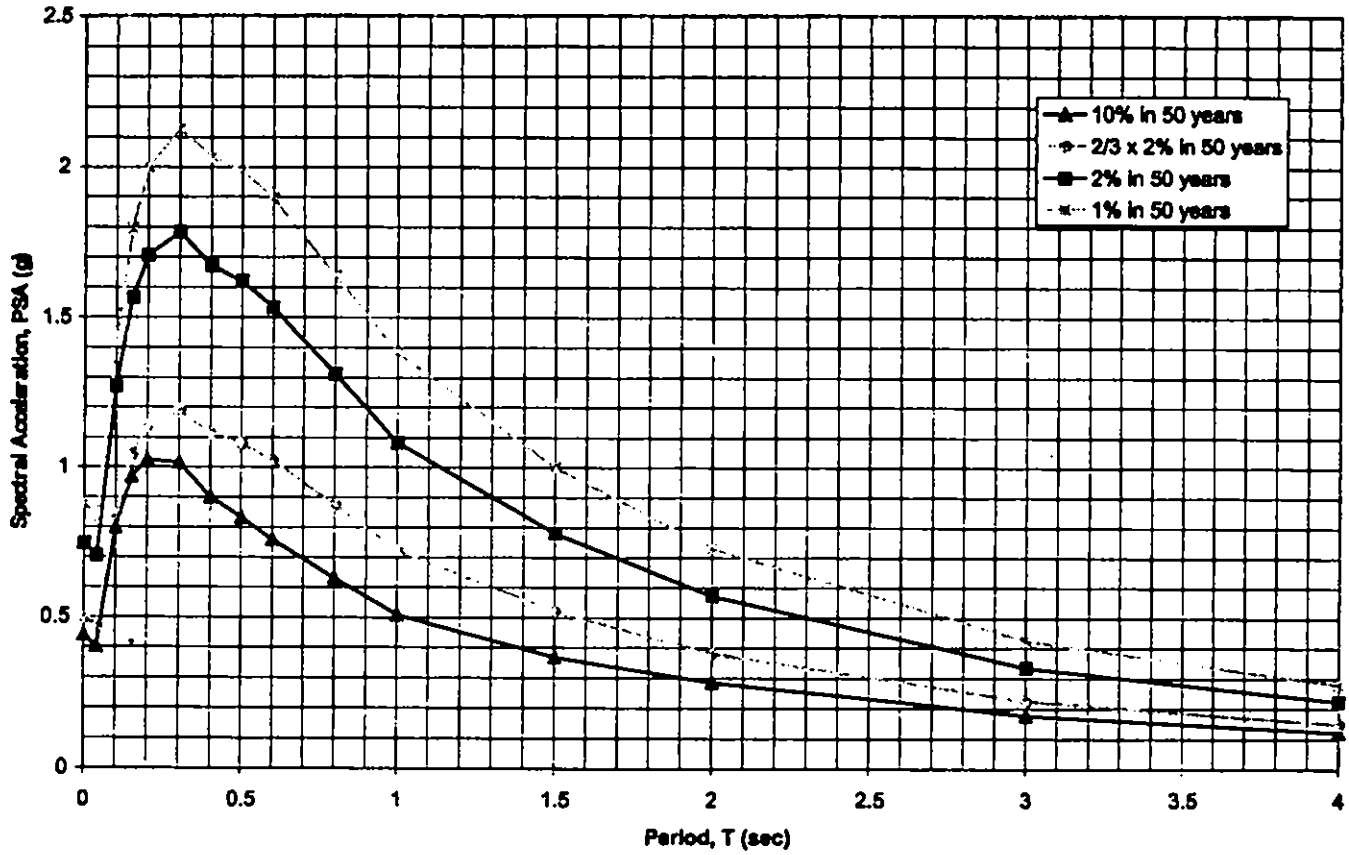

Figure 6-13
Uniform Hazard Spectra, Horizontal Components, 5% Damping

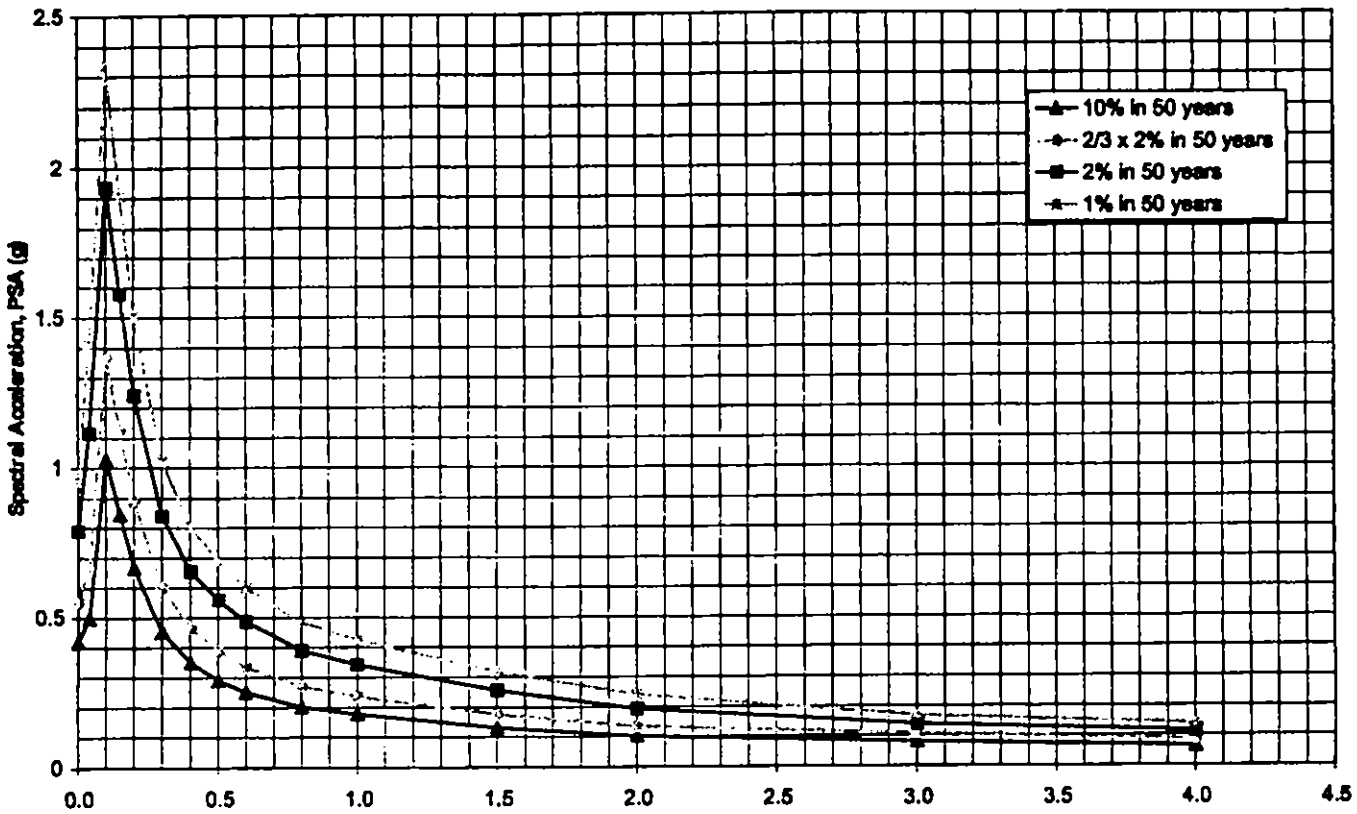

Figure 6-14
Uniform Hazard Spectra, Vertical Component, 5% Damping

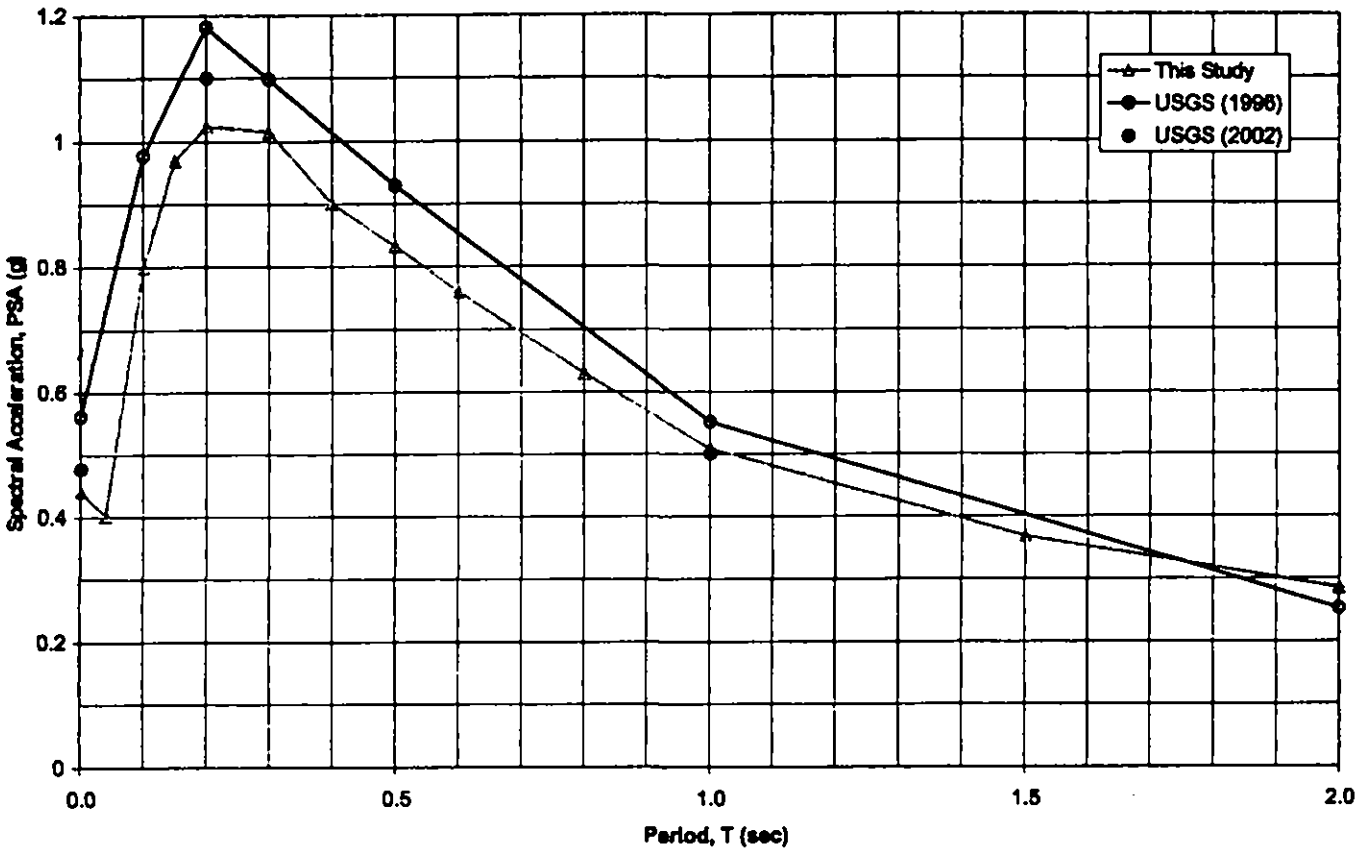

Figure 6-15

Comparison of Uniform Hazard Spectra for a 10% in 50-year Probability of Exceedence Level, Horizontal Components, 5% Damping

7.0 DETERMINISTIC SEISMIC HAZARD ANALYSIS

The 2001 NFPA 59A standard allows the use of a deterministic estimate of the Maximum Considered Earthquake (MCE) response spectrum in the determination of the OBE. Essentially, the 2% in 50 year spectrum from the PSHA is compared to a spectrum resulting from a deterministic seismic hazard analysis (DSHA). To implement the DSHA, maximum earthquakes are postulated on the active seismic sources in the site vicinity. The parameters characterizing each maximum earthquake (magnitude, distance, fault type) are substituted into the same attenuation equations used in the PSHA. The response spectra computed from the equations for each postulated maximum earthquake are averaged using the same weighting in the PSHA. The largest of these average response spectra is the controlling ground motion from the DSHA. This response spectrum is scaled to be 150% of the median spectrum. (Note: The 2001 NFPA 59A shows 50%, but this is a typographical error.)

This scaled spectrum, which is not to be less than a deterministic limit spectrum, is compared with the 2% in 50 year spectrum. The lower of the two spectra in this comparison becomes the controlling MCE spectrum that is used in the determination of the OBE.

7.1 APPLICATION OF DSHA TO SITE

The maximum earthquake producing the largest ground motion at the site is a M_w 7.0 event on the THUMS-HB fault at a distance of 2.2 km from the site. The basis for this magnitude was discussed in Section 5.2. Following the procedure described above, the median and 150% of the median response spectra were computed. A comparison of the 1.5 x median spectrum with the corresponding 2% in 50 year spectrum is shown in Figure 7–1. This figure clearly shows that the 2% in 50 year spectrum is lower, and therefore this spectrum is to be used in the determination of the OBE, as specified in the 2001 NFPA 59A standard. Consequently, the comparison between the 1.5 x median spectrum and the deterministic limit spectrum, also specified in the 2001 NFPA 59A standard, does not apply.

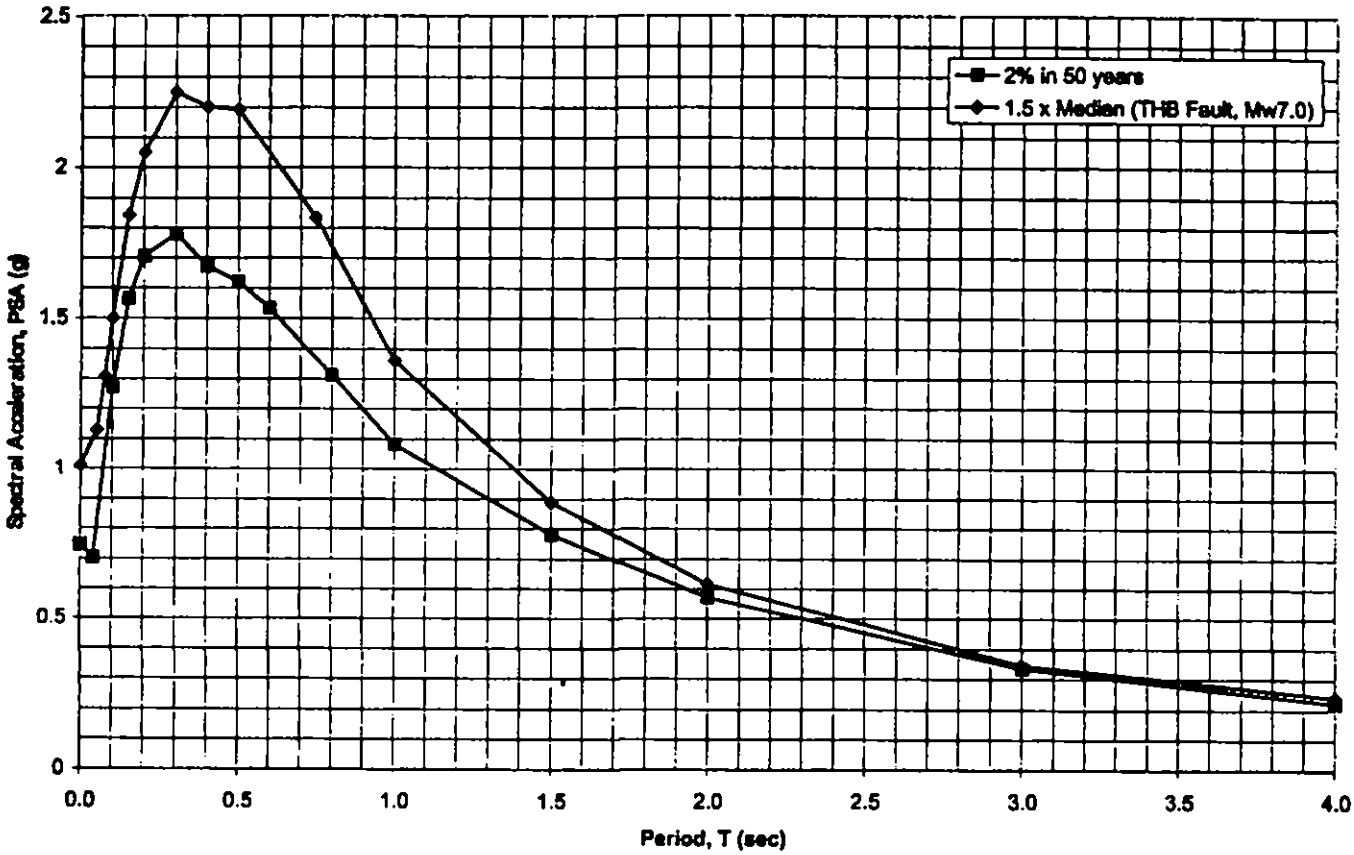

Figure 7-1

Comparison of Probabilistic and Deterministic Spectra, Horizontal Components, 5% Damping

8.0 RECOMMENDED GROUND-MOTION PARAMETERS

The results of the DSHA in the previous section did not govern, so the PSHA results were used as the basis for establishing seismic design parameters for the proposed LNG site. These parameters consisted of effective PGA values and response spectra. For horizontal components, the effective PGA values, which are the zero-period ordinates of the response spectra, were set equal to the spectral ordinates at T = 0.04 sec. This minor adjustment removed the kinks in the spectra at these very short periods (Figure 6-13), and it resulted in an effective PGA that is more consistent with the general level of the response spectra at short periods. For the vertical component, no such adjustments were necessary because kinks in the spectra between 0 and 0.10 sec did not exist.

OBE and SSE response spectra were developed for the seismic design of the LNG tanks. The primary basis for these recommendations was response spectra resulting from the PSHA in Section 6.0 with adjustments for fault directivity effects. Long period ground-motion data from representative strong motion records and URS independent research were used to set the levels of these response spectra at long periods of approximately 9 sec, the fundamental sloshing period estimated for the tank-fluid system.

8.1 RECOMMENDED 5% DAMPED RESPONSE SPECTRA FOR OBE

The seismic design criteria for LNG tanks in the 2001 NFPA 59A standard for the OBE is defined from both the 10% in 50 year and 2% in 50 year ground motions. Essentially, for this application, the 2001 NFPA 59A states that 2/3 of the 2% in 50 year motions need not exceed the 10% in 50 year motions. The PSHA results in Section 6.4 clearly demonstrated that 2/3 of the 2% in 50 year motions exceed the 10% in 50 year motions, and thus the latter were used to define the OBE response spectra.

The 2001 NFPA 59A also states that the vertical-component response spectra shall not be less than 2/3 of the horizontal-component response spectra. Thus, the 10% in 50% vertical-component spectral ordinates in Table 6-4 were adjusted to meet this criterion, and these values, together with the 10% in 50 year horizontal values were further modified for directivity, as discussed below.

The results of the PSHA showed that the Palos Verdes and Newport-Inglewood faults had the majority contribution to the ground-motion hazard at the 10% in 50 year probability level. For these near site sources, fault rupture directivity effects can affect the amplitude of horizontal component ground motions, and according to Somerville et al. (1997), existing attenuation equations do not properly incorporate it. These effects become apparent at periods around 0.6 sec and become more significant at longer periods. Modifications developed by Somerville et al. (1997) were applied to the calculated PSHA ground motions to account for the effects of rupture directivity. These modifications include the directivity effect on the fault-normal (FN) and fault-parallel (FP) components of ground motion.

Table 8-1 lists the 10% in 50 year spectra for the horizontal components that were obtained by applying the two-step directivity modification procedure proposed by Somerville et al. (1997). The Average values in this table are the geometric average of the FN and FP spectra, i.e., Average = $(FN * FP)^{0.5}$. For $T \leq 0.5$ sec, the Average, FN, and FP spectra are equal. Figure 8-1 shows these spectra, and they are the 5% damped, horizontal-component response spectra recommended for the OBE.

Table 8-1. OBE Acceleration Response Spectra (g), 5% Damping Ratio, Horizontal Components.

Period T *(sec)*	PSA_H (T,5%) *(g)*		
	Average	FN	FP
0.00	0.401	0.401	0.401
0.04	0.401	0.401	0.401
0.10	0.799	0.799	0.799
0.15	0.969	0.969	0.969
0.20	1.024	1.024	1.024
0.30	1.015	1.015	1.015
0.40	0.900	0.900	0.900
0.50	0.832	0.832	0.832
0.60	0.759	0.780	0.739
0.80	0.649	0.685	0.615
1.00	0.547	0.593	0.505
1.50	0.423	0.472	0.379
2.00	0.345	0.396	0.301
3.00	0.231	0.281	0.190
4.00	0.169	0.215	0.132
FN = Fault Normal Direction ~ N50E FP = Fault Parallel Direction ~ N40W			

The Somerville two-step procedure was applied as follows. The first step consisted of correcting the 10% in 50 year spectra from the PSHA. As noted in Section 6.0, these spectra were computed by incorporating three attenuation equations in the analysis. These equations compute the geometric average of two orthogonal horizontal components of motion. Rather than adjusting the equations for directivity, average horizontal spectra from the PSHA were multiplied by period-dependent scale factors that were simple functions of (1) the ratio, x, of an assumed fault-rupture length, s, and the total fault length, L, for a given earthquake scenario, and (2) an angle, θ, relating the site location to the position of the epicenter. Based on the locations of the Palos Verdes and Newport-Inglewood faults with respect to the site, values of $x = 1$ and $\theta = 10°$ were selected, which were judged to be a worst case scenario. The resulting scale factors represent the maximum directivity effect without consideration of other rupture scenarios. A recent URS (2003b) PSHA study for a site adjacent to the Hayward fault in northern California showed the effect of incorporating directivity in all possible rupture scenarios in the PSHA. For example, the resulting 5% damped spectral acceleration at $T = 2$ sec (average of two horizontal components) was only about 10% greater than the corresponding acceleration computed with no directivity included. For the POLB site, the corresponding increase was selected as approximately 20%. This scaling was achieved by taking 30% of the maximum directivity effect at each oscillator period. The resulting set of scale factors were judged to better represent an average directivity effect that approximately accounted for all possible rupture scenarios. These scale factors were applied to the 10% in 50 year response spectra to produce directivity-corrected Average spectra.

The second step involved the calculation of spectra for the FP and FN components using period-dependent scale factors that were simple functions of M_w and closest distance from the site to the fault rupture, R_{rup}. For this application $M_w = 7$ and $R_{rup} = 5$ km were selected. The resulting scale factors, one set for each of the FP and FN components, were applied to the directivity-corrected Average spectra to produce the FP and FN response spectra in Table 8-1 and Figure 8-1.

The 2/3 minimum criterion for the vertical component in the 2001 NFPA 59A refers to the ratio between the vertical component and average horizontal component. Thus, the OBE vertical

component was established as the greater of: (1) 2/3 of the Average horizontal component in Table 8-1, or (2) the PSHA results for the vertical component in Table 6-4. The resulting OBE vertical component spectrum for 5% damping ratio is listed in Table 8-2 and plotted in Figure 8-2.

Table 8-2. OBE Acceleration Response Spectra (g), 5% Damping Ratio, Vertical Component.

Period T *(sec)*	PSA_V (T,5%) *(g)*
	Average
0.00	0.417
0.04	0.496
0.10	1.028
0.15	0.846
0.20	0.790
0.30	0.677
0.40	0.600
0.50	0.555
0.60	0.506
0.80	0.433
1.00	0.365
1.50	0.282
2.00	0.230
3.00	0.154
4.00	0.112

8.2 RECOMMENDED 5% DAMPED RESPONSE SPECTRA FOR SSE

The seismic design criteria for the SSE is defined from both the 1% in 50 year and 2 x OBE ground motions. The 2001 NFPA 59A states that 2 x OBE motions need not exceed the 1% in 50 year motions. The PSHA results in Section 5.4 clearly demonstrate that the 1% in 50 year response spectra (corrected for directivity) exceed the 2 x OBE response spectra at most oscillator periods, and thus the latter were used to define the SSE response spectra at these periods. At periods of 0.10, 0.15 and 0.20 sec, the 1% in 50 year spectra governed. The spectral ordinates for the SSE response spectra are presented in Tables 8-3 and 8-4 for the horizontal and vertical components, respectively, and are plotted in Figures 8-3 and 8-4.

Table 8-3. SSE Acceleration Response Spectra (g), 5% Damping Ratio, Horizontal Components.

Period T *(sec)*	PSA_H (T, 5%) *(g)*		
	Average	FN	FP
0.00	0.802	0.802	0.802
0.04	0.802	0.802	0.802
0.10	1.427	1.427	1.427
0.15	1.796	1.796	1.796
0.20	1.999	1.999	1.999
0.30	2.030	2.030	2.030
0.40	1.800	1.800	1.800
0.50	1.664	1.664	1.664
0.60	1.518	1.559	1.479
0.80	1.299	1.370	1.231
1.00	1.094	1.185	1.010
1.50	0.846	0.944	0.759
2.00	0.690	0.792	0.601
3.00	0.462	0.561	0.380
4.00	0.337	0.429	0.265

Table 8-4. SSE Acceleration Response Spectra (g), 5% Damping Ratio, Vertical Component.

Period T *(sec)*	PSA_V (T, 5%) *(g)*
	Average
0.00	0.833
0.04	0.992
0.10	2.056
0.15	1.693
0.20	1.506
0.30	1.353
0.40	1.200
0.50	1.110
0.60	1.012
0.80	0.866
1.00	0.730
1.50	0.564
2.00	0.460
3.00	0.308
4.00	0.225

8.3 RESPONSE SPECTRA AT OTHER DAMPING RATIOS, PSA (T, d%)

For both the OBE and SSE, the following equations, derived from Table 2 of Newmark and Hall (1982), are recommended for tanks designed with and without base isolation. The equations are applicable for horizontal components, damping ratios, $0.5 \leq d\,\% \leq 20$, and periods, $0 < T \leq 4$ sec.

No Base Isolation:

$$PSA_H(T, d\%) = [PSA_H(T, 5\%)] \times [\{3.21 - 0.68 \ln(d\%)\}/2.116] \quad (8\text{-}1)$$

Base Isolation :

$$PSA_H(T, d\%) = [PSA_H(T, 5\%)] \times [\{2.31 - 0.41 \ln(d\%)\}/1.650] \quad (8\text{-}2)$$

PSA_H (T, 5%) is the 5% damped horizontal-component OBE or SSE response spectra. The scale-factor expression in the second pair of [ ] in Equation (8-1) is the median amplification factor for the acceleration-controlled portion of the response spectrum, whereas the corresponding factor in Equation (8-2) is for the velocity-controlled portion. These factors are recommended based on assumed ranges of natural periods for the fundamental impulsive mode. Equations (8-1) and (8-2) are not to be used for the convective mode.

An equation similar to Equation (8-1) is recommended to convert the 5% damped vertical-component OBE and SSE response spectra, PSA_V (T, 5%), to vertical-component spectra at other damping ratios, PSA_V (T, d%). This conversion equation is simply obtained by substituting PSA_V (T, 5%) for PSA_H (T, 5%) in Equation (8-1). The use of this equation assumes that the vertical vibrational periods are less than approximately 0.5 sec. For any vertical vibrational periods greater than 0.5 sec, an equation analogous to Equation (8-2) is recommended.

The zero period (T = 0 sec) PSA values of the OBE and SSE response spectra are the same for all damping ratios. These values represent the effective PGA.

8.4 0.5% DAMPED HORIZONTAL RESPONSE SPECTRA (CONVECTIVE MODE)

The natural period and damping ratio for the fundamental convective (sloshing) mode are approximately 9 sec and 0.5%, respectively (T. Howe, KBR, personal comm., 2003). Response spectral values at this period and damping ratio were estimated from (1) the corresponding response spectra of representative accelerograms, and (2) simulated ground motions for an M_w 7.1 event on the Palos Verdes fault and an M_w 7.8 event on the San Andreas fault.

Few representative accelerograms have been recorded that contain reliable long period motions, which are not contaminated by noise. Representative accelerograms recorded during the 1999 (M_w 7.6) Chi-Chi, Taiwan and 1999 (M_w 7.4) Kocaeli, Turkey, earthquakes were identified as having good signal-to-noise ratios at periods around 9 sec. The digital records of ground motions at Stations TCU 065, 067, 075, 076, and 129 during the Chi-Chi earthquake were representative of site motions from a maximum earthquake (M_w 7) on the THUMS-HB fault. These stations were located adjacent to the portion of the fault where the slip was moderate, corresponding to an M_w 7¼ event. The digital accelerograms recorded at Yarimca and Gebze during the Turkey earthquake are representative of site motions from M_w 7+ events on the Palos Verdes and Newport-Inglewood faults. Both of these records contain forward rupture directivity.

As part of an independent research project (P. Somerville, URS, personal comm., 2003), URS generated ground motions for M_w 7.1 events on the Palos Verdes fault at a distance of 4.25 km. These simulated motions were computed from seismological models of the fault rupture and a geologic medium consisting of horizontally stratified layers. The surface layer of this model had a shear-wave velocity of 1 km/sec. The long period motions computed with this model were increased by 25% to approximately account for the lower site velocity and for basin effects.

Simulation had also been previously generated by URS for an M_w 7.5 event on the San Andreas fault at a distance of 70 km. These simulations incorporated 3D basin effects. The long period motions were increased by 60% to approximate the motions for an M_w 7.8 maximum earthquake on the San Andreas fault.

The results of these investigations indicated that relative response spectral displacements, S_d, at 9-sec period and 0.5% damping ratio, of 75 cm (FN component) and 50 cm (FP component)

were suitable average values for the M_w 7.1 Palos Verdes and M_w 7.8 San Andreas fault scenarios, which were considered representative OBE events (P. Somerville, URS, written comm., 2003). Spectral displacements that are twice these values (i.e., 150 cm - FN, 100 cm - FP) are compatible with the M_w 7 THUMS-HB fault scenario, which is considered representative of an SSE event.

Based on the foregoing discussion, the following equations are recommended for the OBE response spectral displacement in cm.

Average: $$S_d(T, 0.5\%) = 4960 / T^2 \quad (8\text{-}3)$$

FN: $$S_d(T, 0.5\%) = 6075 / T^2 \quad (8\text{-}4)$$

FP: $$S_d(T, 0.5\%) = 4050 / T^2 \quad (8\text{-}5)$$

These equations are applicable for $T \geq 8$ sec. The constant, 4960, in Equation (8-3) is the geometric average of 6075 and 4050 in Equations (8-4) and (8-5), respectively.

Consistent with the investigation results, the values of S_d at $T = 9$ sec are 75 cm and 50 cm for the FN and FP components, respectively.

The corresponding SSE values of S_d are twice the OBE values.

Corresponding acceleration spectra, PSA_H (T, 0.5%), are obtained by multiplying the S_d values by $(2\pi / T)^2$. The acceleration units are cm/sec/sec. These accelerations are converted to units of g by dividing by 980.

8.5 DISCUSSION

The OBE and SSE response spectra recommended in this report represent free field earthquake motions at the ground surface of a site stiffened with stone columns. Alternatively, these response spectra represent a free field outcrop motion at the top of the stiff natural deposits at a depth of approximately 80 feet. This condition applies to an unimproved site with piles as the foundation support.

The Average horizontal spectra represent each of the two orthogonal horizontal components. The FN and FP components are also orthogonal, but the spectra for these two directions are

different. URS recommends the use of either the Average spectra for the two horizontal components or the FN & FP spectra, whichever set produces the largest response.

Linear interpolation is recommended to obtain the spectral ordinates at periods between those in Tables 8-1 and 8-2. Interpolation on linear acceleration versus linear period (i.e., PSA = a + bT, where a and b are constants) is recommended. Interpolation based on the logarithms of acceleration and period could be used at the longer periods (i.e., T > 1 sec) where the point spacing is larger. Although this scheme would better model the spectral decay between these points, the differences between the ordinates computed from either interpolation scheme is considered negligible.

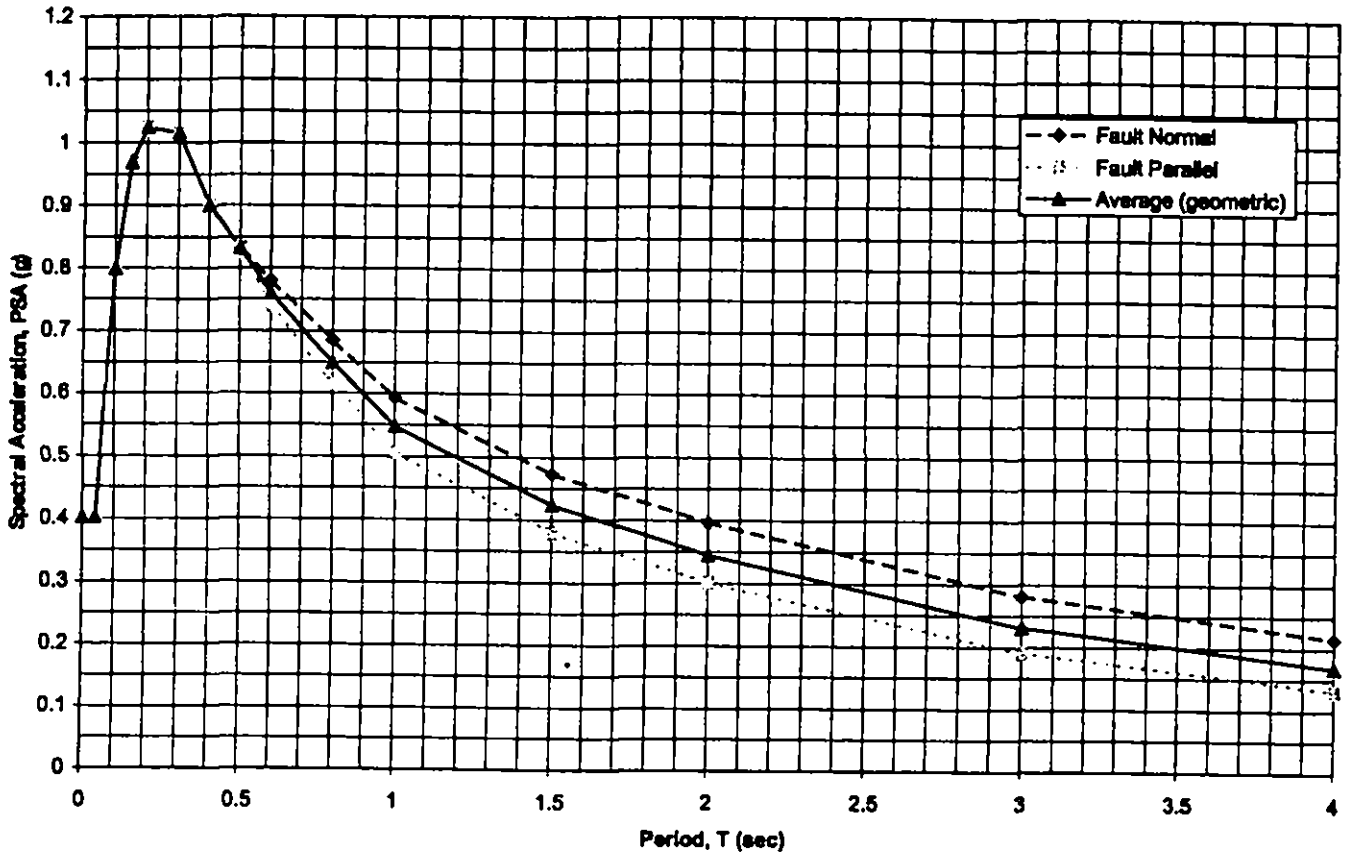

Figure 8-1
OBE (475-yr) Response Spectra, Horizontal Components. 5% Damping. Estimated Directivity Included

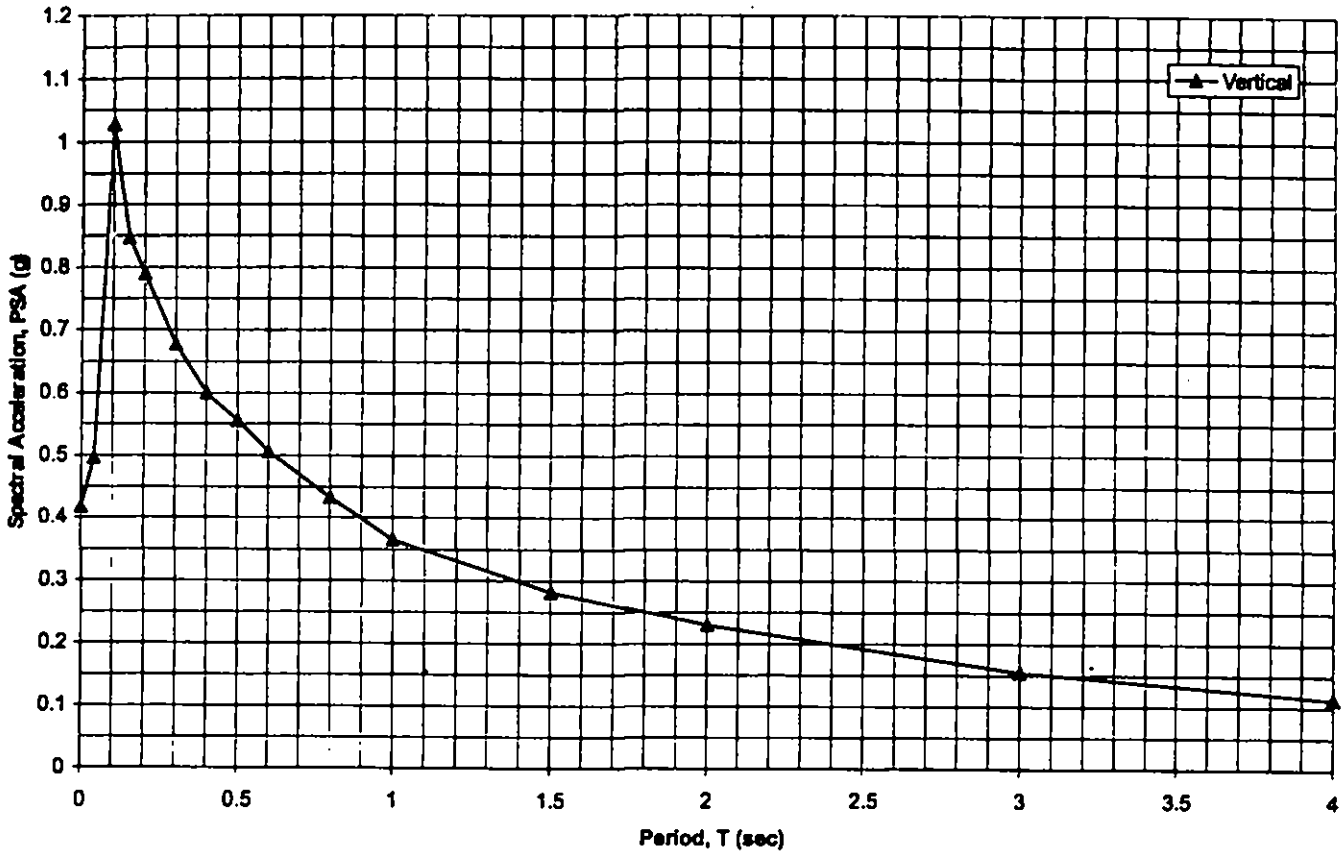

Figure 8-2
OBE (475-yr) Response Spectra, Vertical Component, 5% Damping.

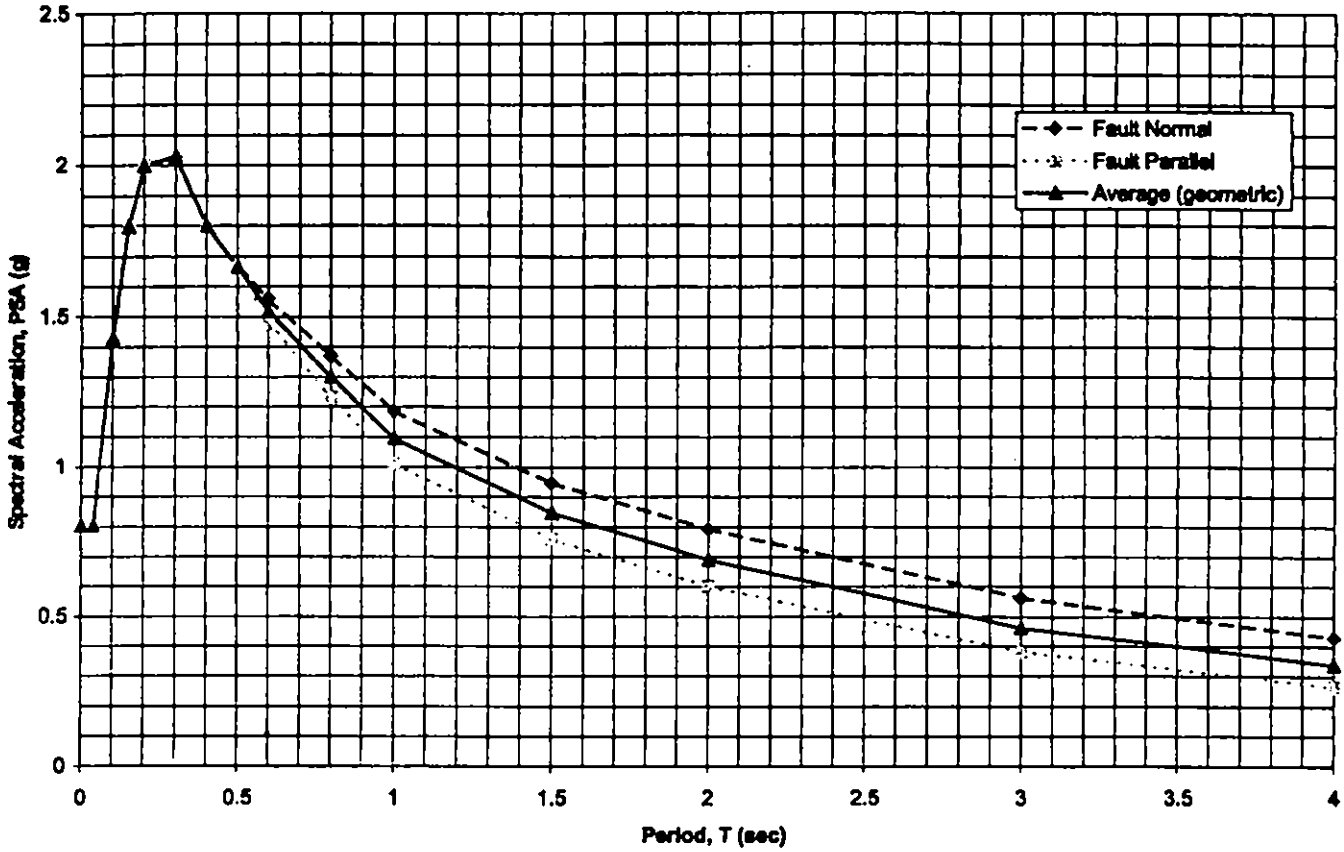

Figure 8-3
SSE Response Spectra, Horizontal Components
5% Damping, Estimated Directivity Included

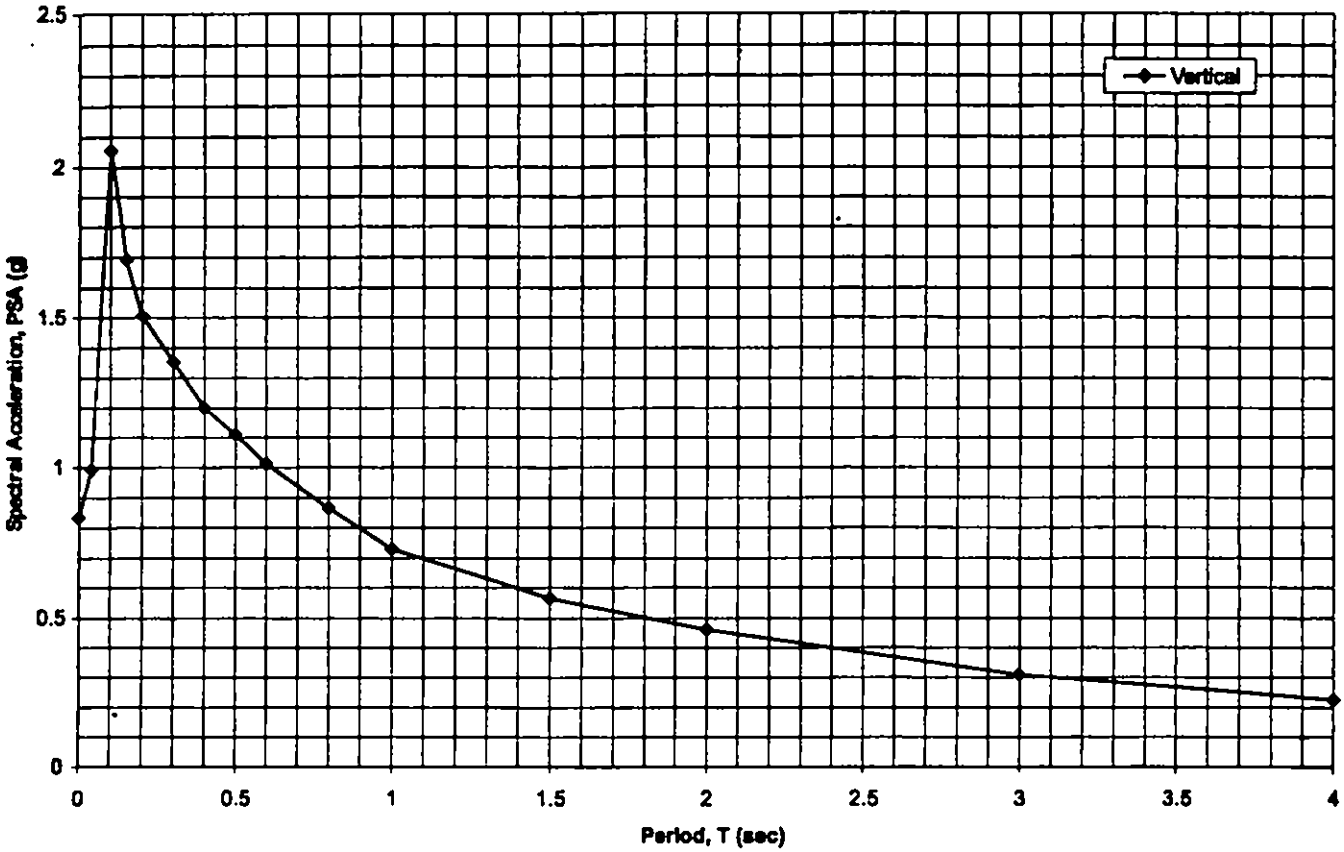

Figure 8-4
SSE Response Spectra, Vertical Component, 5% Damping

9.0 TSUNAMI AND FAULT RUPTURE HAZARDS

9.1 TSUNAMI

Tsunami hazards along the Southern California coast may occur as a result of far-field (distant) earthquakes, local offshore earthquakes and submarine landslides in the continental borderland. There have been several historical tsunamis recorded in Long Beach or Los Angeles Harbors, the largest of which was recorded as a 5 foot range in the tide gauge reading associated with the 1960 Chile earthquake of M_w 9.5, the largest known historical earthquake. Various estimates of runup heights and/or inundation, primarily from far field sources, have been developed. The most recent estimates for the POLB area are a 100-year (R_{100}) runup height of +8 feet and a 500-year (R_{500}) runup of +15 feet (Synolakis, 2003). While these estimates were not developed based on specific tsunami source scenarios with estimated probabilities of occurrence, these heights are considered to be representative values useful for emergency planning. The R_{100} value is considered to be most representative of far field (i.e. Alaska, Japan, South America subduction zone earthquakes) generated tsunamis, and the R_{500} value is more representative of locally (continental borderland earthquakes and/or submarine landslides) generated tsunamis (Synolakis, 2003; J. Borrero, personal communication, 2003). The site elevation is approximately 25 feet above mean low low water, which is above the estimated runup values. Thus, the tsunami hazard at the site is judged to be low.

9.2 SURFACE FAULT RUPTURE

No active surface faults are known to occur within the site boundaries (Dibblee, 1999; Ziony and Jones, 1989; Jennings, 1994) and the site is not located within an Alquist-Priolo Earthquake Fault Zone (California Division of Mines and Geology - CDMG, 2000). Consequently, URS concludes that there is not a potential surface fault rupture hazard at the proposed LNG site.

California has established Alquist-Priolo Earthquake Fault Zones around faults considered to have been geologically active within the Holocene (last 11,000 ybp) and to have a relatively high potential for surface rupture in the event of a large earthquake. In addition, the surface trace(s) of these faults must be sufficiently well-defined (Hart and Bryant, 1997). The closest designated

Alquist-Priolo Earthquake Fault Zone to the site is the Newport-Inglewood fault zone, approximately 6.5 km northeast of the site (Figure 9-1).

Although not formally zoned by the California Geological Survey (formerly Division of Mines and Geology), the Palos Verdes fault has been shown to have been active during the Holocene (Darrow and Fischer, 1983; Fischer et al., 1987; Stephenson et al., 1995; McNeilan et al., 1996). The main trace of this fault is approximately 4.0 km southwest of the site (Figure 3-7), and other active secondary traces are located southwest of the main trace. Consequently, this fault is not considered to pose a potential surface rupture hazard at the site.

The subsurface trace of the THUMS-HB fault has probably been active during the Holocene, dips northeast beneath the site, and the surface projection of the subsurface fault tip is located approximately 1.6 km southwest of the site (Figures 3-7 and 5-2). The available data do not indicate the presence of the THUMS-HB fault or any secondary faults in the Holocene and older, late Pleistocene strata beneath the site. The pertinent data are described below.

The USGS has several high-resolution stratigraphic and geophysical data sets from the Los Angeles-Long Beach harbor area. These data and other data sets clearly show that the THUMS-HB fault is deeply buried (i.e. blind) and does not displace Quaternary strata (Edwards et al., 2001, 2002, 2003; Williams, 2003). The USGS data are reported to clearly document that there are continuous late Quaternary strata beneath the site and Los Angeles Harbor. These data are further supported by the site-specific data obtained by URS during the site geotechnical study (URS, 2003) in conjunction with published and unpublished stratigraphic data (Poland and Piper, 1956; California Department of Water Resources, 1961; D. Ponti and B. Edwards, written communication, 2003). The continuity of strata is shown on the geologic cross-section presented on Figure 3-8. Based on the available data, the THUMS-HB fault is not considered to pose a potential surface rupture hazard at the site.

NON-INTERNET PUBLIC

APPENDIX 6-2: FIGURE 9-1

California Earthquake Fault Study Zone Map

10.0 REFERENCES

Abrahamson, N. and Silva, W., 1997, Empirical response spectral attenuation relations for shallow crustal earthquakes: Seis. Soc. of Am., Seis. Res. Let., v. 68, no. 1, p. 94-127.

Anderson, J., Wesnousky, S.G., and Stirling, M.W., 1996, Earthquake size as a function of fault slip rate: Bull. Seis. Soc. Amer., v. 86, no. 3, p. 683-690.

Anderson, J.G., 1979, Estimating the seismicity from geological structure for seismic risk studies: Bull. Seis. Soc. Am., v. 69, no. 1, p. 135-158.

Bawden, G.W., Thatcher, W., Stein, R.S., Hudnut, K.W. and Peltzer, G., 2001, Tectonic contraction across Los Angeles after removal of groundwater pumping effects: Nature, v. 412, p. 812-815.

Bergmann, M., and Rockwell, T.K., 1993, Preliminary assessment of the late Holocene slip rate for the Wildomar fault in Murrieta, California: Ass. of Eng. Geo. 36th Annual Program and Abstracts, Salt Lake City, Utah, p. 43.

Biasi, G.P., Weldon II, R, Fumal, T., and Seitz, G.S., 2002, Paleoseismic Event Dating and Conditional Probability of Large Earthquakes on the Southern San Andreas Fault, California: Bull. Seis. Soc. Am., v. 92, no. 7, p. 2551-2554.

Bonilla, M.G., 1973, Trench exposures across surface fault ruptures associated with the San Fernando earthquake, in *San Fernando California, earthquake of February 9, 1971, v. 3, Geological and Geophysical studies*: edited by Murphy, L.M., National Oceanic and Atmospheric Administration, p. 173-182.

Bullard, T.F. and Lettis, W.R., 1993, Quaternary fold deformation associated with blind thrust faulting, Los Angeles Basin, California: J. Geophys. Res. v. 98, no. B5, p. 8349-8369.

California Division of Mines and Geology, 1995a, State of California Earthquake Fault Zones, Malibu Beach Quadrangle, scale 1:24000.

California Division of Mines and Geology, 1995b, State of California Earthquake Fault Zones, Point Dume Quadrangle, scale 1:24000.

Campbell, K.W. and Bozorgnia, Y., 2003, Updated near-source ground-motion (attenuation) relations for the horizontal and vertical components of peak ground acceleration and acceleration response spectra: Bull. Seis. Soc. Am., v. 93, no. 1, p. 314-331.

CDMG and USGS, 1996, Probabilistic Seismic Hazard Assessment for the State of California: Calif. Div. Mines Geol. Open-File Report 96-08, U.S. Geol. Surv. Open-File Report 96-706.

CDMG, 2000, Digital Images of Official Maps of Alquist-Priolo Earthquake Fault Zones of California, Southern Region, DMGCD 2000-003.

California Dept of Water Resources, 1961, Planned Utilization of the Ground Water Basins of the Coastal Plain of Los Angeles County. Appendix A, Ground Water Geology, Bulletin No. 104, June.

Catchings, R.D., Gandhok, G., Goldman M.R., and Okaya, D., 2002, Seismic Images and Fault Relations of the Santa Monica Thrust Fault, West Los Angeles, California, U.S. Geological Survey Open-file Report 01-111, July.

Chapman, R.H., and Chase, G.W., 1979, Geophysical investigations of the Santa-Monica-Raymond fault zone, Los Angeles County, California: Calif. Div. Mines Geo., Open-File Report 79-16, p. E-1-E-30.

Clarke, S.H., Greene, H.G., Kennedy, M.P., and Vedder, J.G. (with contributions by Legg, M.R.), 1987, Geologic map of the inner-southern continental margin, California Continental Margin Geologic Map Series: California: Calif. Div. Mines Geo.

Colson, K.B., Rockwell, T.K., Thorup, K.M., and Kennedy, G.L., 1995, Neotectonics of the left-lateral Santa Rosa Island fault, western Transverse Ranges, Southern California, Geol. Soc. Am. Abstr. with Prog. Cordilleran Section, Fairbanks, Abstract No. 30453, p. 11.

Cornell, C.A. 1968, Engineering seismic risk analysis. Bull. Seis. Soc. Am., v. 58, p. 1583-1605.

Crook, R., Jr., Allen, C.R., Kamb, B., Payne, C.M., and Proctor, R.J., 1987, Quaternary geology and seismic hazard of the Sierra Madre and associated faults, western San Gabriel mountains, San Bernardino County, in Recent Reverse Faulting in *The Transverse Ranges, California*, edited by D.M. Mortin and R.F. Yeats, U.S. Geol. Surv. Prof. Pap., 1339, p. 27-64.

Dames & Moore, 1995, Development of Attenuation Equations for Computing Earthquake Ground Motion at Stiff Soil Sites Within Deep Basins: Report to Joint Industry Participants, August.

Darrow, A.C. and Fischer, P.J., 1983, Activity and earthquake potential of the Palos Verdes fault: U.S. Geol. Surv., Open-File Report 82-840, p. 116-119.

Davis, T.L., Namson, J., and Yerkes, R.F., 1989, A cross section of the Los Angeles area: Seismically active fold and thrust belt, the 1987 Whittier Narrows earthquake, and earthquake hazard, J. Geophys. Res., v. 94, p. 9644-9664.

Davis, T.L. and Namson, J.S., 1994, A balanced cross-section of the Northridge earthquake, southern California: Nature, v.372, p. 167-169.

Davis, T.L. and Namson, J.S., 1998, unpublished U.S. Geol. Surv. NEHRP Southern California Cross Section Study, cross sections 12, 13 and 15, www.davisnamson.com.

DeMets, C., Gordon, R.G., Argus, D.F., and Stein, S., 1994, Effect of recent revisions to the geomagnetic reversal time scale on estimates of current plate motions: Geophys. Res. Let., v.21, no. 20, p.2191-2194.

Dibblee, T.W. and Ehrenspeck, H.E., 1994, Geologic map of the Malibu Beach quadrangle, Los Angeles County, California: Dibblee Geological Foundation, Map DF-47, scale 1:24000.

Dibblee, T.W. and Ehrenspeck, H.E., 1993, Geologic map of the Point Dume quadrangle, Los Angeles and Ventura Counties, California: Dibblee Geological Foundation, Map DF-48, scale 1:24000.

Dibblee, T.W. and Ehrenspeck, H.E., ed., 1992, Geologic map of the Topanga and Canoga Park (south 1/2) quadrangles, Los Angeles County, California: Dibblee Geological Foundation, Map DF-35, scale 1:24000.

Dibblee, T.W. and Ehrenspeck, H.E., 1990, Geologic map of the Point Mugu and Triunfo Pass quadrangles, Ventura and Los Angeles Counties, California: Dibblee Geological Foundation, Map DF-29, scale 1:24000.

Dibblee, T.W., Jr., 1989, Geological map of the Palos Verdes Peninsula and Vicinity, Los Angeles County, California, scale 1:24,000, Dibblee Geol. Found. Map DF-70, Santa Barbara, California.

Dolan, J.F., and Sieh, K.E., 1992, Tectonic geomorphology of the northern Los Angeles Basin: Seismic hazards and kinematics of young fault movements, in *Engineering geology field trips: Orange County, Santa Monica Mountains, and Malibu, Guidebook and Volume: Los Angeles, California*, edited by Ehlig, P.L., and Steiner, E.A., Association of Engineering Geologists, p. B20-B26.

Dolan, J.F., Sieh, K., Rockwell, T.K., Yeats, R.S., Shaw, J., Suppe, J., Huftile, G., and Gath, E., 1995, Prospects for larger or more frequent earthquakes in greater metropolitan Los Angeles: Science, v. 267, p.188-205.

Dolan, J.F., Jordan, F., Rasmussen, G., Stevens, D., Reeder, W., and McFadden, L.M., 1996, Evidence for moderate-sized (M_w6.5-7.0) paleoearthquakes on the Cucamonga fault, northeastern Los Angeles metropolitan region, California: EOS, v. 77, p. 461.

Dolan, J.F., and Pratt, T.L., 1997, High-resolution seismic reflection profiling of the Santa Monica fault zone, West Los Angeles, California: Geophys. Res. Let., v. 24, 2051-2054.

Dolan, J., Sieh, K., Rockwell, T. Guptil, P., and Miller, G., 1997, Active tectonics, paleoseismology and seismic hazards of the Hollywood fault, northern Los Angeles basin, California: Bull. Geol. Soc. Am., v. 109, p. 1595-1616.

Dolan, J.F., Sieh, K., and Rockwell, T.K., 2000b, Late Quaternary activity and seismic potential of the Santa Monica fault system, Los Angeles, California: Geol. Soc. Am. Bull., v. 112, p. 1559-1581.

Dolan, J.F., Stevens, D., and Rockwell, T.K., 2000a, Paleoseismologic evidence for an early- to mid-Holocene age of the most recent surface rupture on the Hollywood fault, Los Angeles, California: Bull. Seis. Soc. Am., v. 90, p. 334-344.

Dolan, J.F., Shaw, J.H., and Pratt, T.L., 2001, Methodology for defining concealed earthquake sources - application to the Puente Hills blind thrust system, Los Angeles, California: U.S. Geol. Surv., National Earthquake Hazards Program, 2001 Annual Project Summary.

Dolan, J.F., Marin, M., Owen, L., Hartleb, R.D., and Christofferson, S.A., in review, Slip rate on the Raymond fault determined by 3-D trenching, Implications for fault kinematics and seismic hazards of the Los Angeles metropolitan region, submitted to Bull. Seis. Soc. of Am.

Dolan, J.F., Christofferson, S.A., Shaw, J.H., 2003 Recognition of Paleoearthquakes on the Puente Hills Blind Thrust Fault, California, Science, Vol. 300, pp. 115-118, April 4.

Edwards, B.D., Ehmann, K.D., Ponti, D.J., Tinsley, J.C., III, and Reicherdt, E.G., 2003 (abs.), Offshore stratigraphic controls on saltwater intrusion in Los Angeles area coastal aquifers, in LA Basin 2003, Original Urban Oil Field Legend, Conference Program and Abstracts: American Association of Petroleum Geologists, Pacific Section, Western Region Society of Petroleum Engineers, p. 62.

Edwards, B.D., Ponti, D.J., Ehmann, K.D., Tinsley, J.C., III, and Reicherdt, E.G., 2002, Offshore stratigraphic controls on saltwater intrusion in Los Angeles area coastal aquifers (abs): AGU Fall Meeting, San Francisco, CA, EOS, v., 83, no. 47, p. F567.

Edwards, B.D., Catchings, R.D., Hildebrand, T.G., Miller, M.S., Ponti, D.J., and Wolfe, S.C., 2001, Quaternary Sedimentary Structure of the Southwestern Los Angeles Basin Region, Geol. Soc. Am. Abs. Prog. v. 33, No. 3:A-41.

Edwards, K., and Batson, R.M., 1990, Experimental digital shaded-relief map of California, scale 1:1,000,000, U.S. Geol. Surv. Misc. Investigation Series Map I-1848.

Ellsworth, W.L., 1990, Earthquake History in *The San Andreas Fault System, California,* edited by R.E. Wallace, U.S. Geol. Surv. Prof. Pap. 1515, p. 153–187.

Fisher, M.A., Normak, W.R., Langenheim, V.E., Calvert, A.J., and R. Sliter, 2003 - in review, Marine Geology and Earthquake Hazards for the San Pedro Shelf Region, Southern California

Fischer, P.J., Rudat, J.H., Patterson, R.H., Similia, G., 1987, The Palos Verdes fault zone: Onshore and Offshore, in Geology of the Palos Verdes Peninsula and San Pedro Bay: Guidebook 55, ed. P. Fischer, p. 91-133, Pac. Coast Sect. Soc. of Econ. Paleontol. and Mineralogists, Bakersfield, California.

Frankel, A.D. and Leyendecker, E.V., 2001, Seismic Hazard Curves and Uniform Hazard Response Spectra for the United States: U.S. Geol. Surv. CD Rom, Version 3.10, March.

Frankel, A.D., + 10 coauthors, 2000, USGS national seismic hazard maps: Earthquake Spectra, v. 16, no. 1, p.1-19.

Fumal, T.E., Rymer., M.J., and Seitz, G.G., 2002, Timing of large earthquakes since A.D. 800 on the Mission Creek strand of the San Andreas fault zone at the Thousand Palms Oasis, near Palm Springs, California: Bull. Seis. Soc. Amer., v. 92, no. 7, p. 2841-2860.

Fumal, T.E., Davis, A.B., Frost, W.T., O'Donnell, J., Sega, G., and Schwartz, D.P., 1995, Recurrence studies of Tujunga segment of the 1971 San Fernando earthquake: California, EOS (Supplement), v. 76 (46), p. 364.

Gardner, J.V. and Dartnell, P., 2002, Multibeam mapping of the Los Angeles, California, margin: U.S. Geol. Surv., Open-File Report 02-162.

Gath, E.M., Gonzalez, T., and Rockwell, T.K., 1992, Slip rate of the Whittier fault based on 3-D trenching at Brea, southern California, Geol. Soc. Am. Abs. With Programs, v. 24 p. 26.

Gath, E.M., Gonzalez, T., Drumm, P.L., and Buchiarelli, P., 1994, Paleoseismic investigation at the northern terminus of the Whittier fault zone in the Whittier Narrows area, Rosemead, California (abs): Engineering Geology: Past, Present, and Future; Association of Engineering Geologists, 37th Annual Meeting, Program and Abstracts, p.47.

Grant, L.B., Waggoner, J.T., Rockwell, T.K., and von Stein, C.R., 1997, Paleoseismicity of the North branch of the Newport-Inglewood fault in Huntington Beach, California, from cone penetrometer test data: Bull. Seis. Soc. Am., v. 77, p. 277-293.

Grant, L.B., Mueller, K.J., Gath, E.M., Cheng, H., Edwards, R.L., Munro, R., and Kennedy, G.L., 1999, Late Quaternary uplift and earthquake potential of the San Joaquin Hills, southern Los Angeles Basin, California, Geology, v. 27, p. 1031-1034.

Grant, L.B., Ballenger, L.J., and Runnerstrom, E.E., 2002, Coastal uplift of the San Joaquin Hills, southern Los Angeles basin, California, by a large earthquake since 1635 A.D.: Bull. Seis. Soc. Am., v. 92, no. 2, p. 590-599.

Grant, L.B., and Rockwell, T.K., 2002, A Northward-propagating Earthquake Sequence in Coastal Southern California?: Seismological Research Letters, Vol. 73, no. 4, p. 461-469.

Grant, L.B., and Lettis, W.R., 2002, Introduction to the Special Issue on Paleoseismology of the San Andreas Fault System, Bulletin of Seismological Society of America, vol. 92 no. 7, p. 2551-2554. October.

Hanks, T. and Kanamori, H., 1979, A moment magnitude scale: J. Geophys. Res., v. 84, p. 2348-2350.

Hart, W., and Bryant W.A., 1997, Fault-Rupture Hazard Zones in California: CDMG Ca. Div. Mines Geol., Special Publication No. 42 with Supplements 1-3.

Hauksson, E., Jones, L.M., Hutton, K., 1995, The 1994 Northridge earthquake sequence in California: Seismological and tectonic aspects: J. Geophys. Res., v. 100, no. B7, p. 12,335-12,355.

Hauksson, E., and Jones, L.M., 1989, The 1987 Whittier earthquake sequence in Los Angeles, southern California: seismological and tectonic analysis: J. Geophys. Res., v. 94, no. 87, p. 9569-9589.

Hill, R.L., Sproutte, E.C., Bennett, J.H., Real, C.R., and Slade, R.C., 1979, Location and activity of the Santa Monica fault, Beverly Hills-Hollywood area, California, earthquake hazards associated with faults in the greater metropolitan area, Los Angeles County, including faults in the Santa Monica-Raymond, Verdugo-Eagle Rock, and Benedict Canyon fault zones, Cal. Div. Mines and Geol., Open-file Rept. 79-16 LA, p. B1-B43.

Hudnut, K.W., Shen, Z.K., Murray, M., McClusky, S., King, R., Hager, B., Feng, Y., Fang, P., Donnellan, A., and Bock, Y., 1996, Coseismic displacements on the 1994 Northridge, California earthquake: Bull. Seis. Soc. Am., v. 86, no. 1, Part B, p. S19-S36.

Huftile, G.J., and Yeats, R.S., 1995, Convergence rates across a displacement transfer zone in the western Transverse Ranges, Ventura Basin, California: J. Geophys. Res., v. 100, no. B2, p. 2043-2067.

Hull, A.G., and C. Nicholson, 1992, Seismotectonics of the northern Elsinore fault zone, southern California, Bull. Seis. Soc. Am., v.82, p.800-818.

Jacoby, G.C. Jr., Sheppard, P.R., and Sieh, K.E., 1988, Irregular Recurrence of Large Earthquakes Along the San Andreas Fault: Evidence from Trees. Science, Vol. 241, No. 4862, pp. 196-199.

Jennings, C.W., 1994, Fault Activity Map of California and Adjacent Areas, Cal. Div. Mines and Geol. 1:750,000-Scale Map.

Jones, L.M., Sieh, K.E., Hauksson, E., and Hutton, L.K., 1990, The 3 December Pasadena, California earthquake: Evidence for strike slip motion on the Raymond fault: Bull. Seis. Soc. Am. 80, p. 474-482.

Joyner, W.B., and Boore, D.M., 1992. Quantifying the variability of ground-motion estimates for seismic hazard analysis, submitted to Bulletin of Seismological Society of America.

Kiureghian, A. der, and Ang, A. H-S, 1975, A line source model for seismic risk analysis: Technical Report, University of Illinois.

Lamar, D.L., 1970, Geology of the Elysian Park-Repetto Hills area, Los Angeles County, California, Spec. Rep., Calif. Div. Mines and Geol., 101, p. 45.

Legg, M.R., 2001, Earthquake potential of major faults offshore Southern California: Southern California Earthquake Center, 2001 Annual Report, 9 p.

Leighton and Associates, 1987, Fault activity and recurrence intervals of the western segment of the Whittier fault, California: Final Technical Report to the U.S. Geol. Surv., Contract No. 14-08-0001-21368, 17 p.

Liddicoat, J.C., 1992, Paleomagnetism of the Pico Formation, Santa Paula Creek, Ventura Basin, California, Geophys. J. Int., v. 110, p. 267-275.

Lindvall, S.C., Rockwell, T.K., Walls, C., and Bornyasz, M., 1995, Late Quaternary deformation of Pacoima Wash terraces in the vicinity of the 1971 San Fernando earthquake rupture, northern San Fernando Valley, California, EOS, v. 76, F363.

Lindvall, S.C., Rockwell, T.K., Kasman, G., and Helms, J.G., 2001, Style, activity, and uplift rate of the Hollywood fault in Hollywood and West Hollywood, California, Geol. Soc. Am. Abs. With Program v. 33, No. 3:A-41.

Lung, R., and Weick, R.J., 1987, Exploratory trenching of the Santa Susana fault in Los Angeles and Ventura Counties, in *Recent Reverse Faulting in the Transverse Ranges, California*, edited by D.M. Mortin and R.F. Yeats, U.S. Geol. Surv. Prof. Pap., 1339, p. 65-70.

McGill, J.T., 1989, Geologic maps of the Pacific Palisades area, Los Angeles, California, U.S. Geol. Surv. Miscellaneous Investigations Series Map I-1828, scale 1:48000.

McNeilan, T.W., Rockwell, T.K., and Resnick, G.S., 1996, Style and rate of Holocene slip, Palos Verdes fault, southern California, J. Geophys. Res., v. 101, no. B4, p. 8317-8334.

Magistrale, H., and Rockwell, T., 1996, The central and southern Elsinore fault zone, southern California, Bull. Seis. Soc. Am., v.86, no. 6, p.1793-1803.

Marin, M., Dolan, J.F., Hartleb, R.D., Christofferson, S.A., Tucker, A.Z., and Owen, L.A., 2000, A latest Pleistocene-Holocene slip rate on the Raymond fault based on 3-D trenching, East Pasadena, California, EOS v. 81(48 supplement) F855.

Marlow, M.S., Gardner, J.V., Normark, W.R., 2000, Using high-resolution multibeam bathymetry to identify seafloor surface rupture along the Palos Verdes fault complex in offshore southern California, Geology, v. 28 no. 7 p. 587-590, July.

Morton, D.M. and Matti, S.C., 1987, The Cucamonga fault zone: geologic setting and Quaternary historic, in *Recent Reverse Faulting in the Transverse Ranges, California*, edited by D.M. Mortin and R.F. Yeats, U.S. Geol. Surv. Prof. Pap., 1339, p. 179-203.

Muhs, D.R., Rockwell, T.K., and Kennedy, G.L., 1992, Late Quaternary uplift rates of marine terraces on the Pacific coast of North America, southern Oregon to Baja California Sur: Quat. Intl., v.7/8, p. 81-93.

Newmark, N.M., Hall, W.J., 1982, Earthquake Spectra and Design. Earthquake Engineering Research Institute, Berkeley, CA.

Nicholson, C., 1987, Seismic slip on the southern San Andreas fault: 1948 and 1986: Seis. Soc. Am., Seis. Res. Let., v. 58, p.14.

Oskin, M., and Sieh, K.E. 1998, The Elysian Park anticlinorium: Surficial evidence of an active blind reverse fault beneath downtown Los Angeles, Geol. Soc. Am., Abstracts with Programs, Cordilleran Section, no. 6471, p. 57.

Oskin, M., Sieh, K., Rockwell, T., Miller, G., Guptill, P., Curtis, M., McArdle, S., and Elliot, P., 2000, Active parasitic folds on the Elysian Park anticline: Implications for seismic hazard in central Los Angeles, California, Bull. Geol. Soc. Am., v. 112, p. 693-707.

Peterson, M.D. and Wesnousky, S.G., 1994, Fault slip rates and earthquake histories for active faults in Southern California: Bulletin of the Bull. Geol. Soc. Am., v. 84, no. 5, p. 1608-1649.

Pinter, N., and Sorlien, C., 1991, Evidence for latest Pleistocene and Holocene movement, on the Santa Cruz Island fault, California: Geology, v. 19, p. 909-912.

Poland, J.F., and Piper, A.M., 1956, U.S. Ground-water Geology of the Coastal Zone Long Beach-Santa Ana Area, California, U.S. Geological Surv. Water-Supply Paper 1109.

Ponti, D.J., Lajoie, K.R., and Powell, C.L. II, 1991, Upper Pleistocene marine terraces in San Pedro, southwestern Los Angeles basin, California: Implications for aminostratigraphy and coastal uplift: Geol. Soc. Am. Abst. Prog., v. 23., no. 2, p. 89.

Pratt, T.L., Shaw, J.H., Dolan, J.F., Christofferson, J.F., Williams, R.A., Odum, J.K., Plesch, A., 2002, Shallow seismic imaging of folds above the Puente Hills blind-thrust fault, Los Angeles, California Geophys. Res. Let., v. 29, no. 9, 10.1029/2001GL014313.

Pratt, T.L., Dolan, J.F., Odum, Jackson K., Stephenson, William J., Williams, Robert A., and Templeton, Mary E., 1998, Multiscale seismic imaging of active fault zones for hazard assessment: A case study of the Santa Monica fault zone, Los Angeles, California, Geophysics, Vol. 63 No. 2 pp. 479-489, March-April.

Quinn, J.P., Ponti, D.J., Hillhouse, J.W., Powell, C.L., II, McDougal, K., Sarna-Wojcicki, A.M., Barron, J.A., and Felck, R.J., 2001, Quaternary chronostratigraphic constraints on

deformation and blind thrust faulting, northern Los Angeles Basin, Final Technical Report, 1424-HQ-98-00025 to U.S. Geol. Surv., 22 p.

Real, C.R., 1987, Seismicity and tectonics of the Santa-Monica-Hollywood-Raymond Hill fault zone and northern Los Angeles Basin: in *Reverse Faulting in the Transverse Ranges, California*, edited by D.M. Mortin and R.F. Yeats, U.S. Geol. Surv. Prof. Pap., 1339, p. 113-124.

Rockwell, T.K., Gath, E.M., and Gonzalez, T., 1992, Sense and rate of slip on the Whittier fault zone, eastern Los Angeles basin, California: Assoc. Eng. Geol., Proceedings of the 35th Annual meeting, p. 674-680.

Rockwell, T.K., Gath, E.M., and Crook, K.D. 1988, Sense and rate of slip on the Whittier fault zone near Yorba Linda, California (abstract): Geol. Soc. Am. Abstr. Programs, v. 20, no. 3, p. 224.

Rockwell, T.K., Klinger, R., and Goodmacher, J., 1990, Determination of slip rates and dating of earthquakes for the San Jacinto and Elsinore fault zones: in *Geology around the margins of the eastern San Bernardino Mountains*, Kkooser, M.A. and Reynolds, R.E. (ed.), v. 1, Inland Geol. Soc., Redlands, CA, p. 51-56.

Rockwell, T.K., McElwain, R.S., Millman, D.E., and Lamar, D.L., 1986. Recurrent late Holocene faulting on the Glen Ivy North strand of the Elsinore fault at Glen Ivy Marsh: in *Guidebook and Volume on Neotectonics and Faulting in Southern California*, P. Ehlig (Editor), Cordilleran Section, Geol. Soc. of Am., Boulder, Colorado, p. 167-175.

Rubin, C.M., Lindvall, S.C., and Rockwell, T.K., 1998, Evidence for Large earthquakes in metropolitan Los Angeles: Science. vol. 281, p. 398-402.

Rzonca, G.F., Spellmane, H.A., Fall, E.W., and Shlemon, R.F., 1991, Holocene dsiplacement of the Malibu Coast fault zone, Winter Mesa, Malibu, California: engineering geologic implications: Bull. Assoc. Eng. Geol., v. 28, no. 2, p. 147-158.

SCEC (Southern California Earthquake Center) Group C, 2001, Active Faults in the Los Angeles Metropolitan Region: SCEC Special Publications Series, no. 001, 2001 September.

Schneider, C.L., Hummon, C., Yeats, R.S., and Huftile, G.J., 1996, Structural evolution of the northern Los Angeles basin, California, based on growth strata: Tectonics, v. 15, p. 341-355.

Seitz, G., Weldon, R. II, and Biasi, G. P., 1997, The Pitman Canyon paleoseismic record: A reevaluation of southern San Andreas fault segmentation: Jour. Geodyn., v.24, p.129-138.

Shaw, J., 1999, Seismic-reflection transect and geologic cross-section across the central Los Angeles basin and San Pedro Bay, Southern California Earthquake Center, 1999 Annual Report, 2 p.

Shaw, J.H., Plesch, A., Dolan, J.F., Pratt, T.L., and Fiore, P., 2002, Puente Hills blind-thrust system, Los Angeles, California: Bull. Seis. Soc. Am., v. 92, no. 8, p. 2946-2960.

Shaw, J.H., and Suppe, J., 1996, Earthquake hazards of active blind thrust faults under the central Los Angeles basin, California: J. Geophys. Res., v. 101, p. 8623-8642.

Shaw, J.H. and Shearer, P.M., 1999, An elusive blind-thrust fault beneath metropolitan Los Angeles: Science, v. 283, p. 1516-1518.

Sieh, K., Stuiver, M. and Brillnger, D., 1989, A more precise chronology of earthquakes produced by the San Andreas fault in Southern California: J. Geophys. Res., v. 94, p. 603-623.

Sieh, K.E., and Williams, P.L., 1990, Behavior of the southernmost San Andreas Fault during the past 300 years: J. Geophys. Res., v. 95, p. 6629-6645.

Slosson, J.E. and Gray, C.H.J., 1984, Geology and man, San Bernardino – Cajon Pass Region: American Association of Petroleum Geologists, Pacific Section Guidebook for the San Andreas fault – Cajon Pass to Wrightwood.

Somerville, P.G., 2003, Magnitude scaling of the near fault rupture directivity pulse: Physics of the Earth and Planetary Interiors, v. 137, p. 201-212.

Somerville, P.G., Smith, N.F., Graves, R.W., and Abrahamson, N.A., 1997, Modification of empirical strong motion attenuation relations to include the amplitude and duration effects of rupture directivity: Seism. Soc. of Am., Seis. Res. Let., v. 68, no. 1, p.199-222.

Sorlein, C.C., 1994, Faulting and uplift of the northern Channel Islands, California: in Proceedings, The Fourth California Islands Symposium: Update on the Status of Resources, Santa Barbara Museum of Natural History, p. 281-296.

Stein, R.S. and Hanks, T.C., 1998, M≥6 earthquakes in southern California during the twentieth century: no evidence for a seismicity or moment deficit: Bull. Seis. Soc. of Am., v. 88, no. 3, p. 635-652.

Stephenson, W. J., Rockwell, T.K., Odum, J.K., Shedlock, K.M., and Okaya, D.A., 1995, Seismic reflection and geomorphic characterization of the onshore Palos Verdes fault zone, Los Angeles, California: Bull. Seis. Soc. Am., v. 85, no. 3, p. 943-950.

Synolakis, Costas, 2003, Tsunami and Seiche, Earthquake Engineering Handbook, Chapter 9, CRC Press.

Toppozada, T., Brandum, D., Peterson, M., Hallstrom, C., Cramer, C., and Reichle, M., 2002, Epicenters of and Areas Damaged by M ≥ 5 California Earthquakes, 1800 – 1899: California Division of Mines and Geology, Map Sheet 49.

Treiman, J.A., 1994, The Malibu Coast fault: California Division of Mines and Geology Fault Evaluation Report FER 229, p. 42.

Truex, J.N., 1974, Structural evolution of Wilmington , California, anticline: Amer. Assoc. Pet. Geol. Bull., v. 58,p. 2398-2410.

Truex, J.N. and Hunter, W.J., 1973, Development of the offshore Wilmington Oil field: Pacific Sections, AAPG-SEPM-Society of Exploration Geophysicists Guidebook, Trip 1, p. 3-9

Tsutsumi, H., Yeats, R.S., and Huftile, G.J., 2001, Late Cenozoic tectonics of the northern Los Angeles fault system, California: Bull. Geol. Soc. Am., v. 113, p. 454-468.

Tsutsumi, H., and Yeats, R.S., 1999, Tectonic setting of the 1971 Sylmar and 1994 Northridge earthquakes in the San Fernando Valley, California: Bull. Seis. Soc. Amer., v. 89, no. 5, p. 1232-1249.

Tucker, A.Z. and Dolan, J.F., 2001, Paleoseismologic evidence for a >8 ka age of the most recent surface rupture on the eastern Sierra Madre fault, northern Los Angeles metropolitan region, California: Bull. Seis. Soc. Amer., v. 91, no. 1, p. 232-249

URS, 2003a, Final Geotechnical Report, Proposed LNG Import Terminal Development, Pier Echo, Terminal Island, Port of Long Beach, California: submitted to Kellogg Brown & Root, Inc., November.

URS, 2003b, Draft Report, Appendix I – Probabilistic ground motion analysis for the central campus, Section 2.4 – Earthquake Hazard Levels, UC Berkeley Seismic Guidelines.

USGS (U.S. Geological Survey), 1988, Probabilities of large earthquakes occurring in California on the San Andreas fault: U.S. Geol. Surv., Open-File Report 88-398, p. 62.

Walls, C., Rockwell, T.K., Mueller, K., Back, Y., Williams, S., Pfanner, J., Dolan, J., and Fang, P., 1998, Escape tectonics in the Los Angeles metropolitan region and implications for seismic risk: Nature, v. 394, p. 356-360.

Ward, S. N., and Valensise, G., 1994, The Palos Verdes terraces, California: bathtub rings from a buried reverse fault: J. Geophys. Res., v. 99, p. 4485-4494.

Weaver, K.D., and Dolan, J.F., 2000, Paleoseismology and geomorphology of the Raymond fault, Los Angeles County, California: Bull. Seis. Soc. Am., v. 90, p. 1409-1429.

Weaver, K.D., and Dolan, J.F., 2001, Evaluation Event Chronologies on the Raymond Fault, Los Angeles County, California: Geol. Soc. Am. Abs. With Program v. 33, no. 3 p. A-41.

Weber, F.H., Bennett, J.H., Chapman, R.H., et al., Chase, G.W. and Saul, R.B., 1980, Earthquake hazards associated with the Verdugo-Eagle Rock and Benedict Canyon fault zones, Los Angeles County, California: Cal. Div. Mines Geol., Open-File Report 80-10LA. 4 plates, p. 166.

Weldon, R.J. II, Fumal, T.E., Powers, T.J., Pezzopane, S.K., Scharer, K.M., and Hamilton, J.C., 2002, Structure and earthquake offsets of the San Andreas fault at the Wrightwood, California, paleoseismic site, Bull. Seis. Soc. Amer., v. 92, no. 7, p. 2704-2725

Wells, D.L., and Coppersmith, K.J., 1994, New empirical relationships among magnitude, rupture length, rupture width, rupture area, and surface displacement: Bull. Seis. Soc. Am., v. 84, no. 4, p. 974-1002.

Williams, N., 2003, An Earthquake Hazard Assessment of the THUMS-HB fault, Long Beach, California, BA Thesis to The Dept. of Earth and Planetary Science, Harvard College.

WGCEP (Working Group on California Earthquake Probabilities), 1995, Seismic hazards in southern California: Probable earthquakes, 1994 to 2024: Bull. Seis. Soc. of Am., v. 85, no. 2, p. 379-439.

Wright, T.L., 1991, Structural geology and tectonic evolution of the Los Angeles Basin, in Biddle, K.T., ed., Active margin basins: AAPG Memoir, v. 52, p. 35-134.

Yeats, R.S., G.J. Huftile, and L.J. Stitt, 1994, Late Cenozoic tectonics of the east Ventura basin, Transverse Ranges, California: Am. Assoc. Pet. Geol. Bull., v. 78, p. 1040-1074.

Yeats, R.S., 1987, Late Cenozoic Structure of the Santa Susana fault zone, in *Recent Reverse Faulting in the Transverse Ranges, California*, edited by D.M. Mortin and R.F. Yeats, U.S. Geol. Surv. Prof. Pap. 1339, p. 137-160.

Yerkes, R.F., McCulloh, T.H. Schoellhamer, J.E. and Vedder J.G., 1965. Geology of the Los Angeles Basin, California – and Introduction: U.S. Geol. Surv., Prof. Pap. 420-A.

Ziony, J.I. and Jones, L.M., 1989, Map showing late Quaternary faults and 1978-1984 seismicity of the Los Angeles region, California: U.S. Geol. Surv., Misc. Field Studies map MF-1964.